Supporting Information

Sterically hindered phenanthroimidazole ligands drive the structural flexibility and unprecedented lability of cyclometalated iridium(III) complexes

Sergei V. Tatarin, Paulina Kalle, Ilya V. Taydakov, Evgenia A. Varaksina, Vladislav M. Korshunov and Stanislav I. Bezzubov

1. **NMR and mass spectra.**

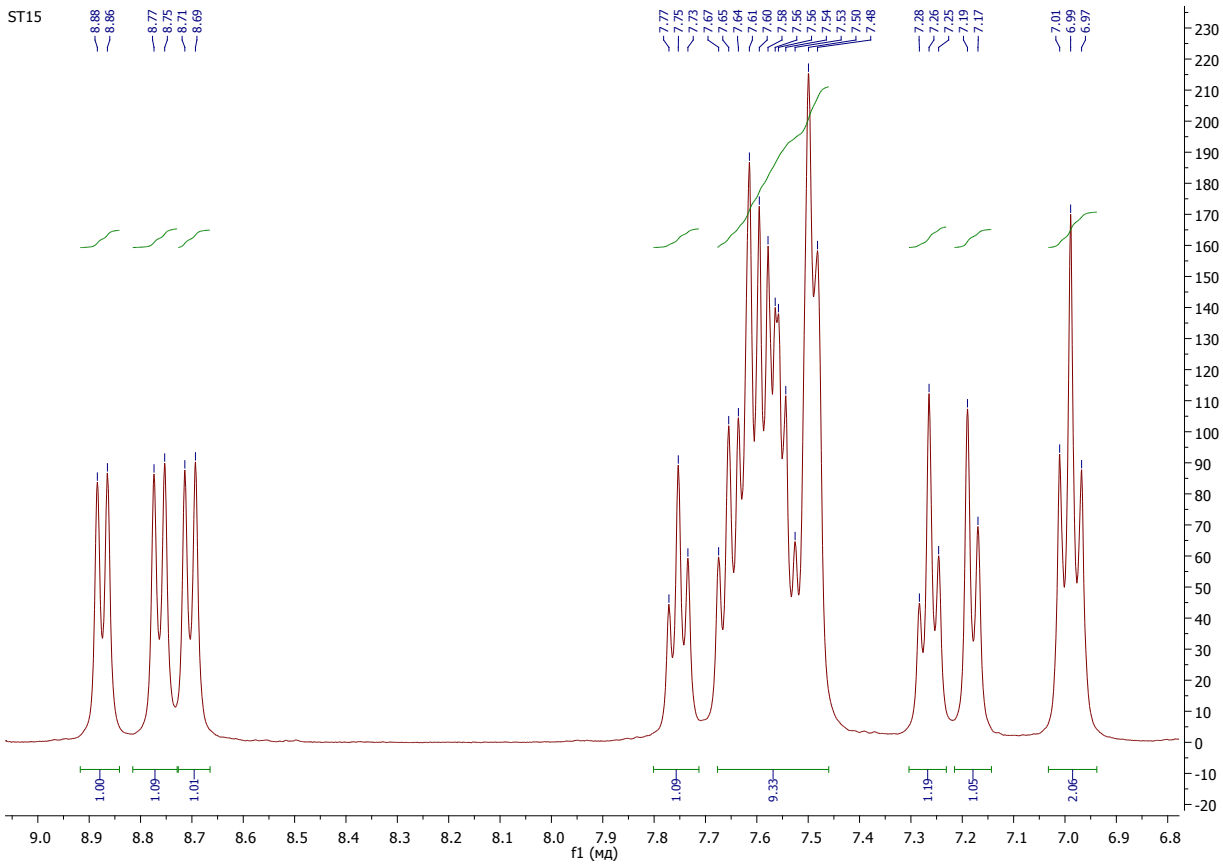

Figure S1. ^{1}H NMR spectrum of fphi (400 MHz, 298K, $CDCl_3$).

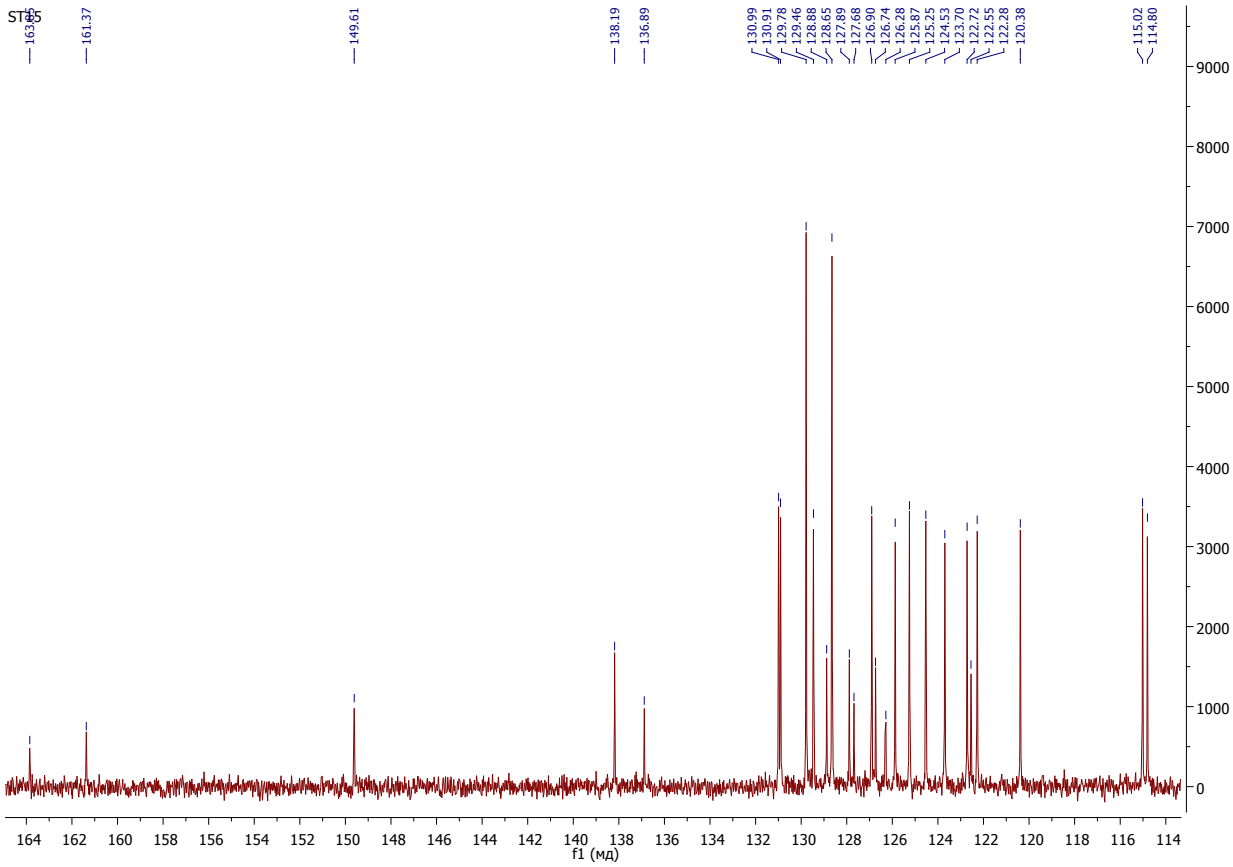

Figure S2. ^{13}C {^{1}H} NMR spectrum of fphi (101 MHz, 298K, $CDCl_3$).

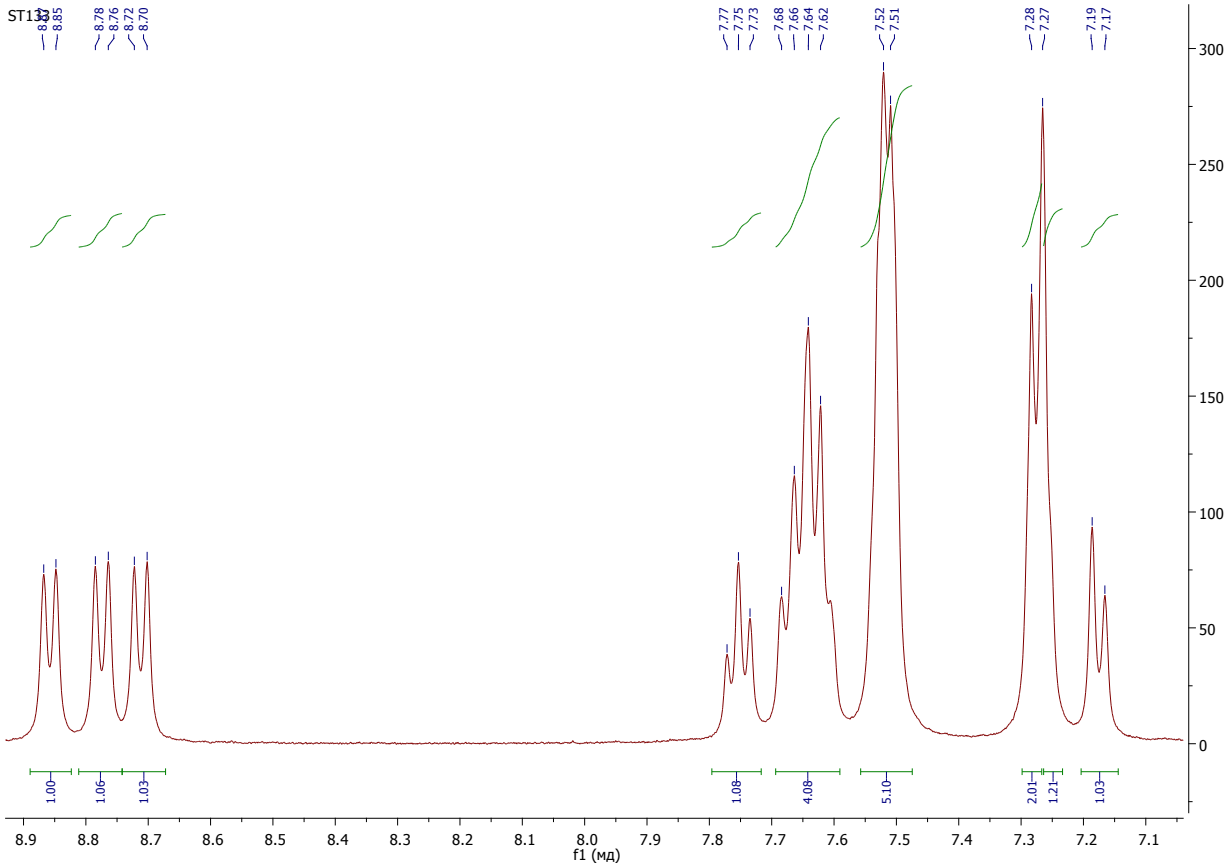

Figure S3. ^{1}H NMR spectrum of cphi (400 MHz, 298K, $CDCl_3$).

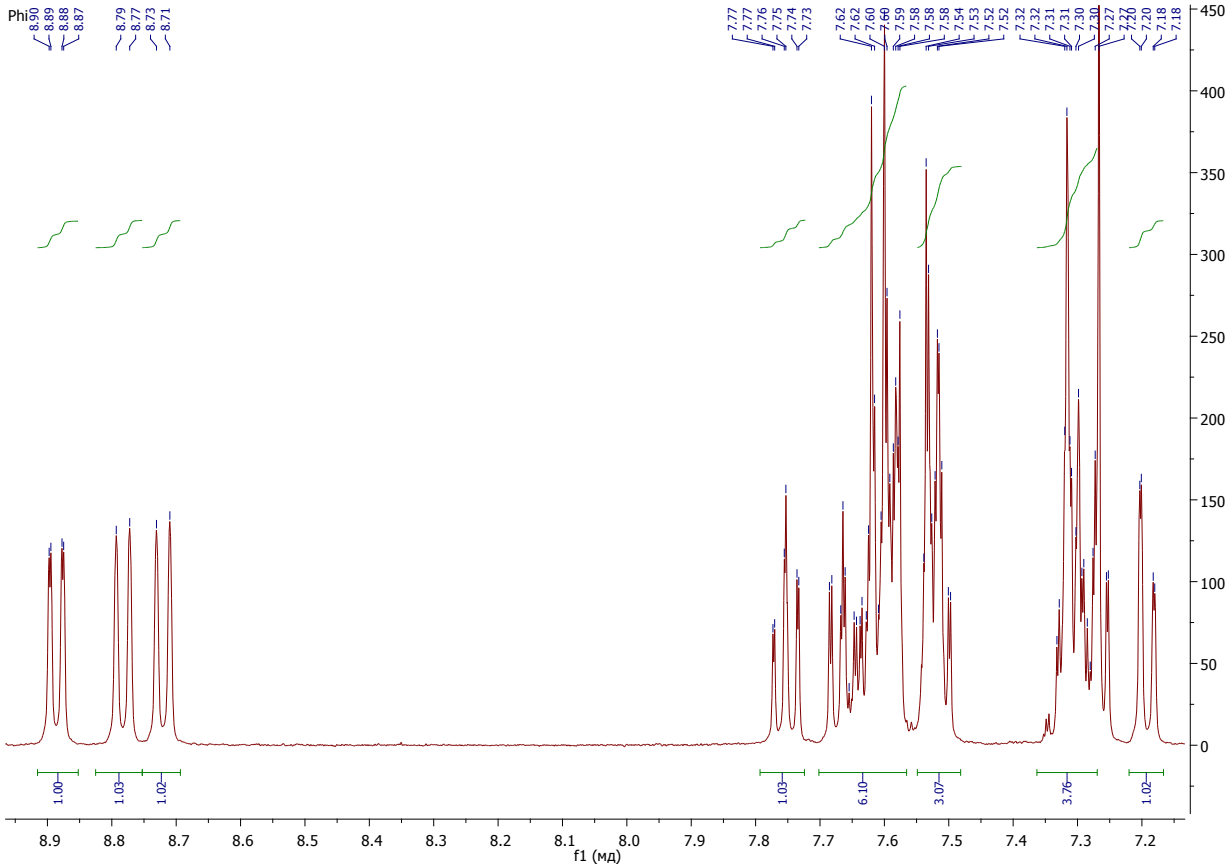

Figure S4. ^{1}H NMR spectrum of phi (400 MHz, 298K, $CDCl_3$).

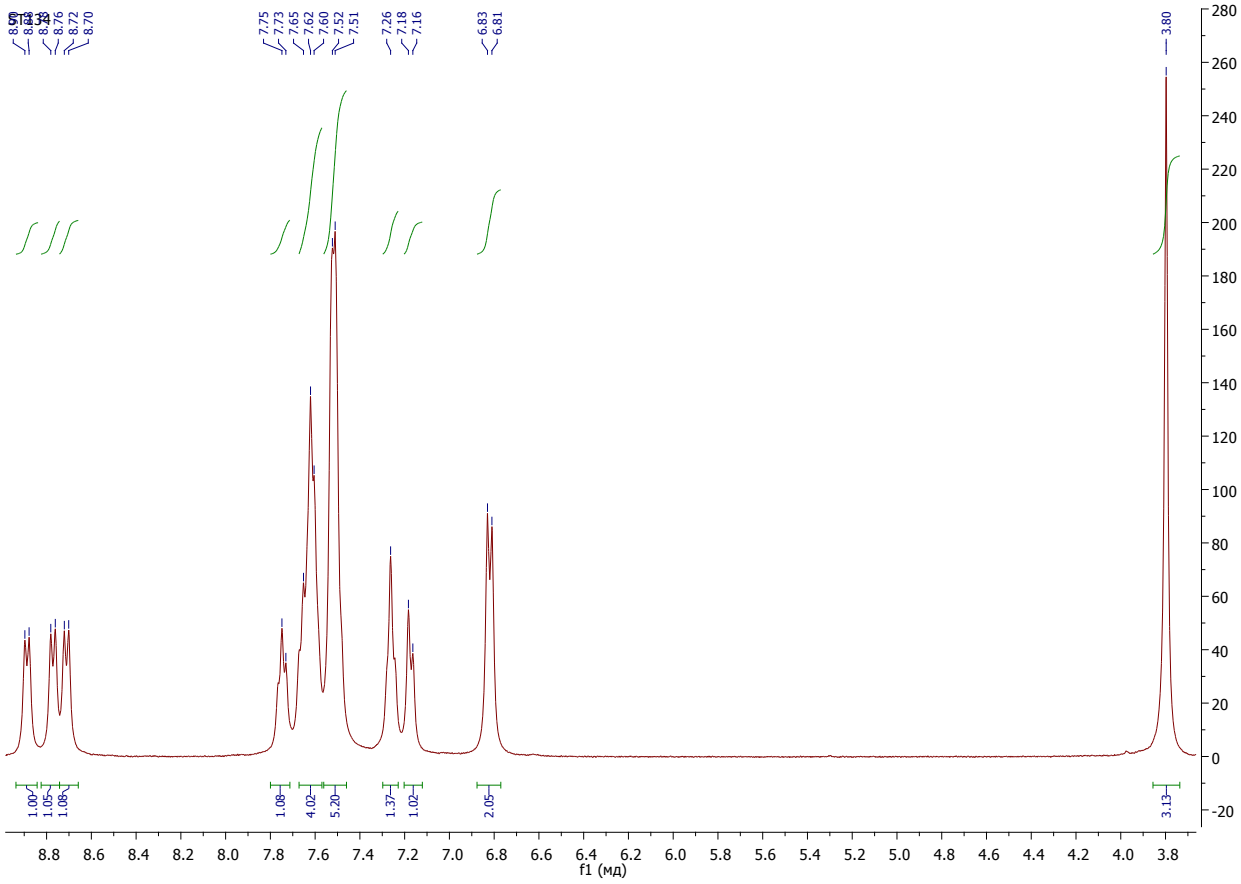

Figure S5. ^{1}H NMR spectrum of mphi (400 MHz, 298K, $CDCl_3$).

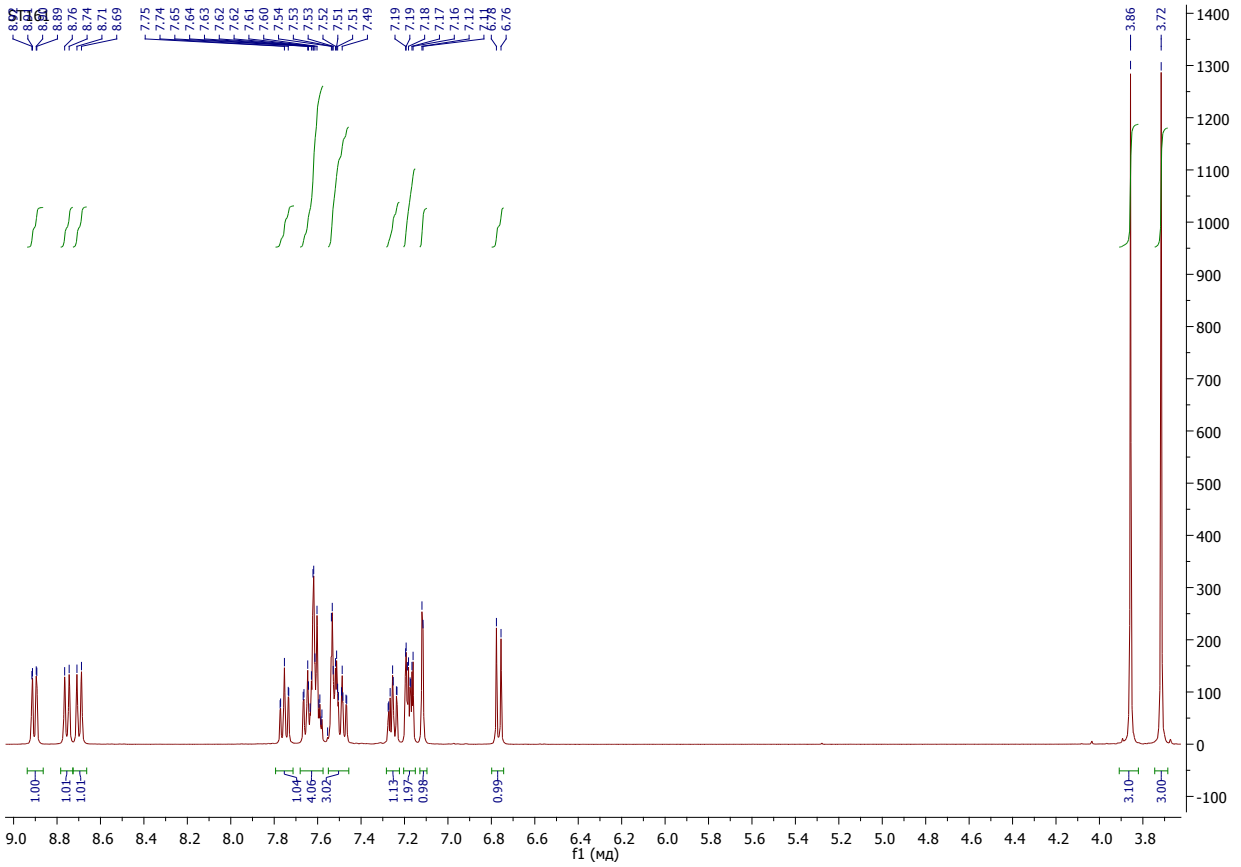

Figure S6. ^{1}H NMR spectrum of dmphi (400 MHz, 298K, $CDCl_3$).

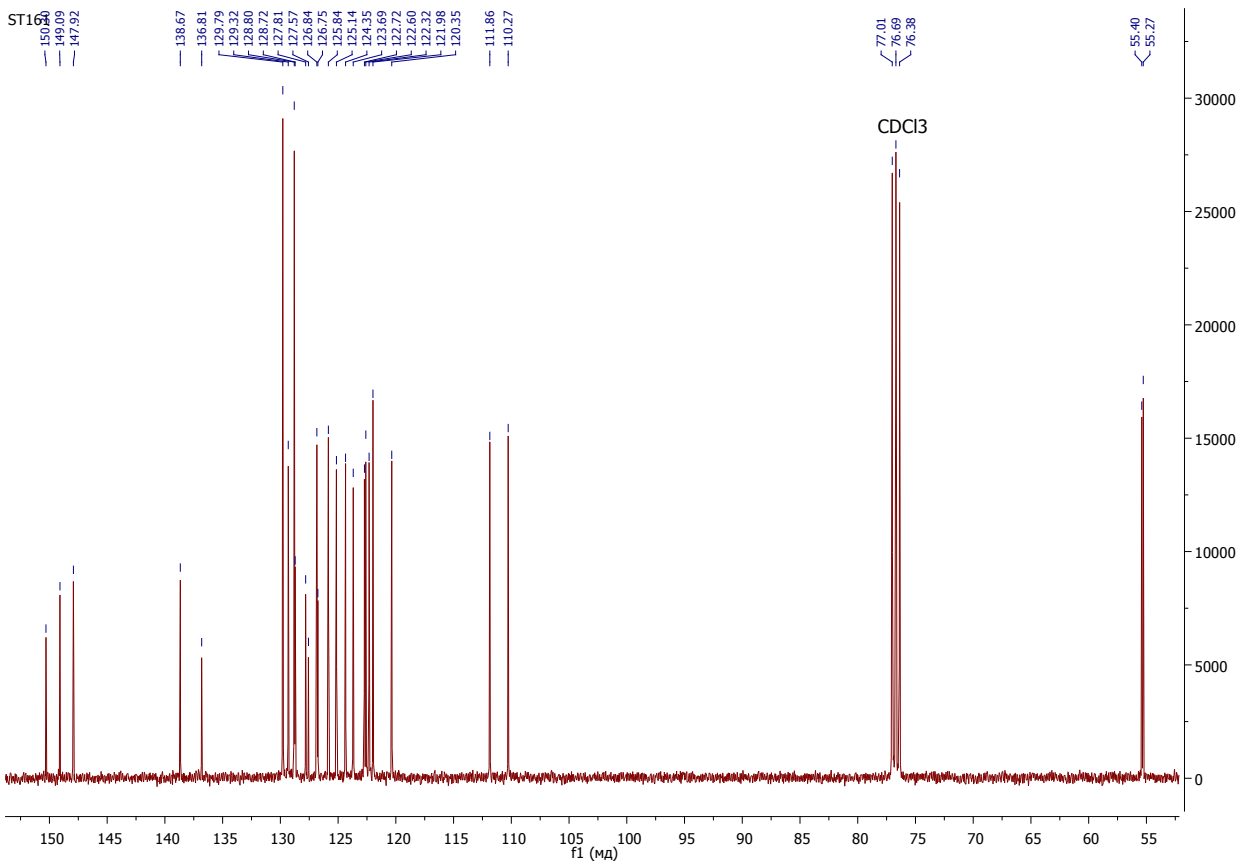

Figure S7. ^{13}C {^{1}H} NMR spectrum of dmphi (101 MHz, 298K, $CDCl_3$).

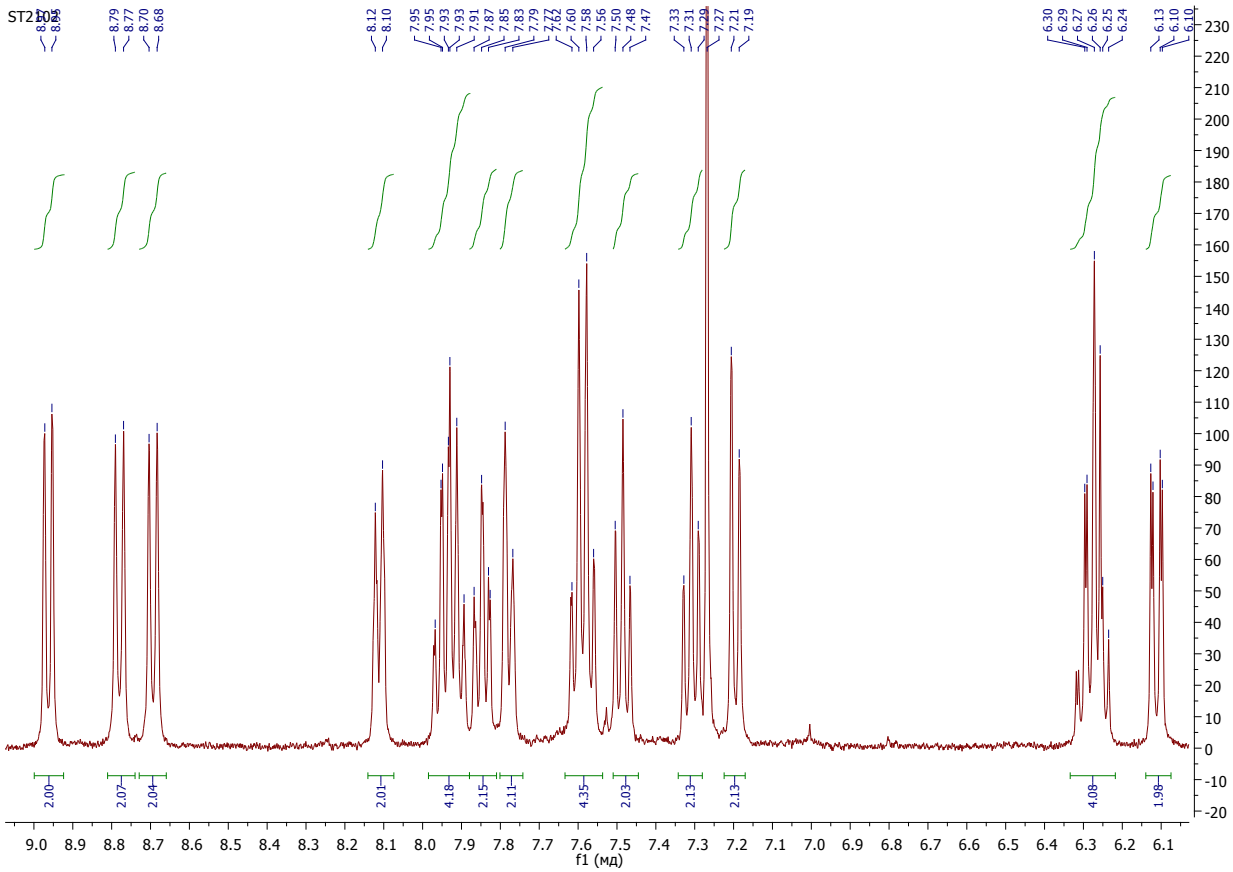

Figure S8. ^{1}H NMR spectrum of $[Ir(fphi)_2Cl]_2$ (400 MHz, 298K, $CDCl_3$).

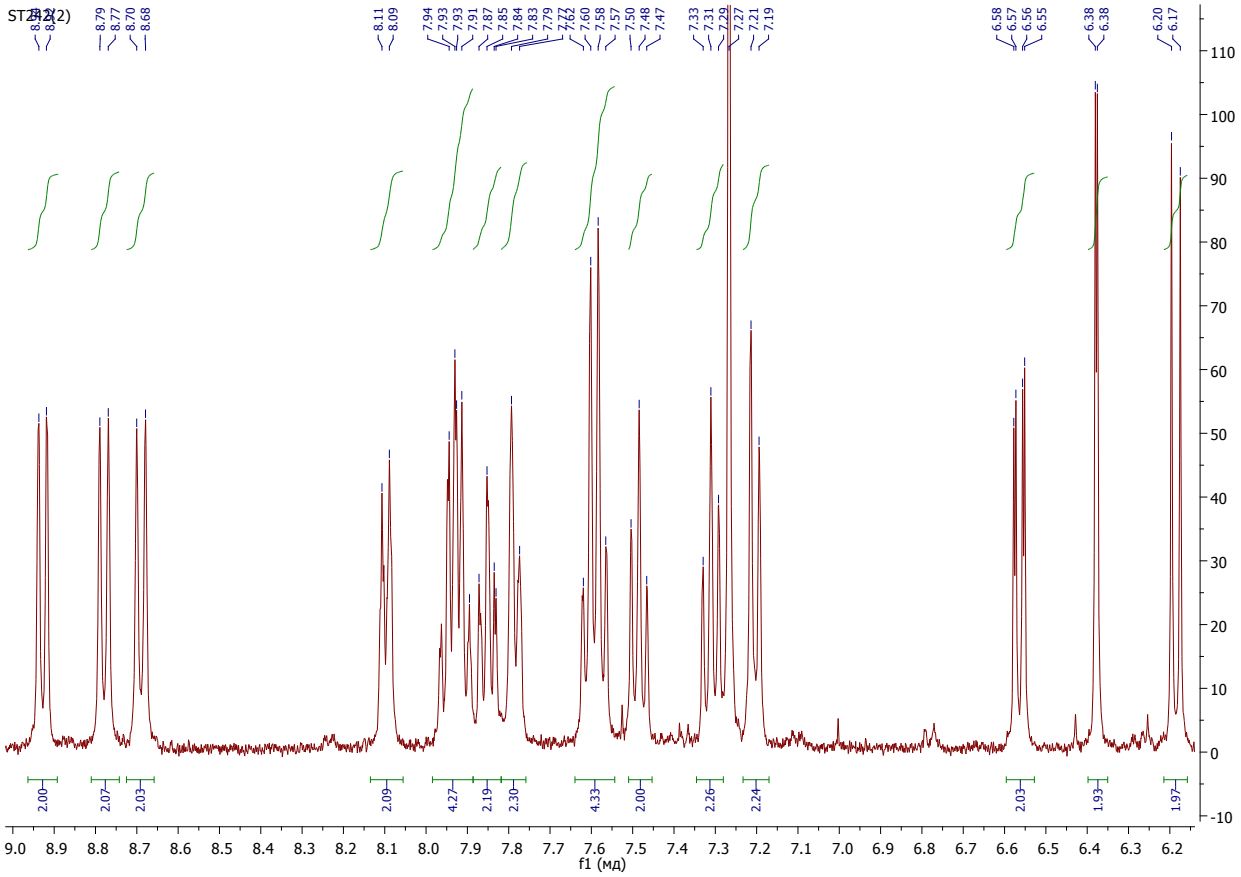

Figure S9. ^{1}H NMR spectrum of $[Ir(cphi)_2Cl]_2$ (400 MHz, 298K, $CDCl_3$).

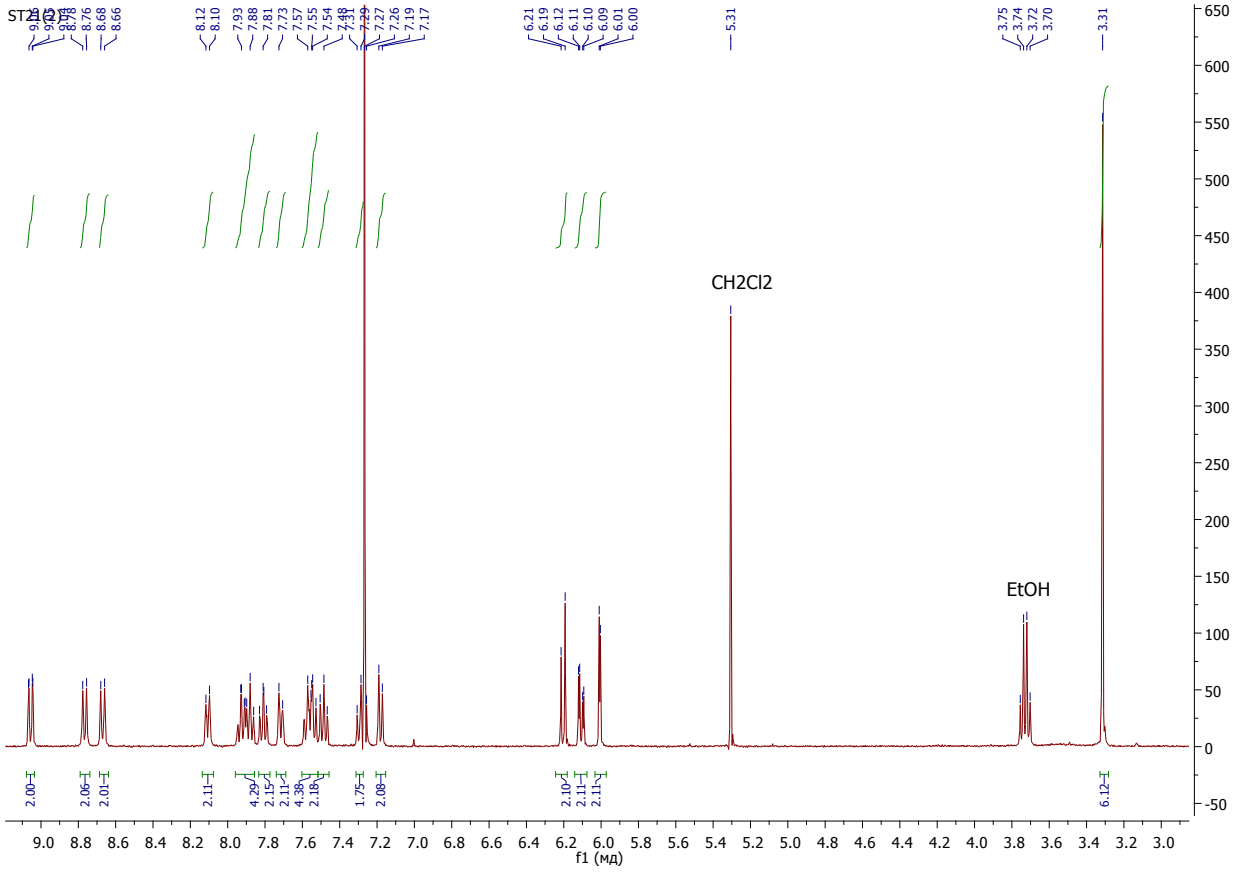

Figure S10. ^{1}H NMR spectrum of $[Ir(mphi)_2Cl]_2$ (400 MHz, 298K, $CDCl_3$).

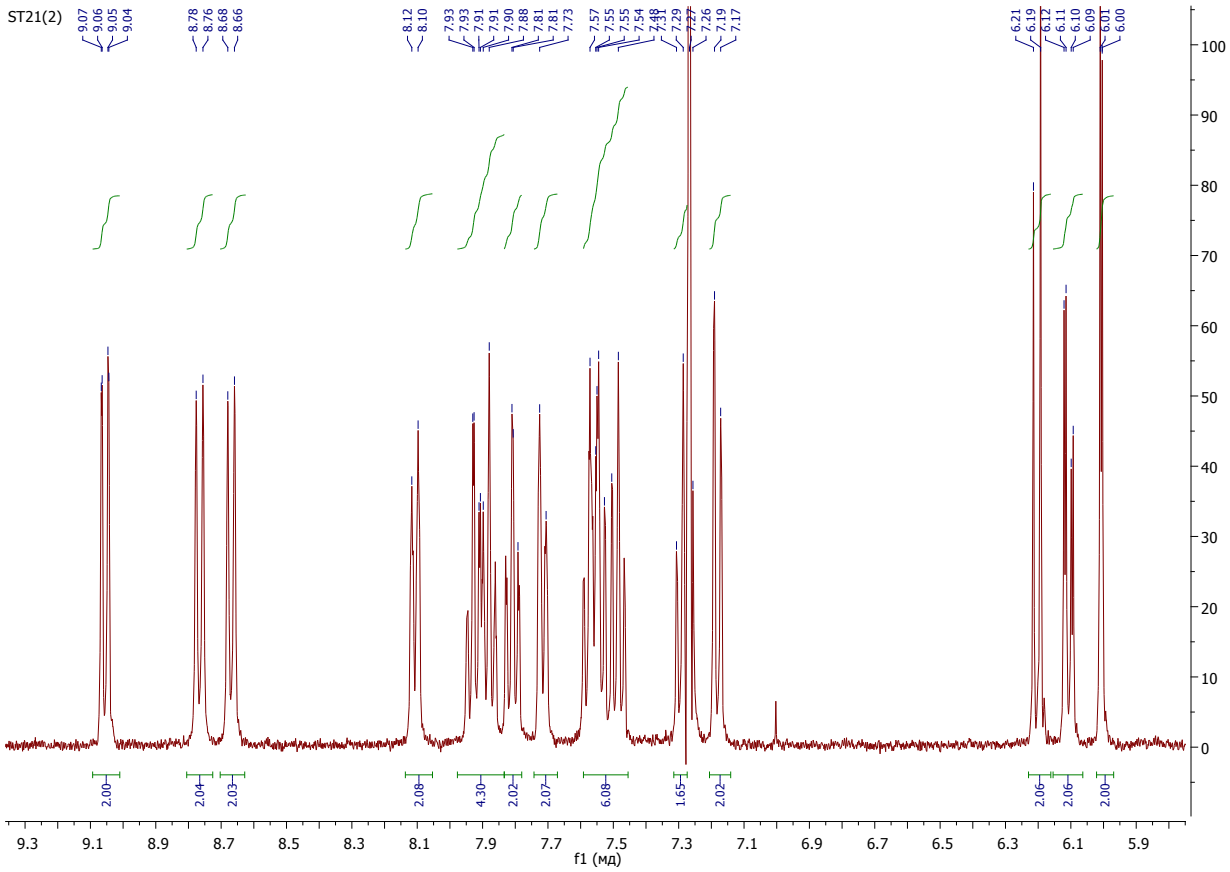

Figure S11. Aromatic region of ^{1}H NMR spectrum of $[Ir(mphi)_2Cl]_2$ (400 MHz, 298K, $CDCl_3$).

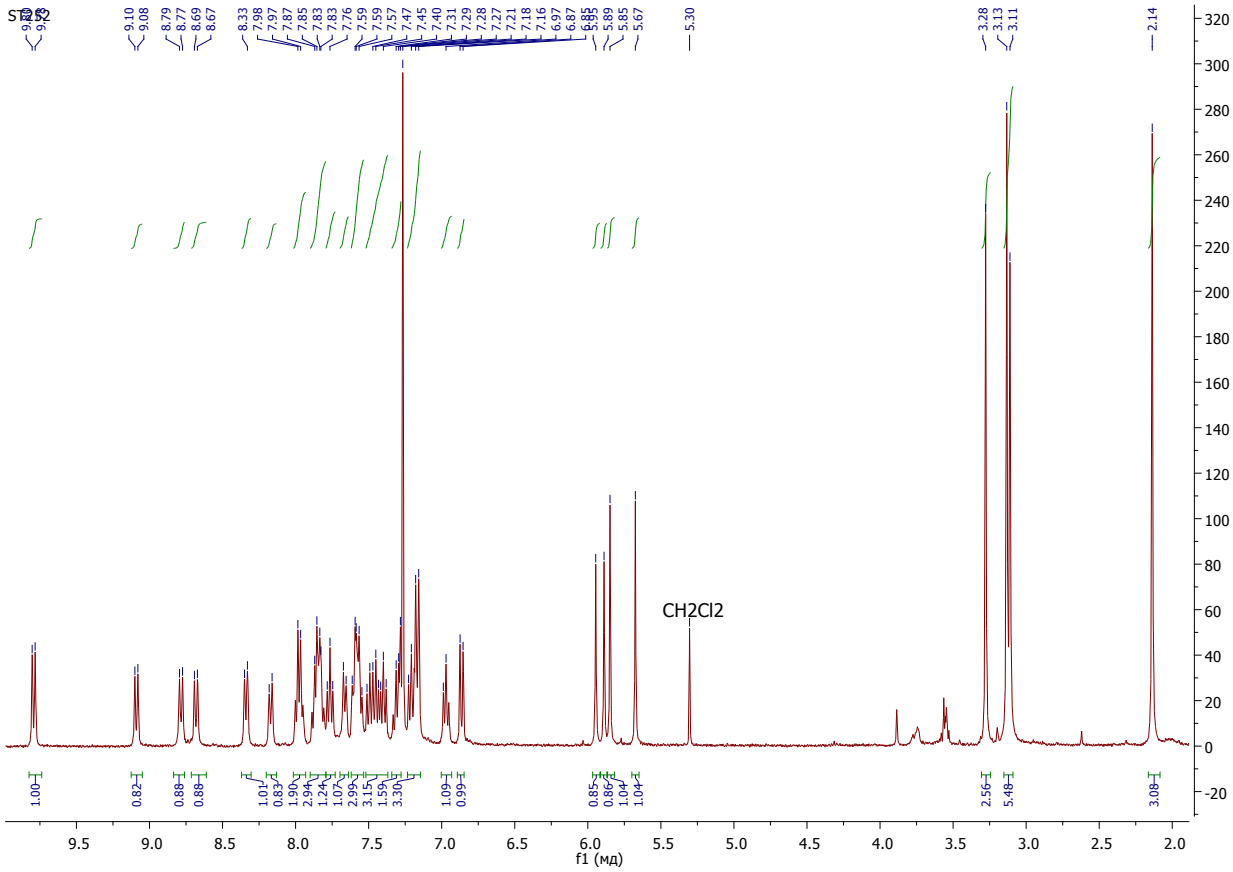

Figure S12. ^{1}H NMR spectrum of $[Ir(dmphi)_2Cl]_2$ (400 MHz, 298K, $CDCl_3$).

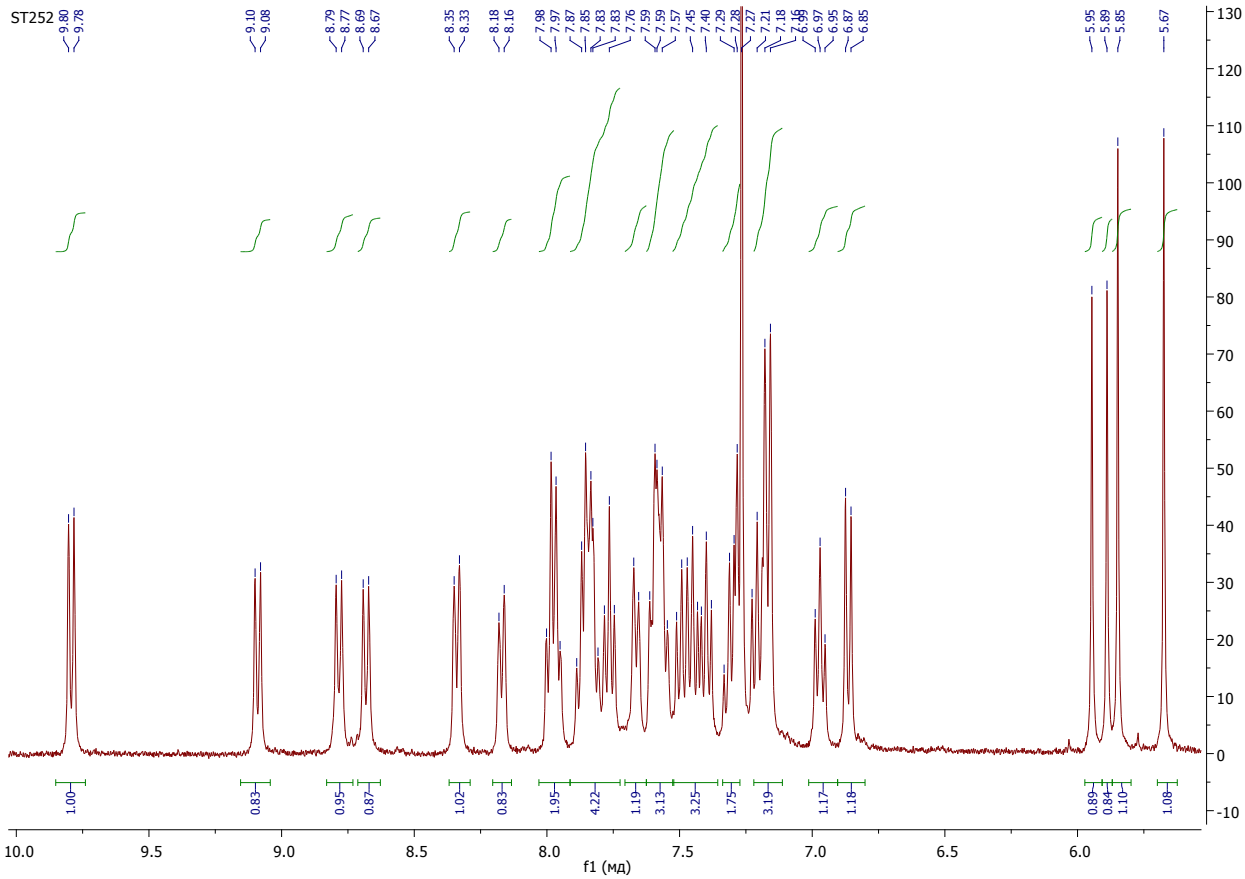

Figure S13. Aromatic region of ^{1}H NMR spectrum of $[Ir(dmphi)_2Cl]_2$ (400 MHz, 298K, $CDCl_3$).

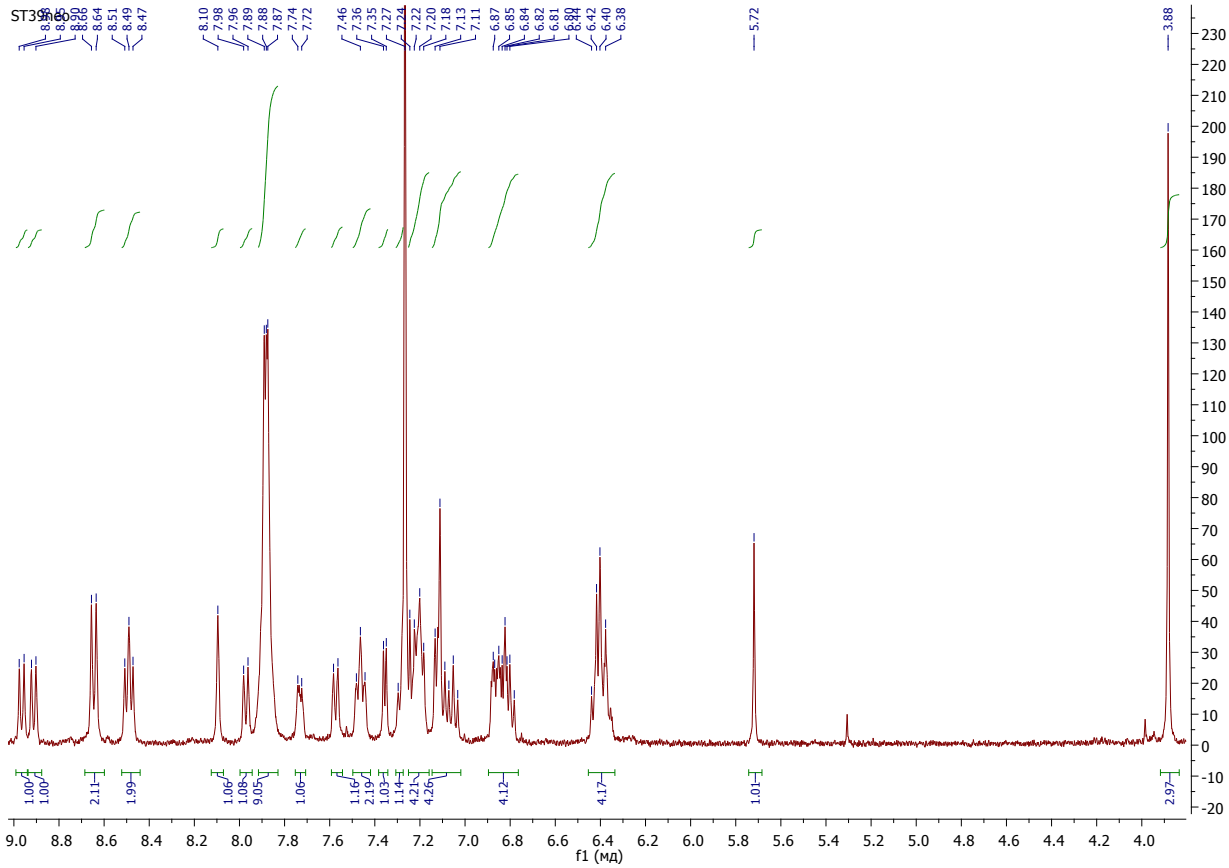

Figure S14. ^{1}H NMR spectrum of **1** (400 MHz, 298K, $CDCl_3$).

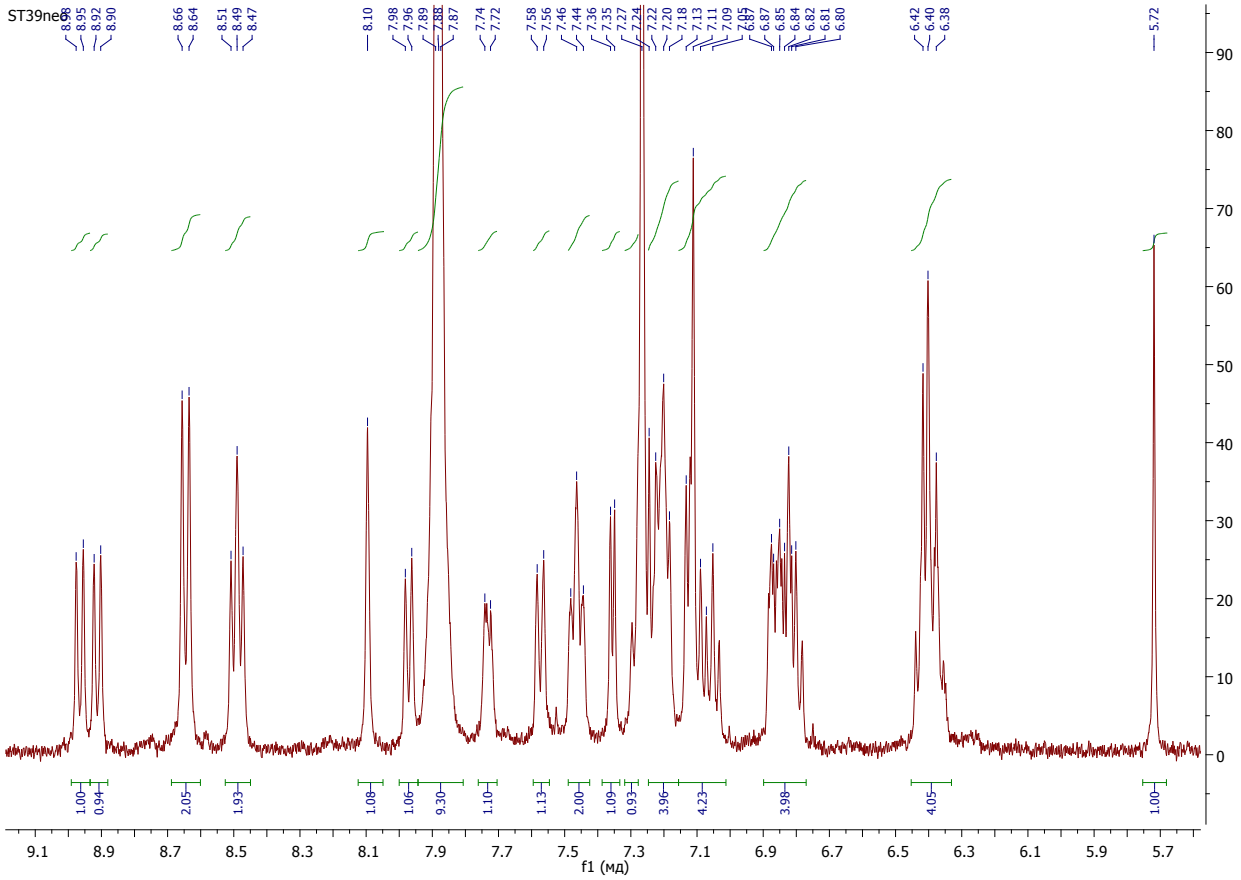

Figure S15. Aromatic region of ^{1}H NMR spectrum of **1** (400 MHz, 298K, $CDCl_3$).

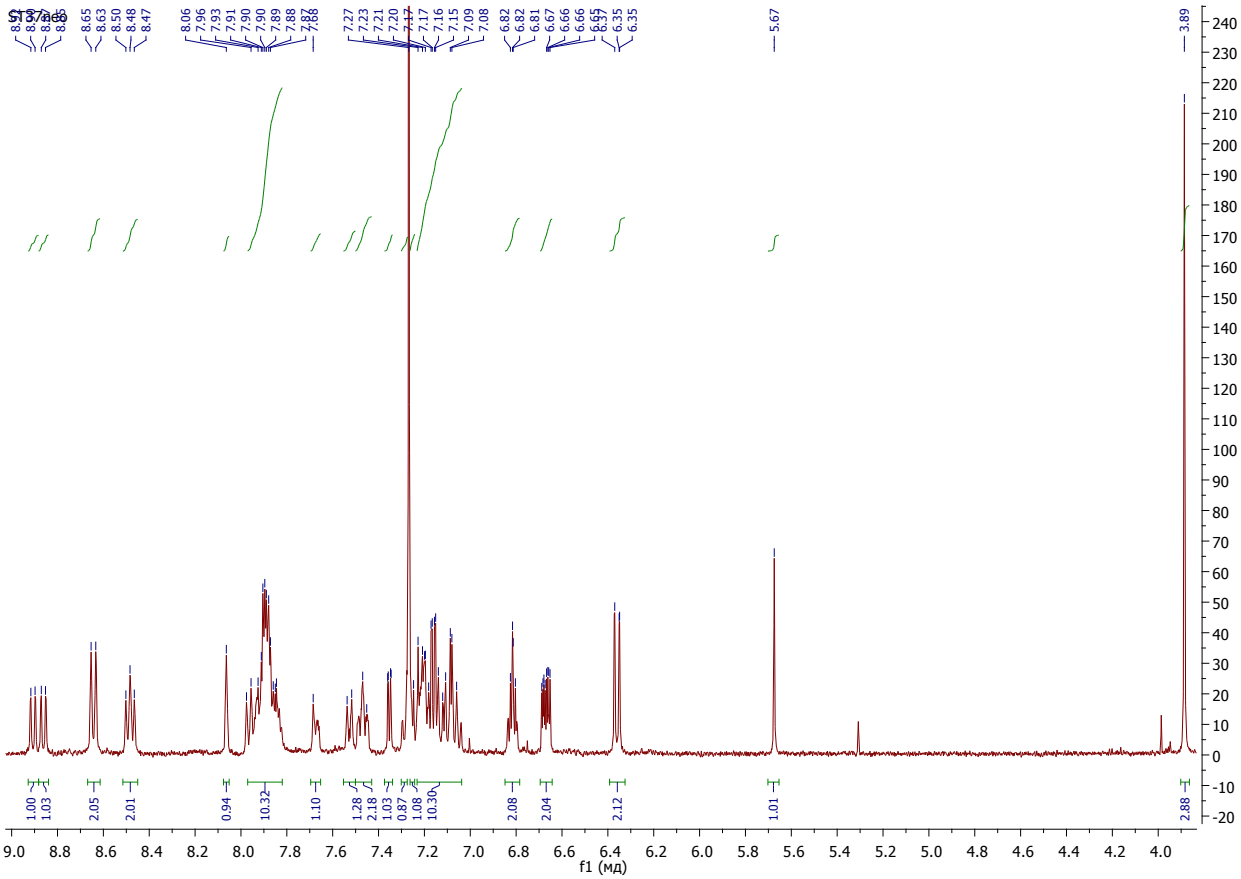

Figure S16. ^{1}H NMR spectrum of **2** (400 MHz, 298K, $CDCl_3$).

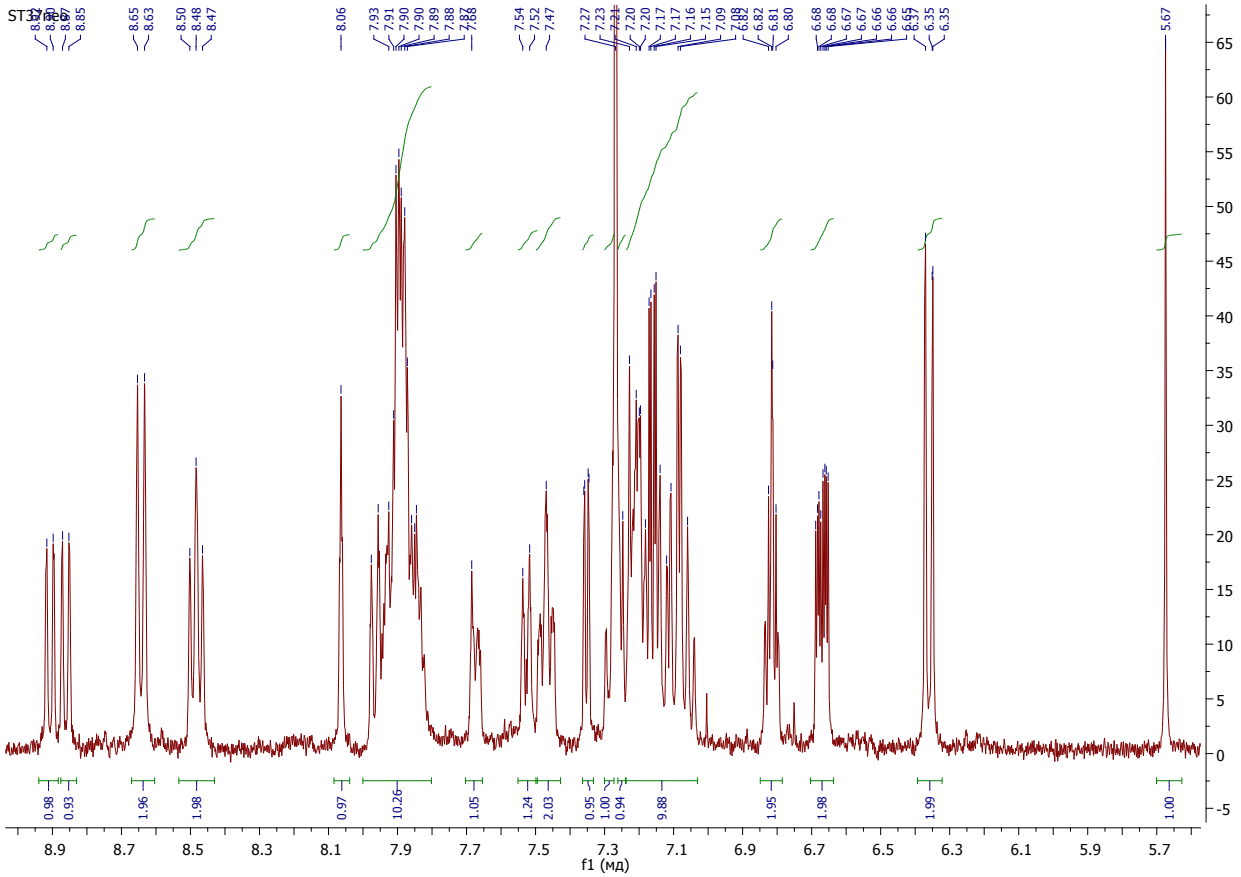

Figure S17. Aromatic region of ^{1}H NMR spectrum of **2** (400 MHz, 298K, $CDCl_3$).

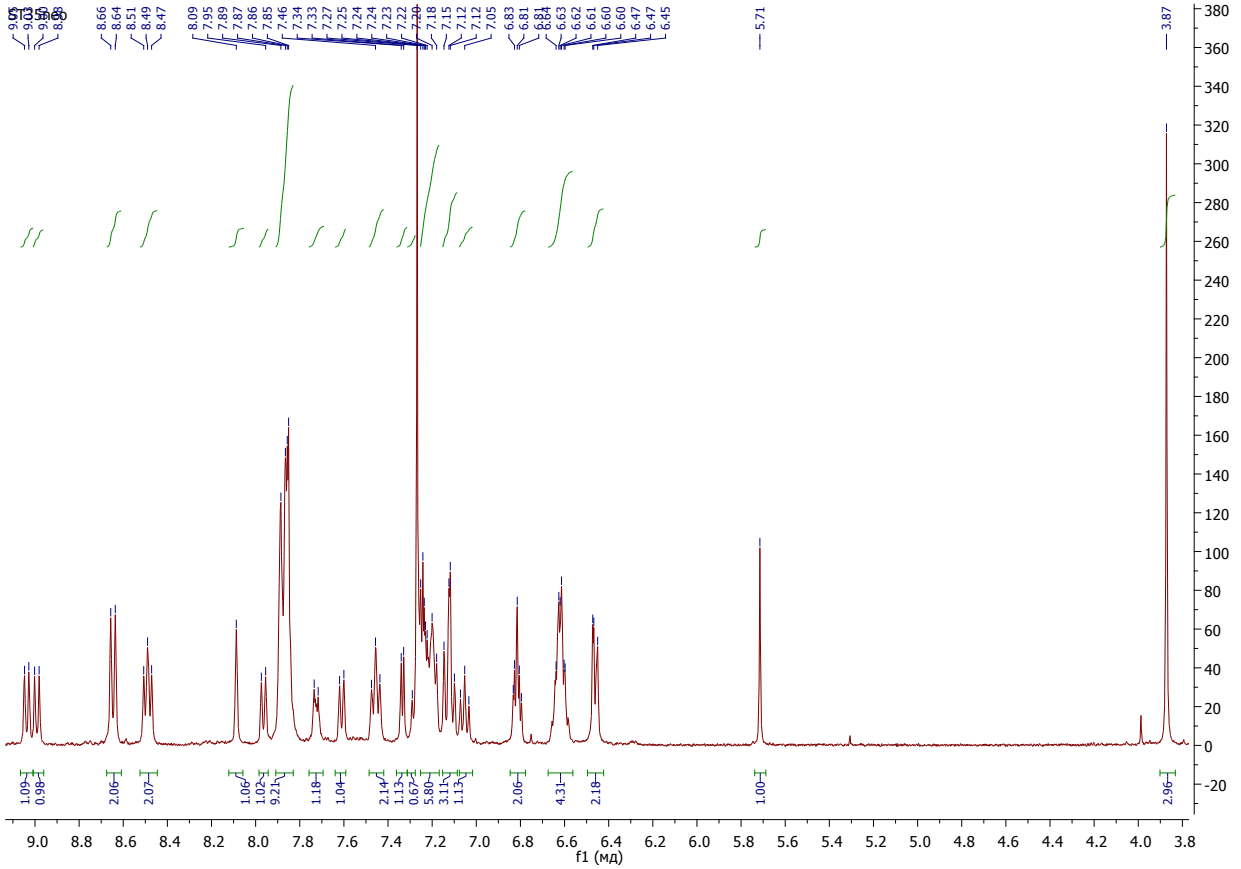

Figure S18. ^{1}H NMR spectrum of **3** (400 MHz, 298K, $CDCl_3$).

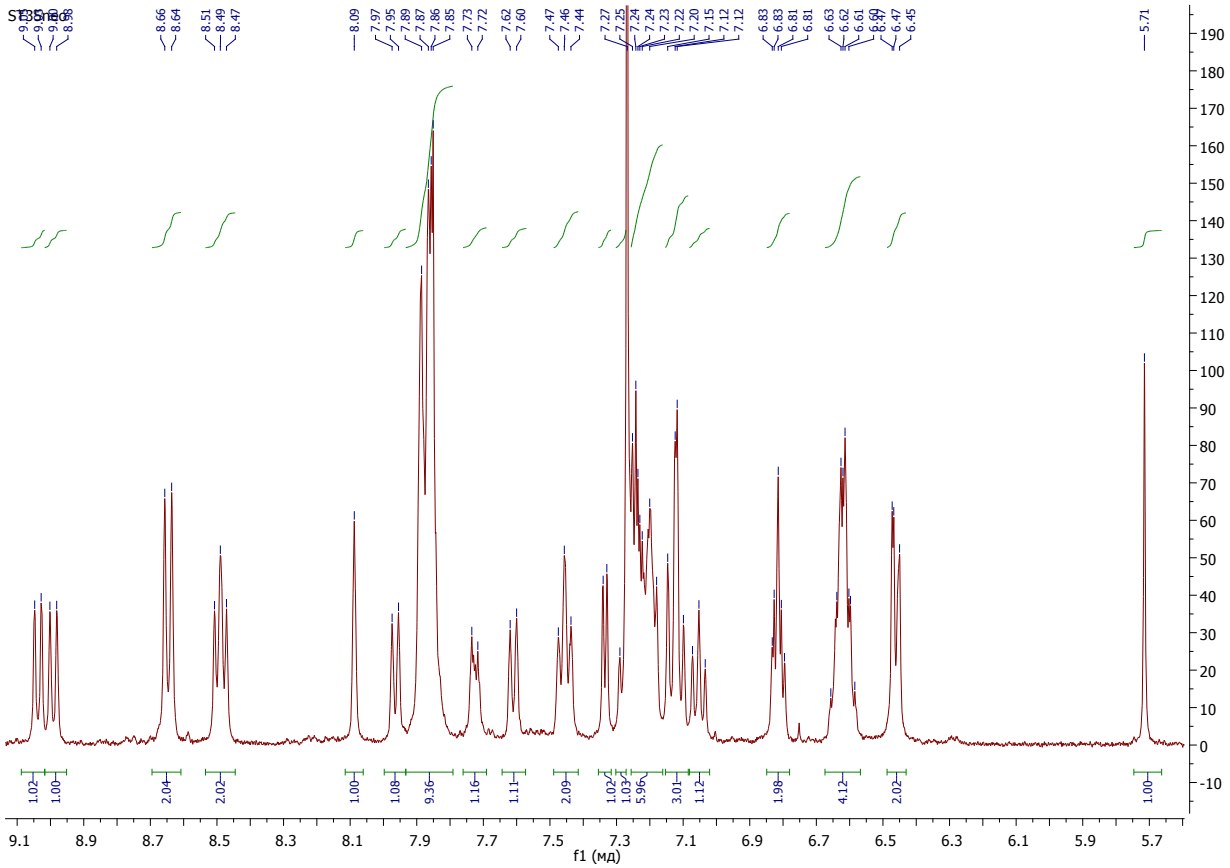

Figure S19. Aromatic region of ^{1}H NMR spectrum of **3** (400 MHz, 298K, $CDCl_3$).

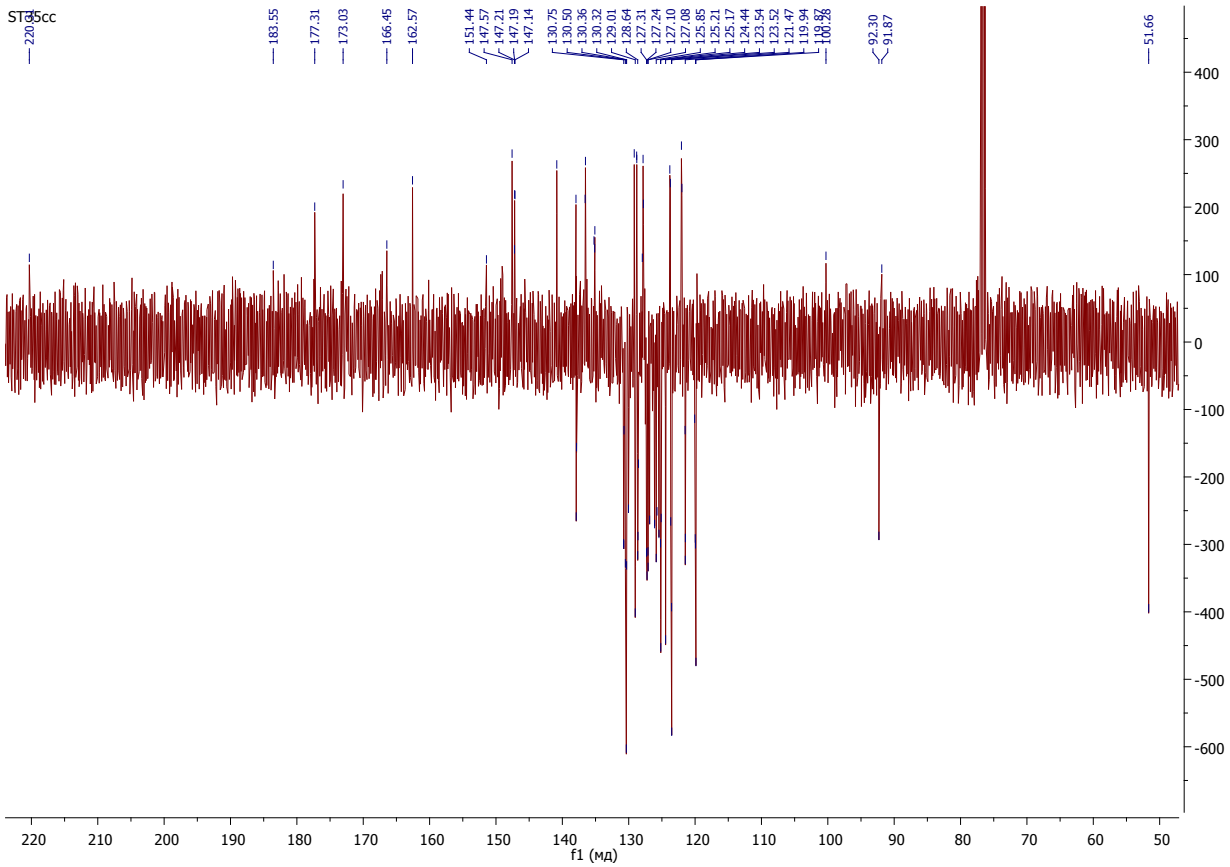

Figure S19b. ^{13}C{^{1}H} APT NMR spectrum of **3** (101 MHz, 298K, $CDCl_3$).

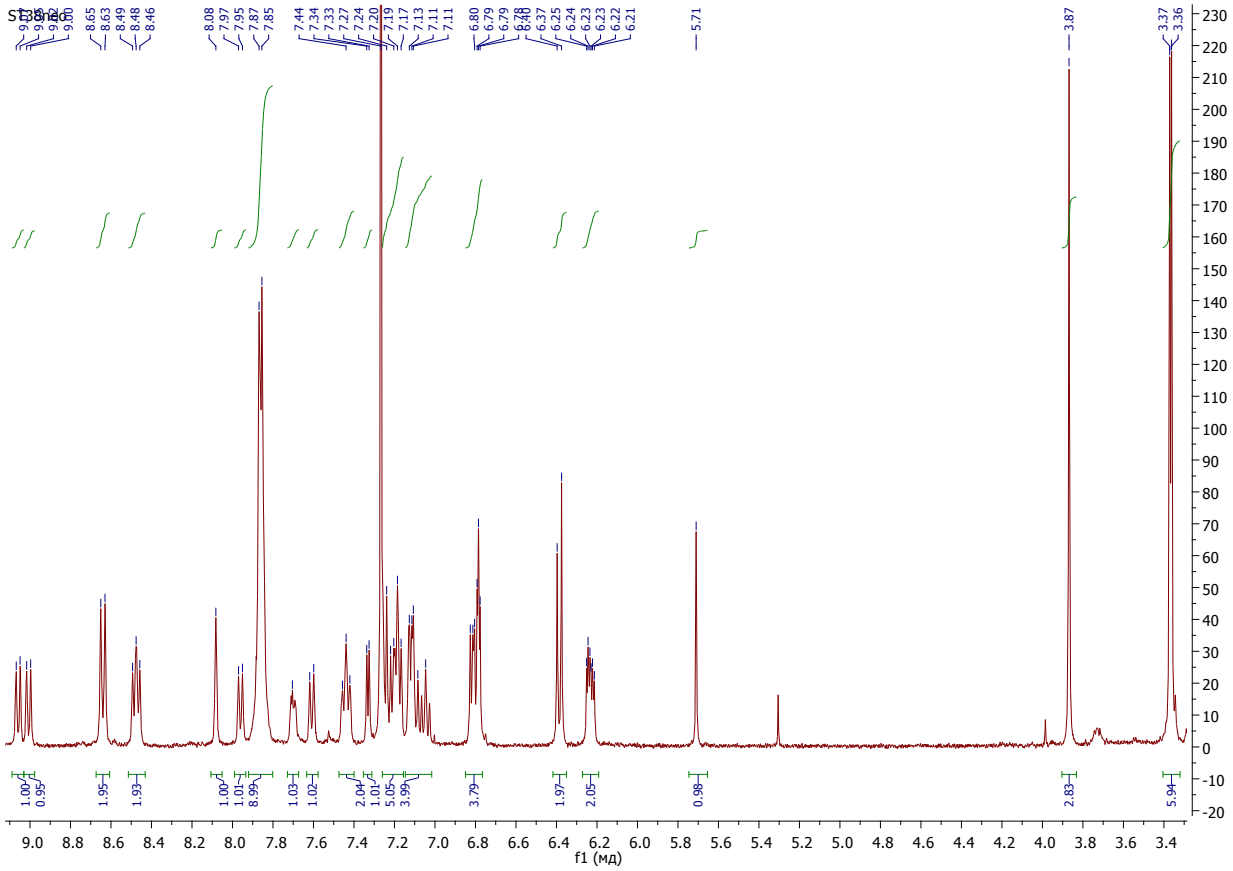

Figure S20. ^{1}H NMR spectrum of **4** (400 MHz, 298K, $CDCl_3$).

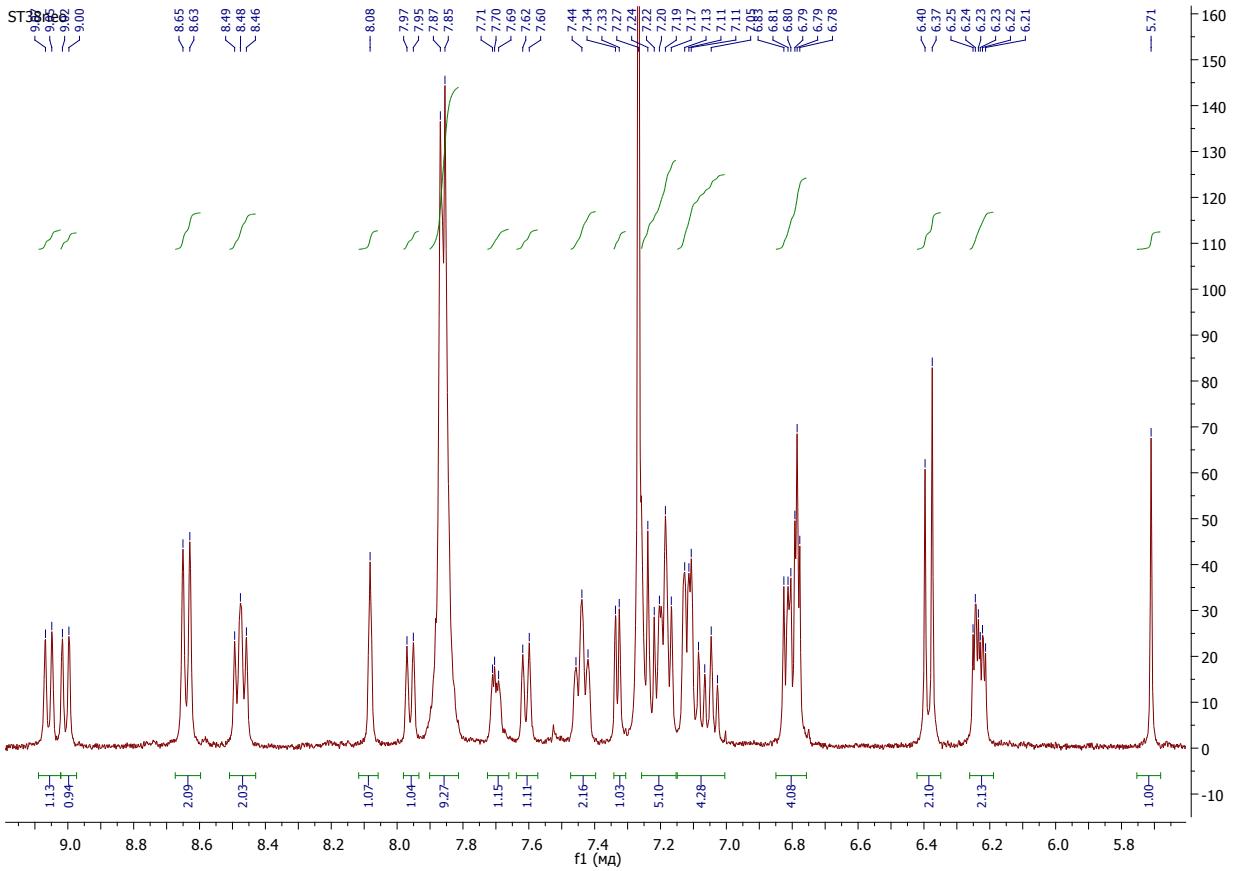

Figure S21. Aromatic region of ^{1}H NMR spectrum of **4** (400 MHz, 298K, $CDCl_3$).

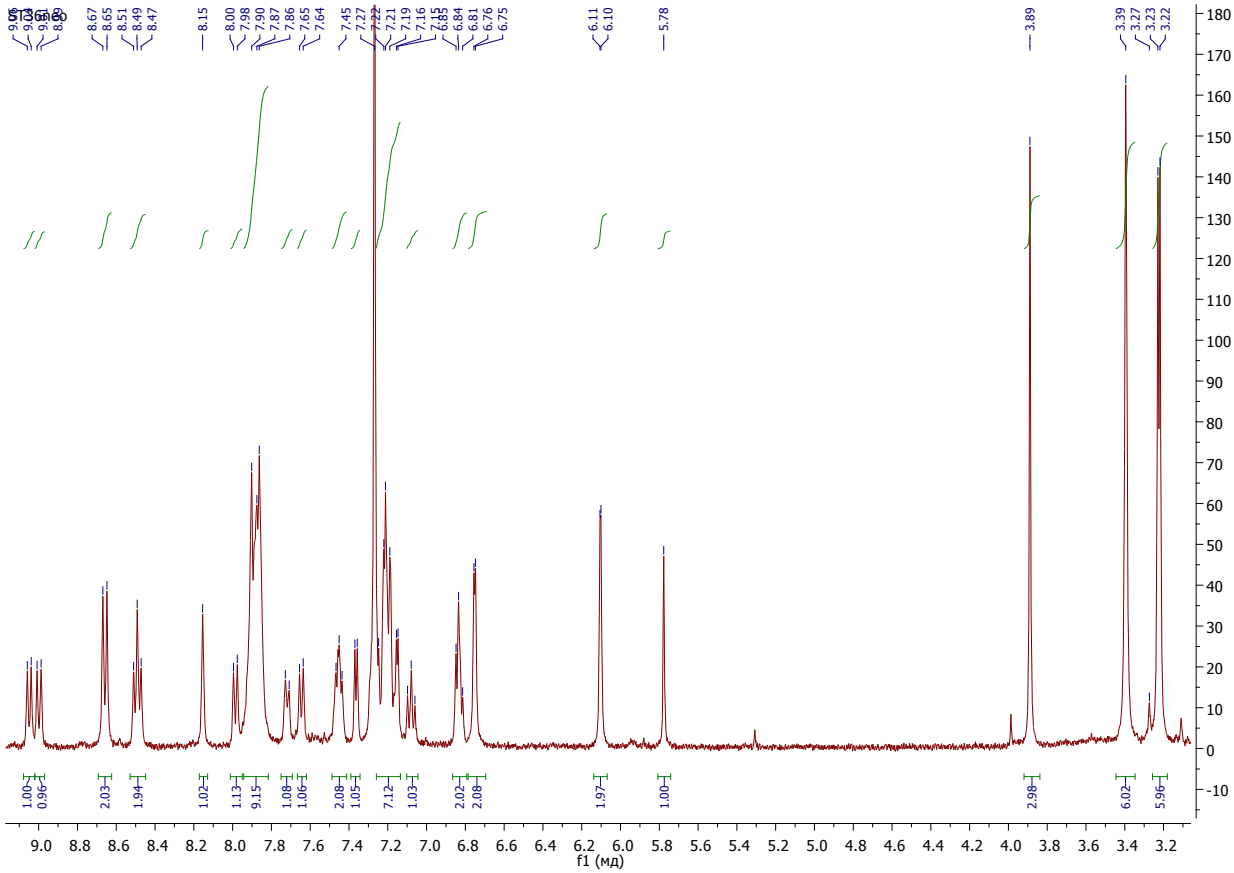

Figure S22. ^{1}H NMR spectrum of **5** (400 MHz, 298K, $CDCl_3$).

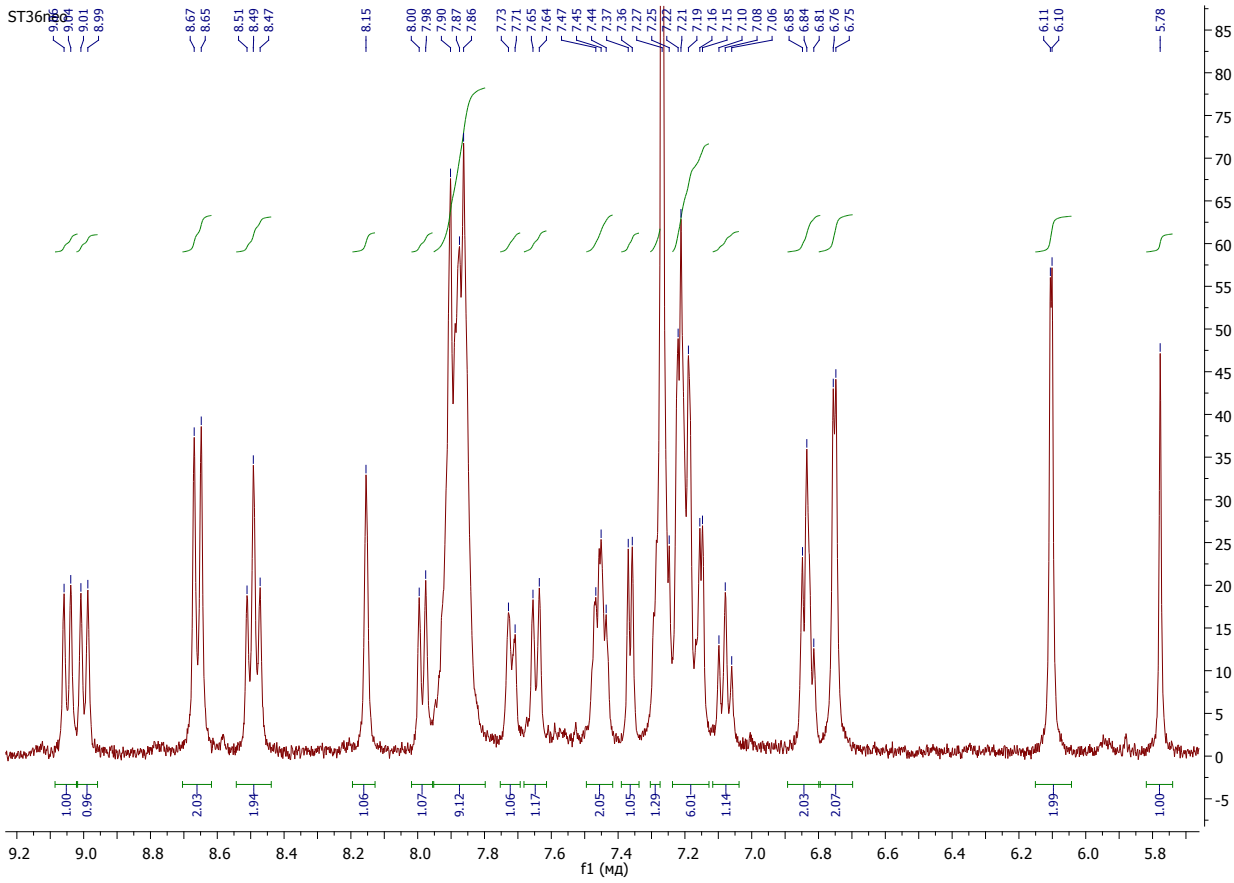

Figure S23. Aromatic region of ^{1}H NMR spectrum of **5** (400 MHz, 298K, $CDCl_3$).

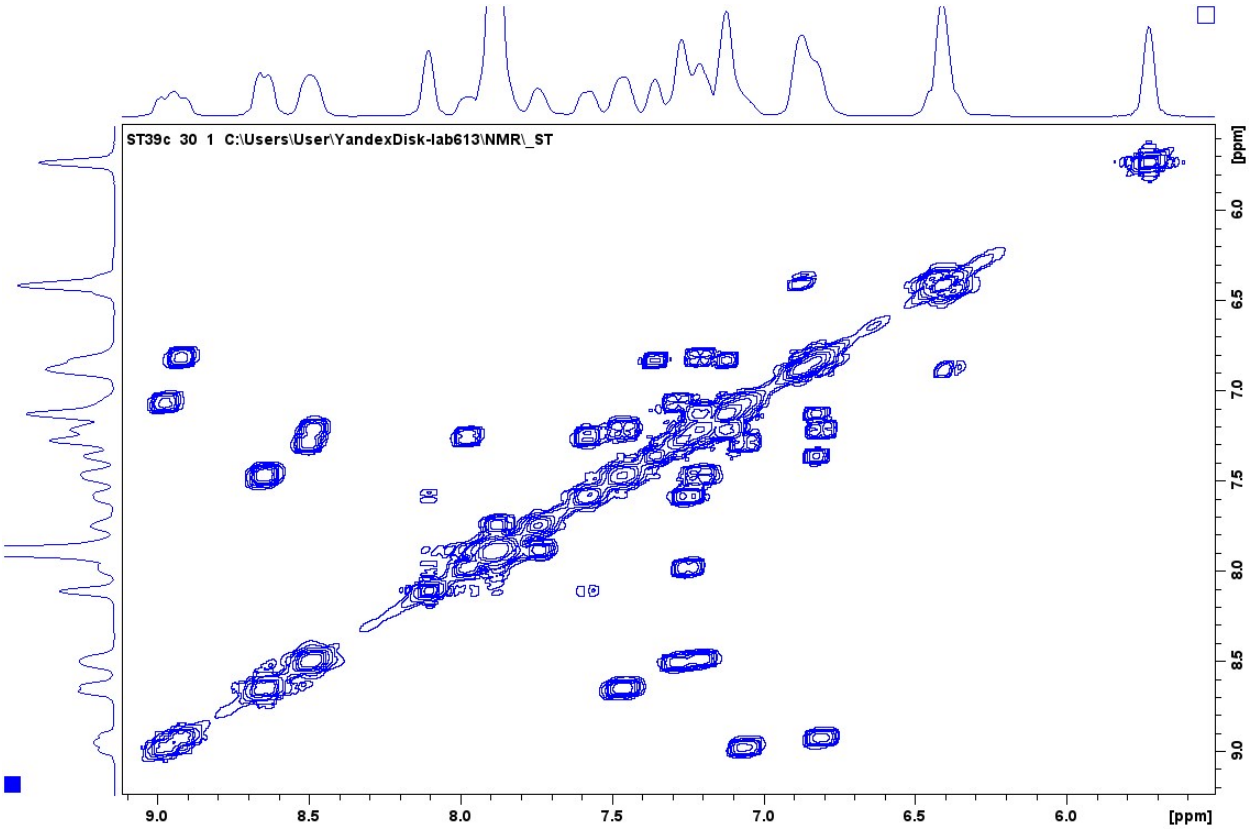

Figure S24. Aromatic region of COSY ^{1}H, ^{1}H NMR spectrum of **1**

Assignment:

8.97 (d, *J*=7.9 Hz, 1 H)	**q'/q**
8.91 (d, *J*=7.9 Hz, 1 H)	**q/q'**
8.65 (d, *J*=8.4 Hz, 2 H)	**m, m'**
8.52 – 8.45 (m, 2 H)	**n, n'**
8.12 – 8.08 (m, 1 H)	**r**
7.97 (d, *J*=7.7 Hz, 1 H)	**u/s**
7.93 – 7.81 (m, 9 H); 7.76 – 7.71 (m, 1 H)	
residual signals	
7.57 (d, *J*=7.9 Hz, 1 H)	**s/u**
7.50 – 7.43 (m, 2H)	**l, l'**
7.36 (d, *J*=4.9 Hz, 1 H)	**y/w**
7.30 – 7.27 (m, 1H)	**o'/o**
7.25 – 7.17 (m, 4 H)	**k, k'; o/o'; t**
7.15 – 7.03 (m, 4 H)	**p'/p; w/y; j, j'**
6.89 – 6.78 (m, 4H)	**(c, c')/(d, d'); p/p'; x**
6.46 – 6.34 (m, 4H)	**a, a'; (d, d')/(c, c')**
5.72 (s, 1 H)	**v**
3.88 (s, 3 H)	**COO*CH₃***

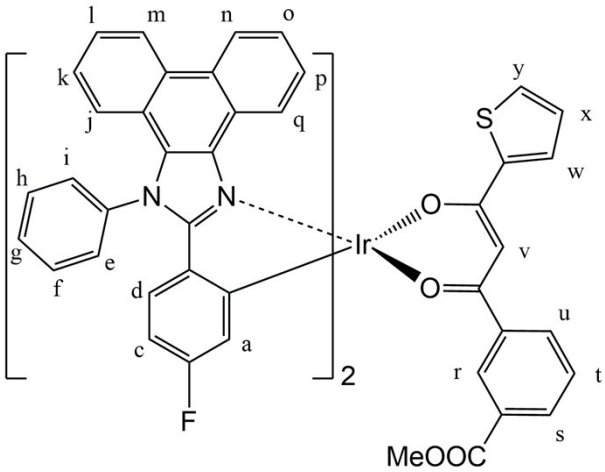

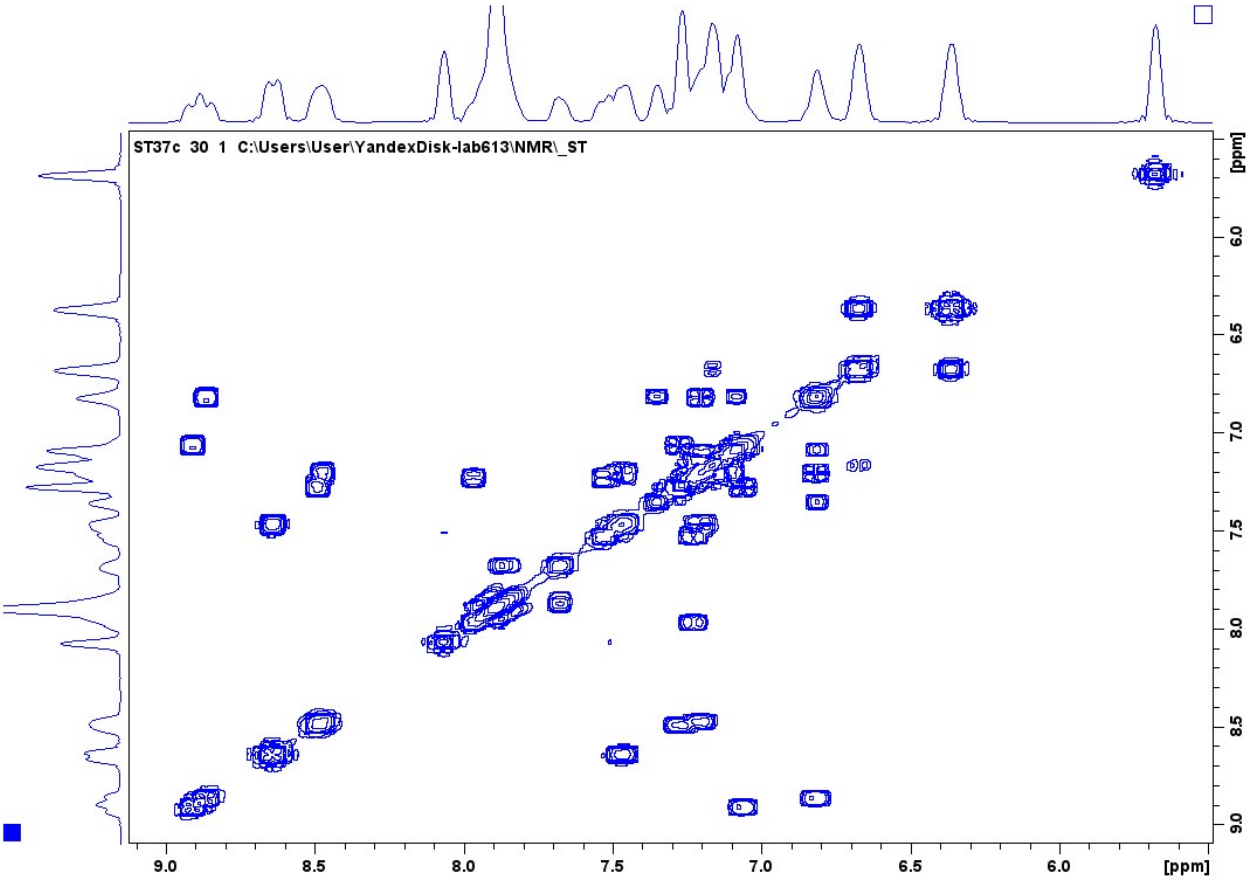

Figure S25. Aromatic region of COSY ^{1}H, ^{1}H NMR spectrum of **2**

Assignment:

8.91 (d, *J*=7.4 Hz, 1 H) **q'/q**
8.86 (d, *J*=7.4 Hz, 1 H) **q/q'**
8.64 (d, *J*=8.2 Hz, 2 H) **m, m'**
8.52 – 8.44 (m, 2 H) **n, n'**
8.08 – 8.05 (m, 1 H) **r**
7.96 (d, *J*=7.7 Hz, 1 H) **u/s**
8.00 – 7.80 (m, 10 H); 7.70 – 7.65 (m, 1 H)
11 residual signals
7.55 – 7.50 (m, 1 H) **s/u**
7.50 – 7.44 (m, 2 H) **l, l'**
7.35 (dd, *J*=5.0, 1.0 Hz, 1 H) **w/y**
7.30 – 7.27 (m, 1H) **o/o'**
7.26 – 7.04 (m, 10H) **t; o'/o; k, k'; j, j'; a, a'; y/w; p'/p**
6.86 – 6.77 (m, 2H) **x, p/p'**
6.67 (ddd, J = 8.5, 3.8, 2.2 Hz, 2H) **c, c'**
6.39 – 6.32 (m, 2H) **d, d'**
5.67 (s, 1 H) **v**
3.89 (s, 3 H) **COO*CH₃***

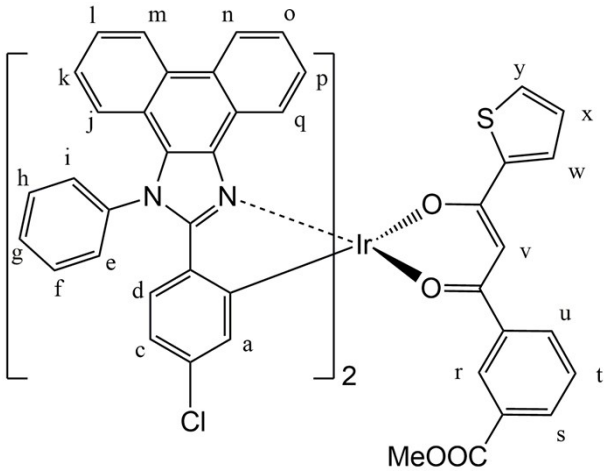

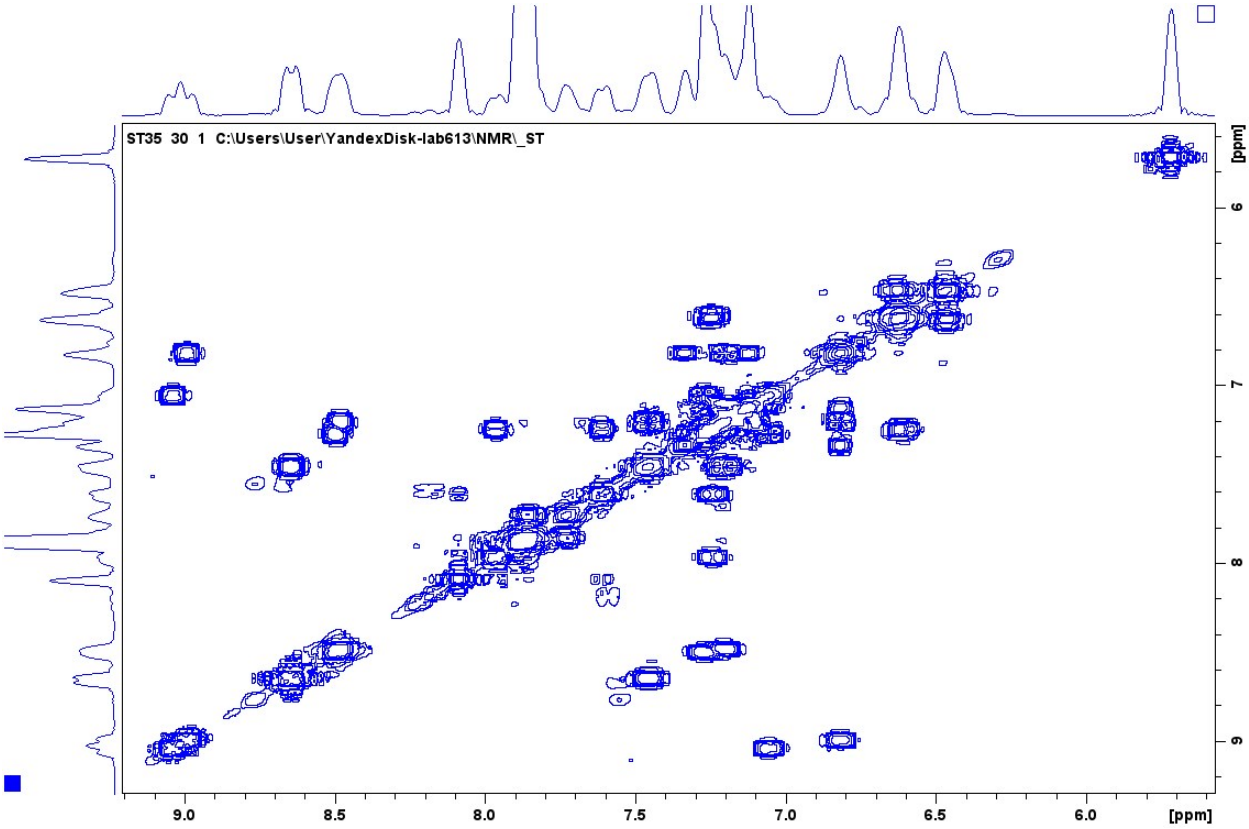

Figure S26. Aromatic region of COSY ^{1}H, ^{1}H NMR spectrum of **3**

Assignment:

9.04 (d, *J*=7.8 Hz, 1 H)	**q'/q**
8.99 (d, *J*=8.1 Hz, 1 H)	**q/q'**
8.65 (d, *J*=8.3 Hz, 2 H)	**m, m'**
8.54 – 8.42 (m, 2 H)	**n, n'**
8.10 – 8.07 (m, 1 H)	**r**
7.96 (d, *J*=7.7 Hz, 1 H)	**u/s**
7.92 – 7.81 (m, 9 H); 7.75 – 7.70 (m, 1 H)	
10 residual signals	
7.61 (d, *J*=7.7 Hz, 1 H)	**s/u**
7.49 – 7.42 (m, 2 H)	**l, l'**
7.33 (d, *J*=4.4 Hz, 1 H)	**w/y**
7.30 – 7.17 (m, 7H)	**c, c'; o, o'; k, k'; t**
7.16 – 7.09 (m, 3H)	**j, j'; y/w**
7.05 (t, *J*=7.7 Hz, 1 H)	**p'/p**
6.87 – 6.76 (m, 2H)	**x, p/p'**
6.68 – 6.53 (m, 4H)	**b, b'; d, d'**
6.50 – 6.41 (m, 2H)	**a, a'**
5.71 (s, 1 H)	**v**
3.87 (s, 3 H)	**COO*CH₃***

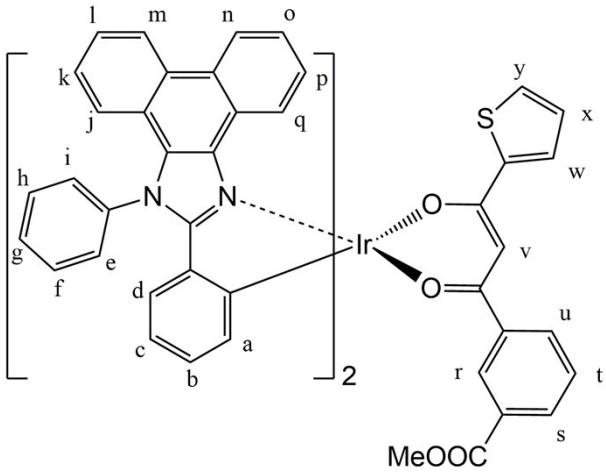

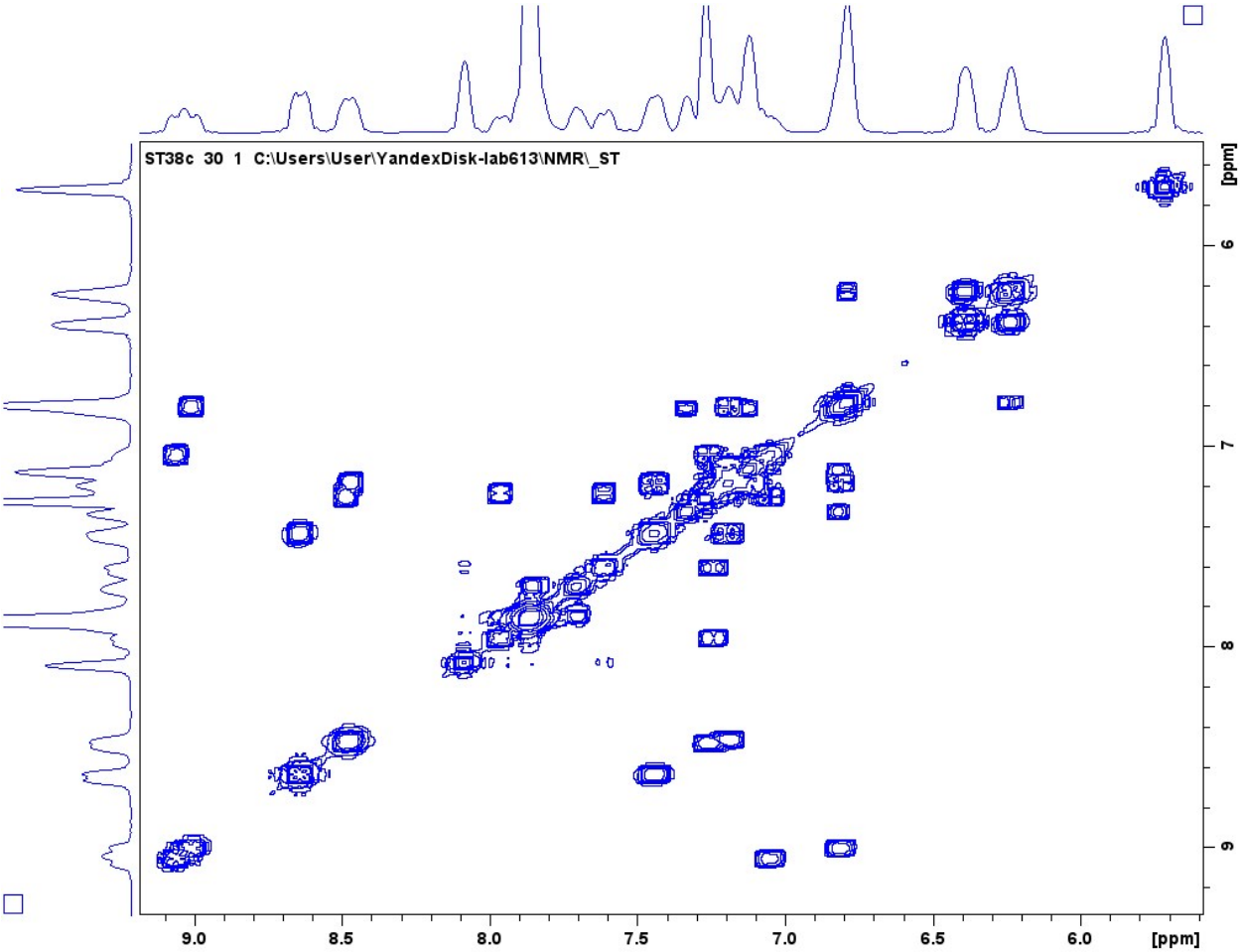

Figure S27. Aromatic region of COSY ^{1}H, ^{1}H NMR spectrum of **4**

Assignment:

9.06 (d, *J*=7.6 Hz, 1 H)	**q'/q**
9.01 (d, *J*=8.1 Hz, 1 H)	**q/q'**
8.64 (d, *J*=8.3 Hz, 2 H)	**m, m'**
8.51 – 8.43 (m, 2 H)	**n, n'**
8.10 – 8.07 (m, 1 H)	**r**
7.96 (d, *J*=7.7 Hz, 1 H)	**u/s**
7.90 – 7.81 (m, 9 H); 7.73 – 7.67 (m, 1 H)	
10 residual signals	
7.61 (d, *J*=7.7 Hz, 1 H)	**s/u**
7.47 – 7.40 (m, 2 H)	**l, l'**
7.33 (d, *J*=4.6 Hz, 1 H)	**w/y**
7.25 – 7.14 (m, 5H); 7.13 – 7.00 (m, 4H);	
j, j'; o, o'; k, k'; t; y/w; p'/p	
6.84 – 6.76 (m, 4H)	**x; p/p'; a, a'**
6.39 (d, *J* = 8.7 Hz, 2H)	**d, d'**
6.26 – 6.20 (m, 2H)	**b, b'**
5.71 (s, 1 H)	**v**
3.87 (s, 3 H)	**COO*CH₃***
3.39-3.33 (m, 6H).	O*CH₃*, (O*CH₃*)'

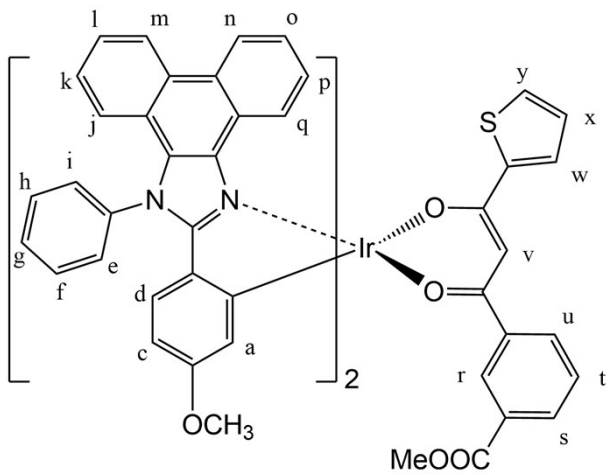

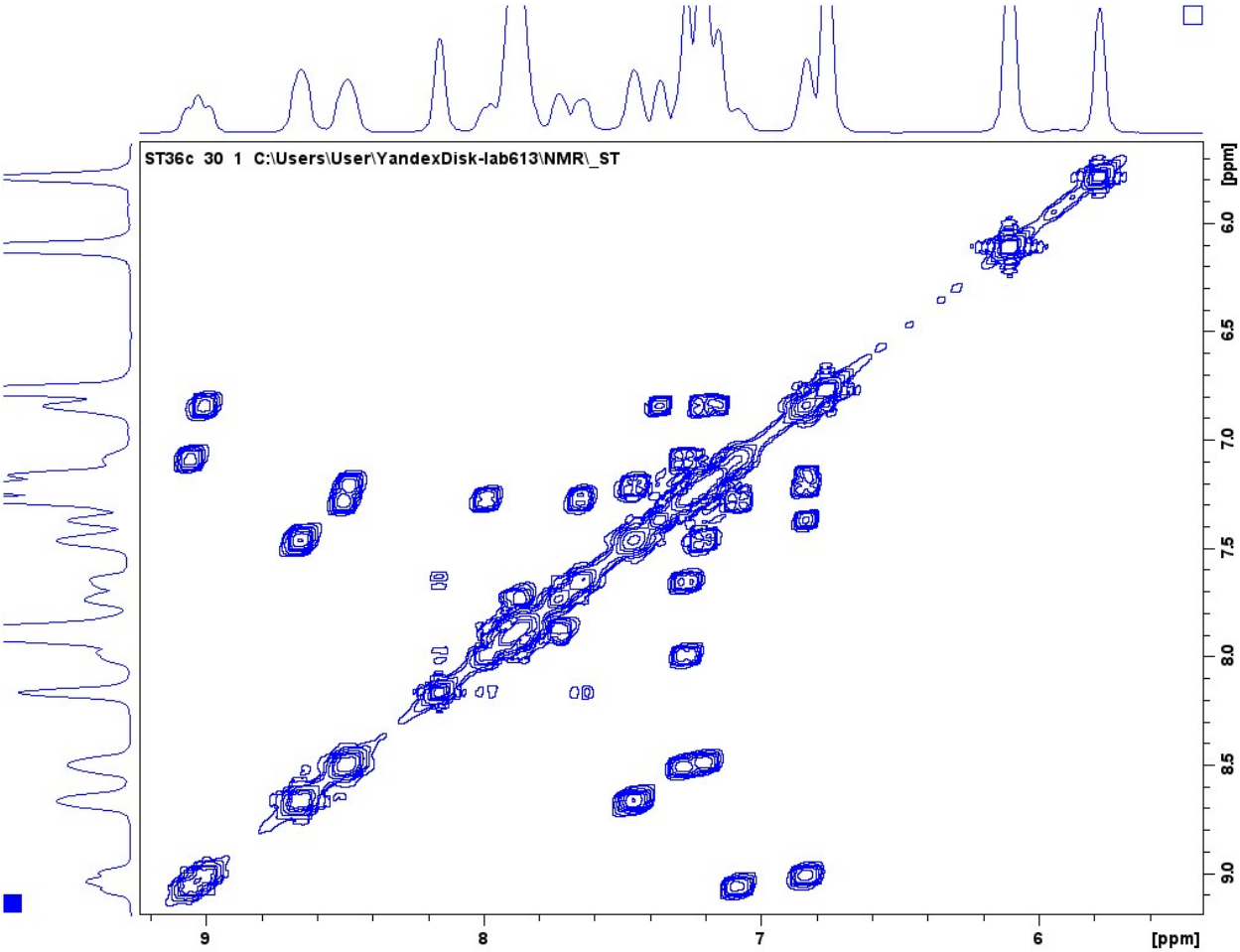

Figure S28. Aromatic region of COSY ^{1}H, ^{1}H NMR spectrum of **5**

Assignment:

9.05 (d, *J*=8.0 Hz, 1 H)	**q'/q**
9.00 (d, *J*=8.3 Hz, 1 H)	**q/q'**
8.66 (d, *J*=8.4 Hz, 2 H)	**m, m'**
8.49 (t, *J*=7.9 Hz, 2 H)	**n, n'**
8.17 – 8.14 (m, 1 H)	**r**
7.99 (d, *J*=7.8 Hz, 1 H)	**u/s**
7.94 – 7.81 (m, 9 H); 7.75 – 7.69 (m, 1 H) 10 residual signals	
7.65 (d, *J*=7.6 Hz, 1 H)	**s/u**
7.48 – 7.42 (m, 2 H)	**l, l'**
7.36 (d, *J*=4.8 Hz, 1 H)	**w/y**
7.29 – 7.27 (m, 1H); 7.26 – 7.14 (m, 7H); **j, j'; o, o'; k, k'; t; y/w**	
7.08 (t, *J*=7.6 Hz, 1 H)	**p'/p**
6.86 – 6.80 (m, 2H)	**x; p/p'**
6.77 – 6.73 (m, 2H)	**(d, d')/(a, a')**
6.12 – 6.09 (m, 2H)	**(a, a')/(d, d')**
5.71 (s, 1 H)	**v**
3.89 (s, 3 H)	**COO*CH₃***
3.39 (s, 6H).	$(OCH_3, OCH_3')_b/((OCH_3, OCH_3')_c$
3.26 – 3.19 (m, 6H).	$(OCH_3, OCH_3')_c/((OCH_3, OCH_3')_b$

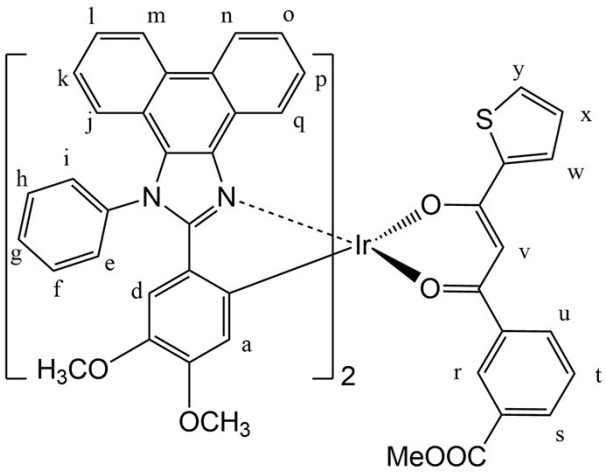

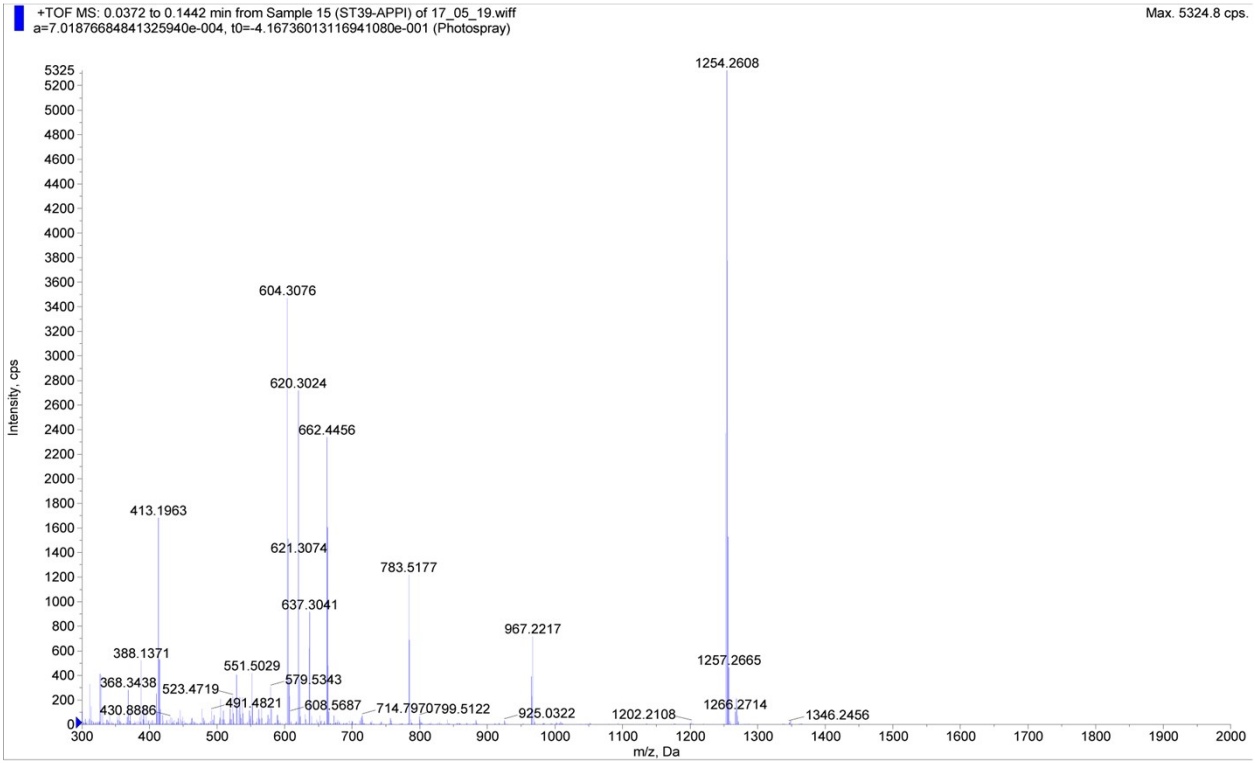

Figure S29. High resolution mass spectrum of **1**.

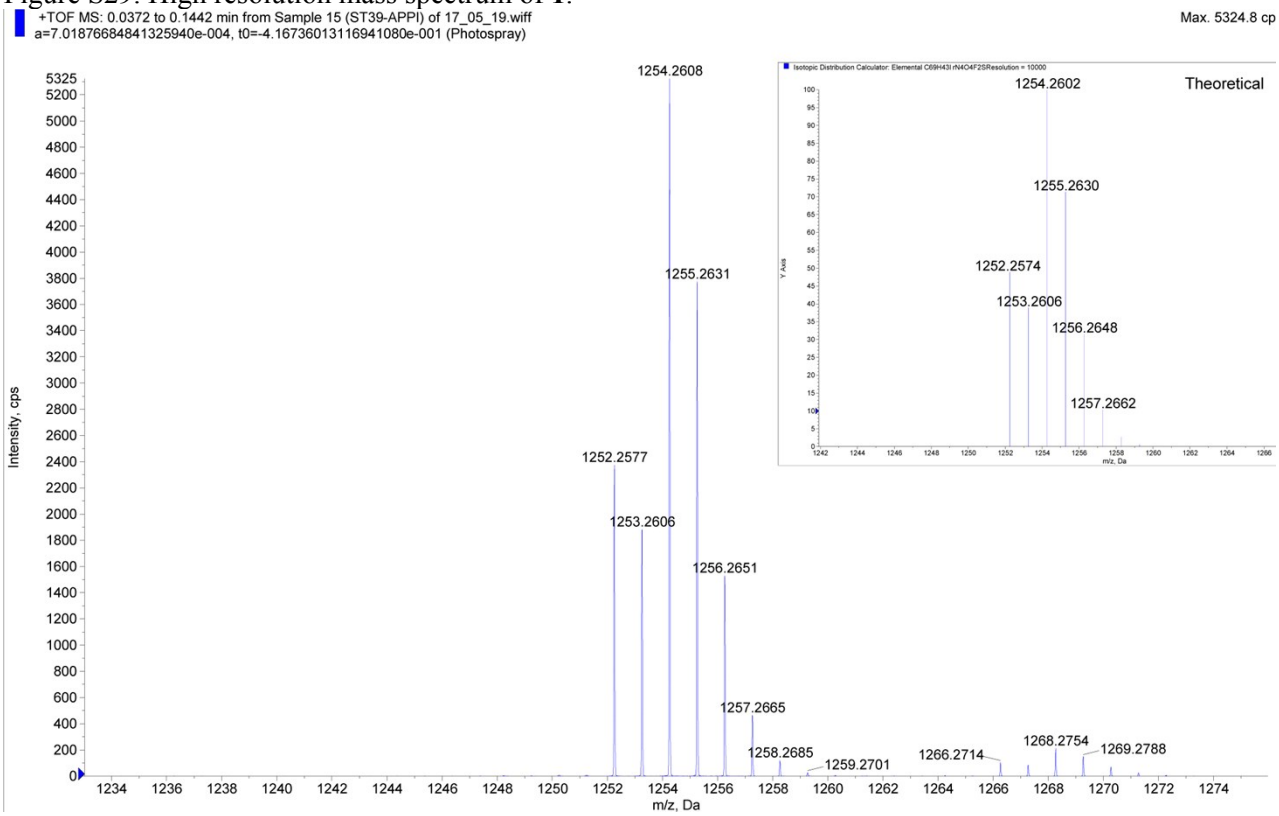

Figure S30. High resolution mass spectrum of **1**.

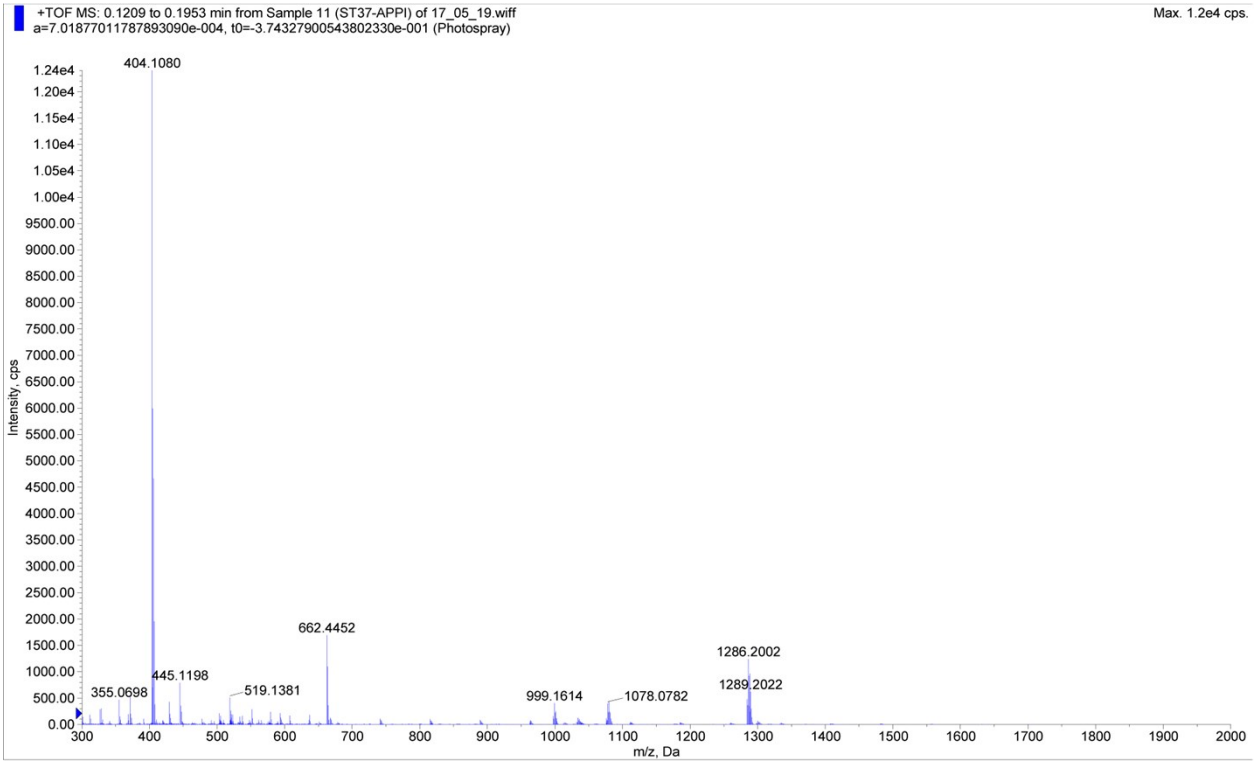

Figure S31. High resolution mass spectrum of **2**.

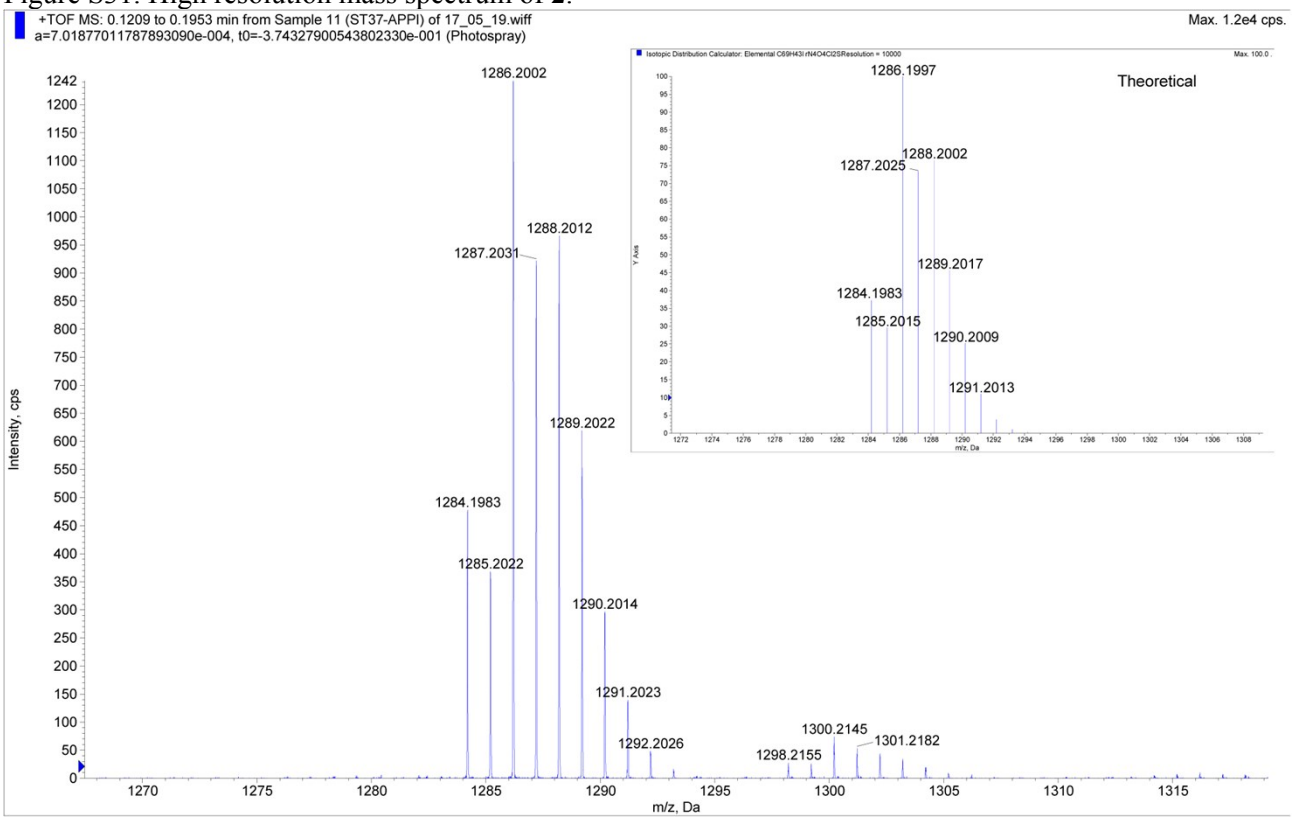

Figure S32. High resolution mass spectrum of **2**.

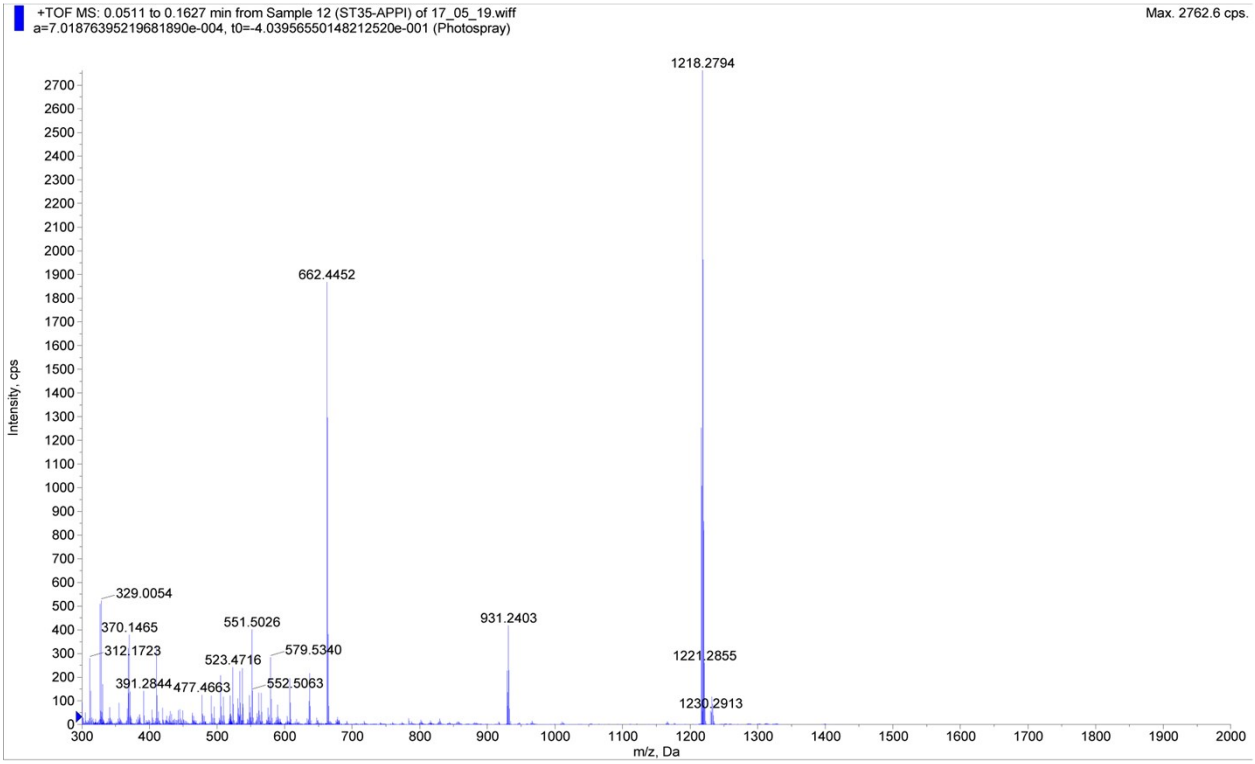

Figure S33. High resolution mass spectrum of **3**.

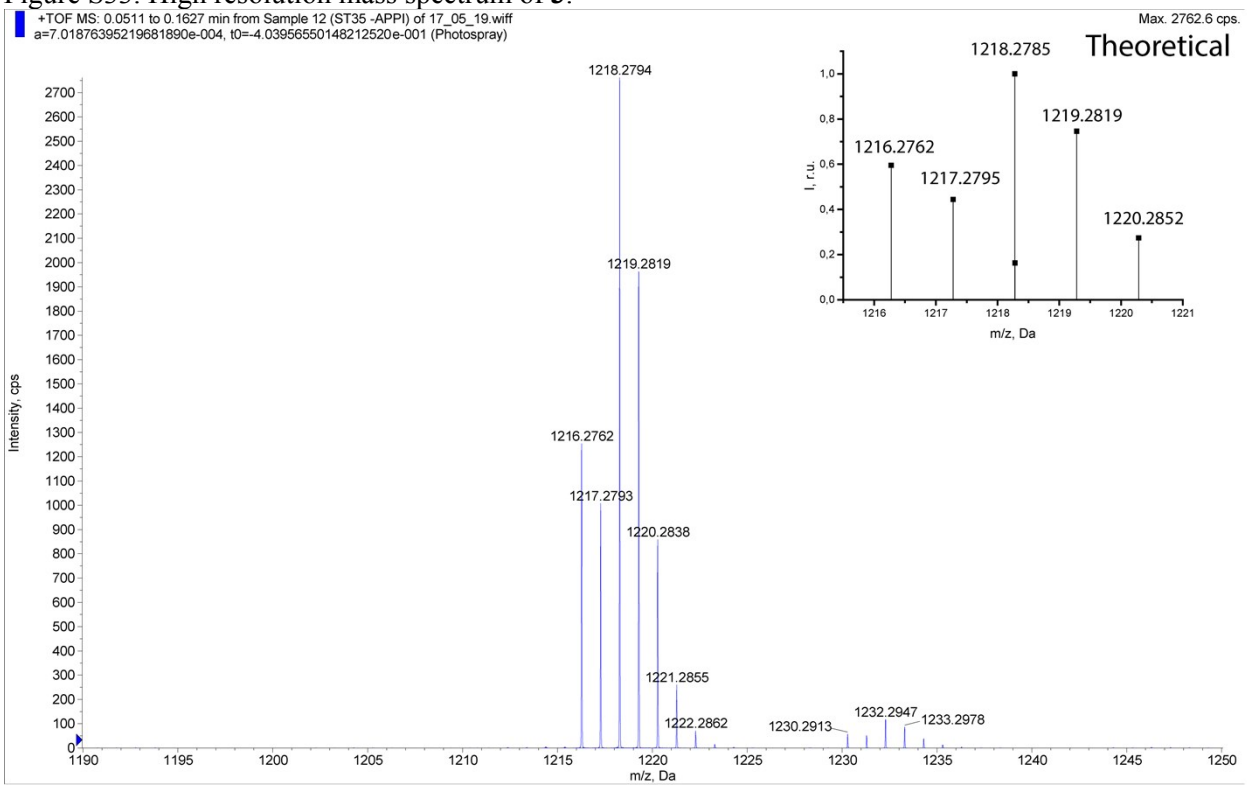

Figure S34. High resolution mass spectrum of **3**.

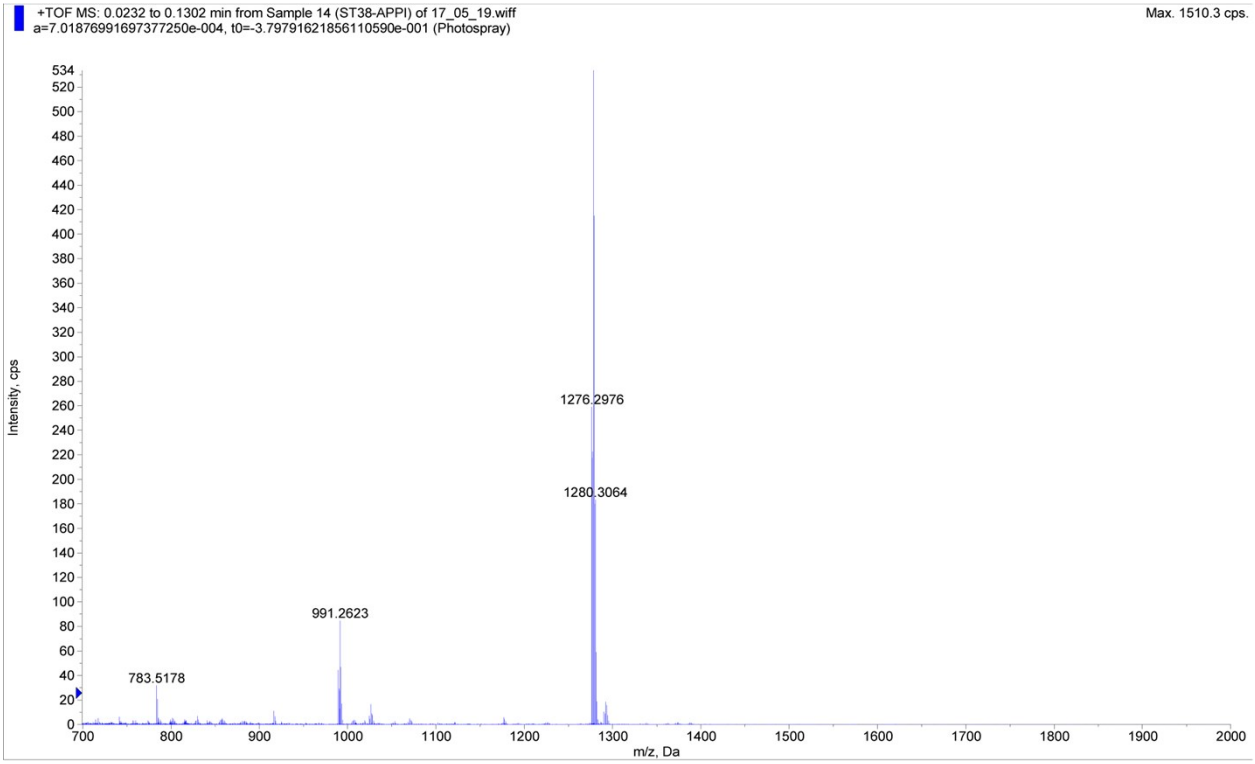

Figure S35. High resolution mass spectrum of **4**.

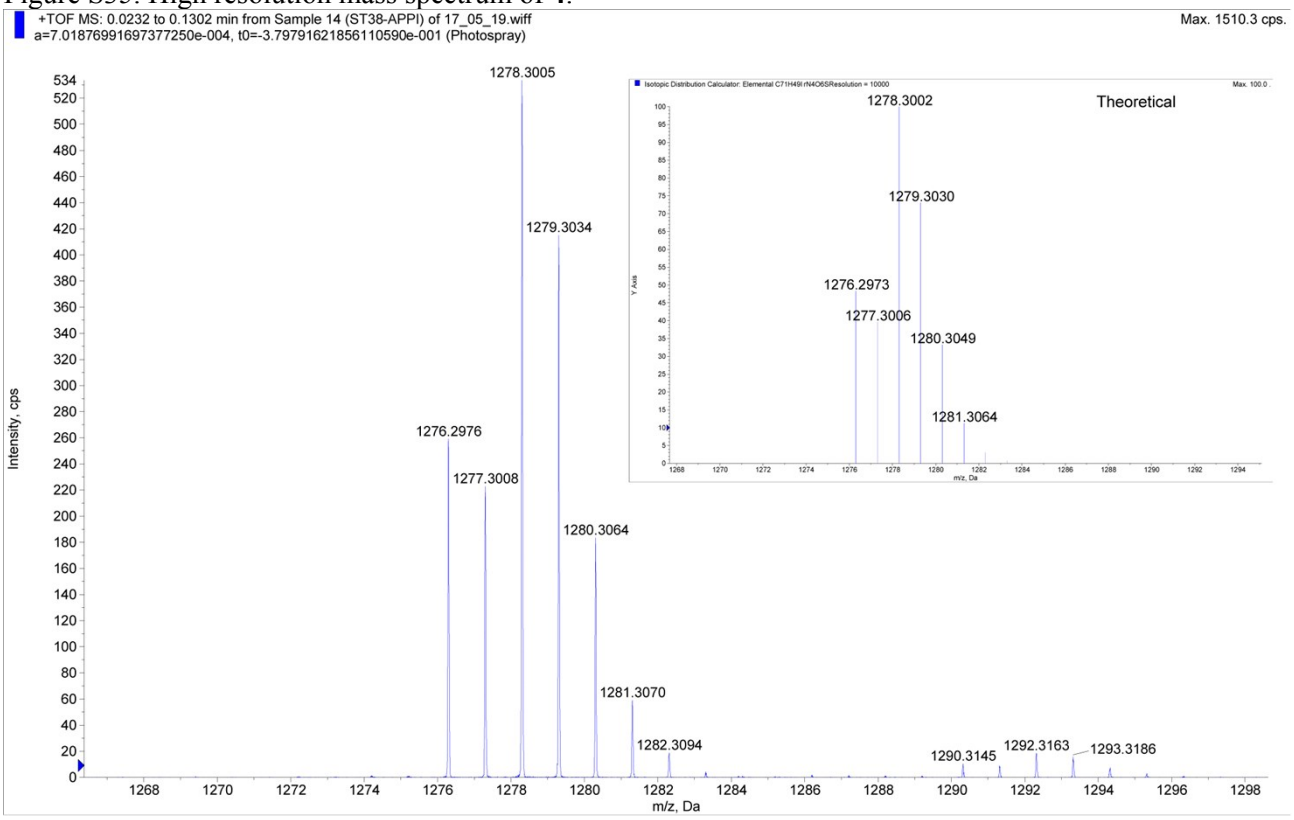

Figure S36. High resolution mass spectrum of **4**.

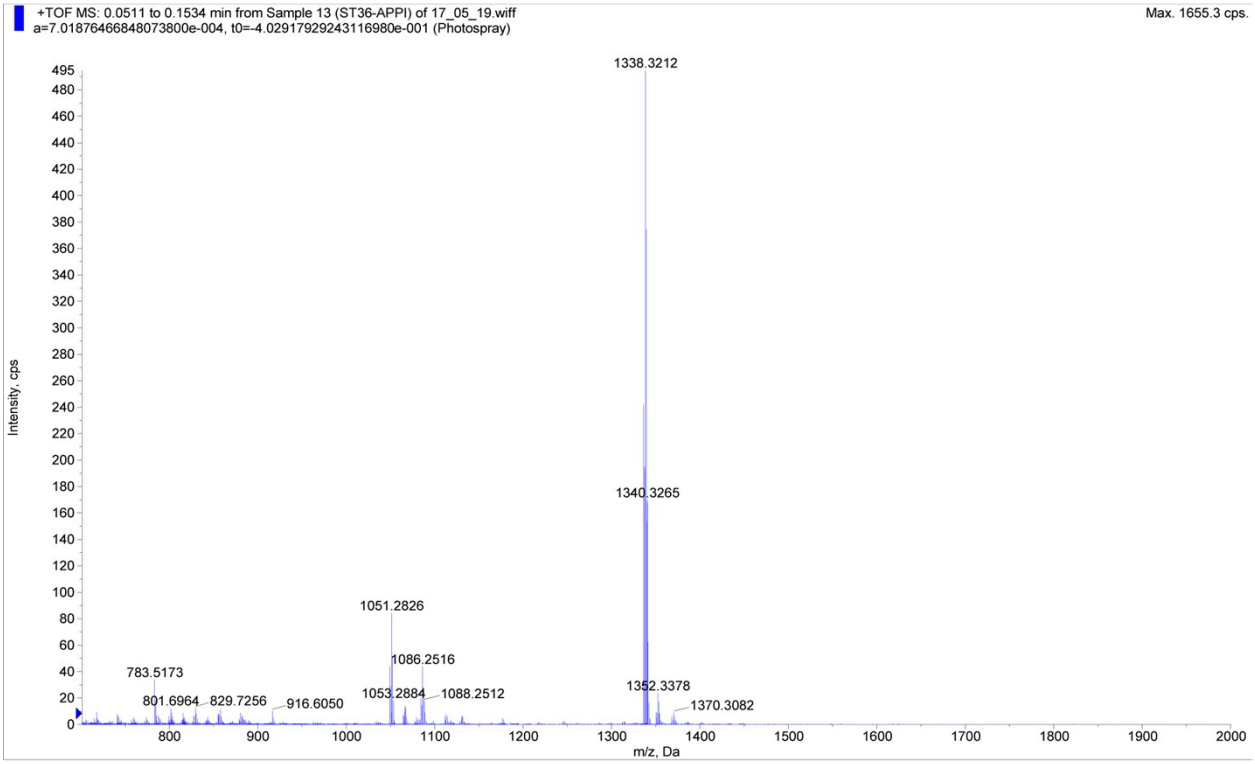

Figure S37. High resolution mass spectrum of **5**.

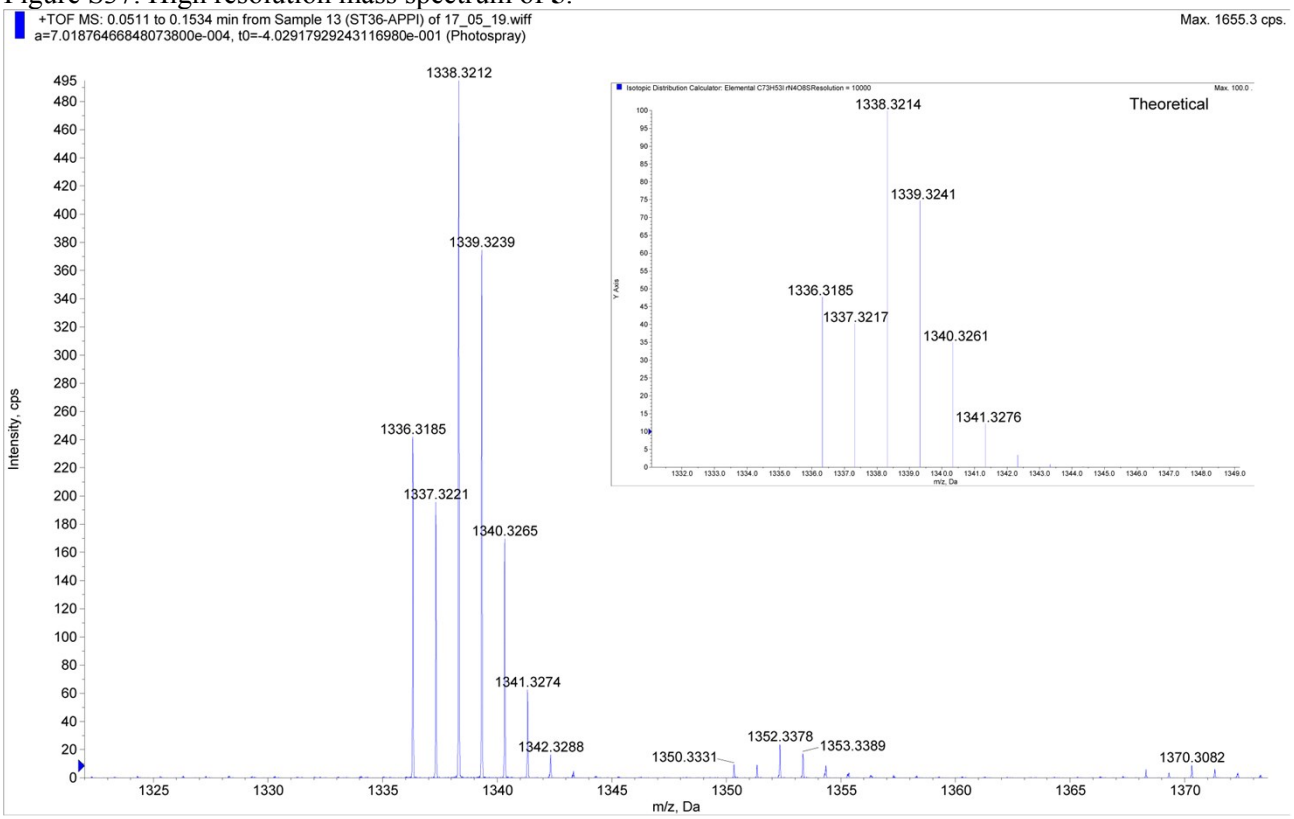

Figure S38. High resolution mass spectrum of **5**.

Table S1. Complex species (with their relative masses) in mass spectra of **1** – **5**.

	$Ir(C^N)_2^+$	$Ir(C^N)_2(O^O)^+$
1	967.2217	1254.2608
2	999.1614	1286.2002
3	931.2403	1218.2794
4	991.2623	1278.3005
5	1051.2826	1338.3212

2. **X-ray experiments.**

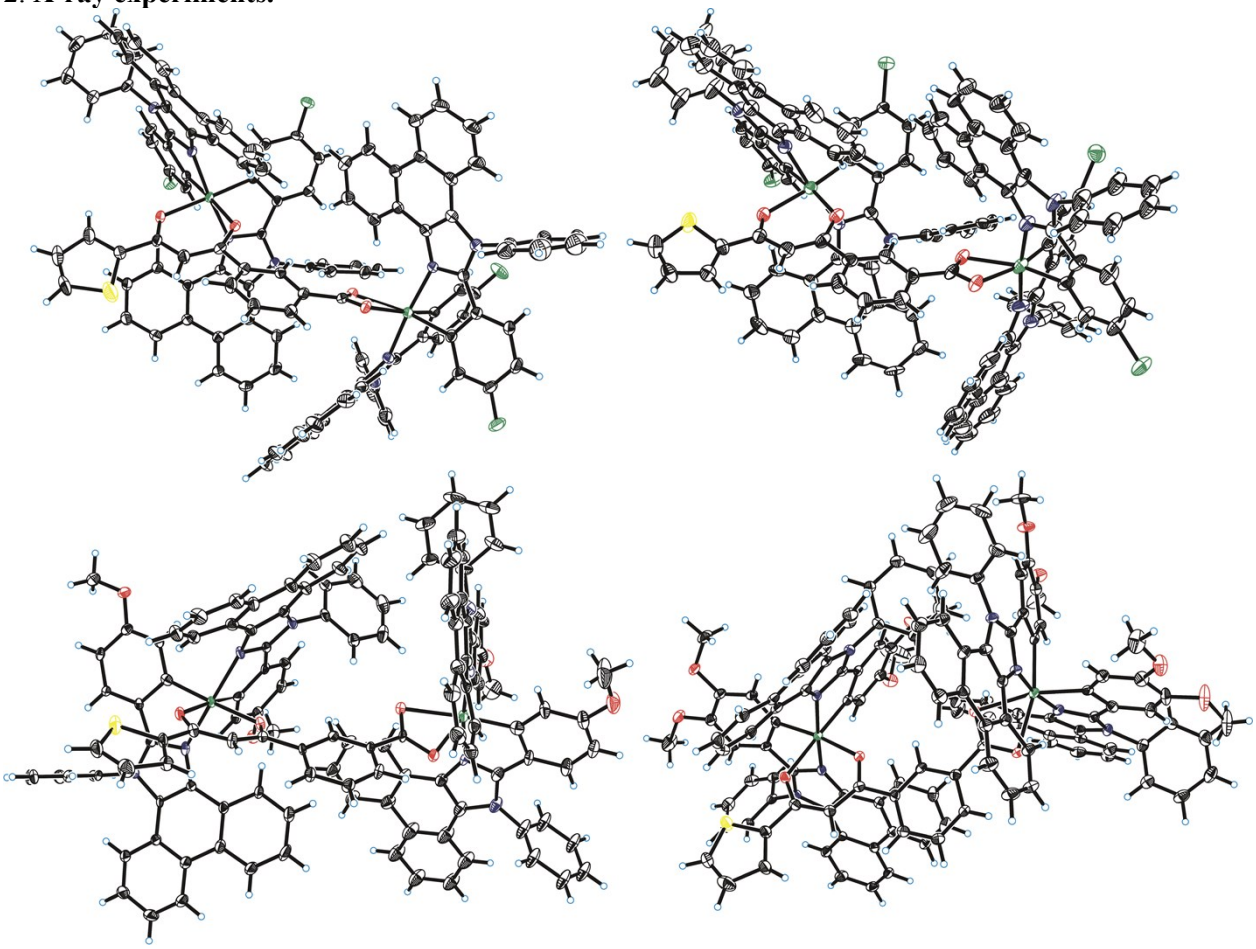

Figure S39. Binuclear structures of reaction products of **1H** (upper left), **2H** (upper right), **4H** (lower left) and **5H** (lower right) with TiO_2.

Table S2. Details of the X-ray crystal data collection and structure refinement for dimeric compounds

	$[Ir(dmphi)_2Cl]_2$	$[Ir(cphi)_2Cl]_2$	$[Ir(fphi)_2Cl]_2$	$[Ir(mphi)_2Cl]_2$
Empirical formula	$C_{116}H_{84}Ir_2N_8O_8Cl_2$ +solvent	$C_{108}H_{64}Cl_6Ir_2N_8$ +solvent	$C_{108}H_{64}Cl_2F_4Ir_2N_8$ +solvent	$C_{112}H_{76}Cl_2Ir_2N_8O_4$ +solvent
M_w	2173.21	2070.77	2004.97	2053.10
Temperature (K)	150	150	230	150
Size (mm)	0.30 x 0.27 x 0.04	0.35 x 0.20 x 0.07	0.36 x 0.12 x 0.1	0.30 x 0.18 x 0.05
Cryst. system	monoclinic	triclinic	monoclinic	triclinic
Space group	C2/c	P-1	C2/c	P-1
a (Å)	24.510(3)	17.8595(11)	29.578(10)	13.8139(5)
b (Å)	22.242(3)	18.4756(10)	24.131(8)	19.0358(8)
c (Å)	22.805(3)	19.4513(11)	20.493(8)	20.5748(7)
α(°)		69.415(2)		73.4120(10)
β (°)	115.060(2)	64.151(2)	126.799(9)	70.6910(10)
γ(°)		79.109(2)		74.1020(10)
V (Å^3)	11262(2)	5402.4(5)	11712(7)	4796.1(3)
Z	4	2	4	2
ρ_{cald} (g·cm^{-3})	1.282	1.273	1.137	1.422
Abs coeff (mm^{-1})	2.463	2.655	2.363	2.885
F(000)	4352	2048	3968	2048
θ range (deg)	$1.98< \theta < 27.00$	$1.94< \theta < 26.3$	$1.72< \theta < 25.05$	$2.15< \theta < 25.01$
no. of collected/unique rflns	48294/12241	58725/21930	28161/10334	47688/16918
Completeness to θ (%)	99.5	98.8	99.3	99.4
no. of data/restraints/params	12241/6/627	21930/0/117	10334/0/560	16918/0/1157
Goodness of fit on F^2	1.069	1.045	0.979	1.027
Final *R* indices ($I > 2\sigma(I)$)	$R_1 = 0.0502$, $wR_2 = 0.1117$	$R_1 = 0.0485$, $wR_2 = 0.1327$	$R_1 = 0.0544$, $wR_2 = 0.1315$	$R_1 = 0.0386$, $wR_2 = 0.0928$
R indices (all data)	$R_1 = 0.0751$, $wR_2 = 0.1197$	$R_1 = 0.0612$, $wR_2 = 0.1405$	$R_1 = 0.0914$, $wR_2 = 0.1488$	$R_1 = 0.0460$, $wR_2 = 0.0963$
Largest diff peak/hole (e/Å^3)	1.96/-2.44	3.94/-2.83	1.57/-2.60	3.28/-0.78

Table S3. Details of the X-ray crystal data collection and structure refinement for complexes **1 – 5**.

	1	**2**	**3**	**4**	**5**
Empirical formula	$C_{69}H_{43}IrN_4O_4F_2S\cdot$ 0.5 CH_2Cl_2	$C_{69}H_{43}IrN_4O_4Cl_2S\cdot$ 1.3 CH_2Cl_2	$C_{69}H_{45}IrN_4O_4S\cdot$ 0.65 CH_3CN	$C_{71}H_{49}IrN_4O_6S\cdot$ 1.3 $CH_2Cl_2\cdot$0.27 H_2O	$C_{73}H_{53}IrN_4O_8S\cdot$ 0.45 CH_3OH
M_w	1381.72	1397.64	1245.03	1538.04	1352.87
Temperature (K)	100	150	150	150	150
Size (mm)	0.20 x 0.12 x 0.10	0.20 x 0.18 x 0.12	0.30 x 0.25 x 0.05	0.17 x 0.14 x 0.08	0.32 x 0.23 x 0.18
Cryst. system	monoclinic	triclinic	Triclinic	triclinic	orthorhombic
Space group	C2/c	P-1	P-1	P-1	$Pna2_1$
a (Å)	23.5656(15)	14.6748(9)	15.7615(4)	11.3617(4)	23.0818(17)
b (Å)	17.6138(11)	15.3911(8)	19.7594(6)	11.4387(4)	11.7771(8)
c (Å)	29.183(2)	15.5092(10)	21.2004(6)	25.1626(9)	22.3446(16)
α(°)		93.940(2)	84.9820(10)	87.1280(10)	
β (°)	98.663(2)	107.762(2)	68.2350(10)	82.5430(10)	
γ(°)		106.996(2)	77.2280(10)	82.4970(10)	
V ($Å^3$)	11974.9(13)	3141.9(3)	5980.1(3)	3213.0(2)	6074.1(7)
Z	8	2	4	2	4
ρ_{cald} ($g\cdot cm^{-3}$)	1.533	1.477	1.383	1.590	1.479
Abs coeff (mm^{-1})	2.460	2.406	2.320	2.419	2.296
F(000)	5528	1397	2505	1545	2736
θ range (deg)	$1.75< \theta < 25.05$	$2.37< \theta < 25.03$	$2.11 < \theta < 25.05$	$2.29 < \theta < 30.54$	$1.94< \theta <29.00$
no. of collected/unique rflns	57032/10610	45730/10988	50466/21080	38911 / 19375	70959/16116
Completeness to θ (%)	99.9	98.9	99.5	98.3	99.9
no. of data/restraints/params	10610/15/627	10988/42/750	21080/123/1426	19375 /0 / 836	16116/10/699
Goodness of fit on F^2	1.061	1.046	1.066	1.043	1.023
Final *R* indices ($I > 2\sigma(I)$)	$R_1 = 0.0733$, $wR_2 = 0.2026$	$R_1 = 0.0699$, $wR_2 = 0.1847$	$R_1 = 0.0528$, $wR_2 = 0.1554$	$R_1 = 0.0427$, $wR_2 = 0.0986$	$R_1 = 0.0400$, $wR_2 = 0.0964$
R indices (all data)	$R_1 = 0.0930$, $wR_2 = 0.2188$	$R_1 = 0.0934$, $wR_2 = 0.2006$	$R_1 = 0.0727$, $wR_2 = 0.1676$	$R_1 = 0.0531$, $wR_2 = 0.1028$	$R_1 = 0.0493$, $wR_2 = 0.1010$
Largest diff peak/hole ($e/Å^3$)	2.72/-1.56	2.17/-1.85	2.26/-1.51	1.91 /-1.51	1.59/-1.16

Table S4. Details of the X-ray crystal data collection and structure refinement for binuclear compounds obtained by partial decomposition of hydrolysed complexes (**1H – 5H**)

	1H	**2H**	**3H**	**4H**	**5H**
Empirical formula	$C_{122}H_{72}Ir_2N_8O_4F_4S\cdot$ 4.5 CH_3CN	$C_{122}H_{72}Cl_4Ir_2N_8O_4S\cdot$ 7 CH_3CN	$C_{122}H_{76}Ir_2N_8O_4S\cdot$ 0.5 CH_3CN+solvent	$C_{126}H_{84}Ir_2N_8O_8S$ $\cdot$5 CH_3CN	$C_{130}H_{92}Ir_2N_8O_{12}S\cdot$ 7 CH_3CN
M_w	2391.07	2354.24	2175.42	2459.79	2661.95
Temperature (K)	100	100	150	100	100
Size (mm)	0.12 x 0.10 x 0.03	0.20 x 0.10 x 0.02	0.16 x 0.08 x 0.07	0.14 x 0.11 x 0.09	0.15 x 0.12 x 0.07
Cryst. system	triclinic	triclinic	triclinic	triclinic	triclinic
Space group	P-1	P-1	P-1	P-1	P-1
a (Å)	17.471(2)	12.202(3)	13.7602(5)	15.9214(10)	14.2021(15)
b (Å)	17.750(2)	20.438(5)	18.4965(5)	19.4903(12)	19.393(2)
c (Å)	18.145(2)	21.092(6)	22.4727(6)	20.8240(13)	23.025(2)
α(°)	104.068(4)	99.336(8)	111.7180(10)	89.263(2)	105.080(3)
β (°)	107.253(2)	101.460(9)	97.9180(10)	69.208(2)	101.124(3)
γ(°)	93.552(4)	102.695(8)	105.2410(10)	68.446(2)	90.032(4)
V ($Å^3$)	5157.9(10)	4911(2)	4947.4(3)	5567.1(6)	5999.5(11)
Z	2	2	2	2	2
ρ_{cald} ($g\cdot cm^{-3}$)	1.540	1.592	1.460	1.467	1.474
Abs coeff (mm^{-1})	2.671	2.902	2.770	2.474	2.305
F(000)	2394	2348	2176	2480	2691
θ range (deg)	$1.98< \theta < 26.00$	$1.94< \theta < 25.05$	$2.00< \theta < 26.38$	$2.15< \theta < 26.00$	$2.00< \theta < 26.00$
no. of collected/unique rflns	84068/20266	83692/17415	54309/20035	89775/21855	98817/23568
Completeness to θ (%)	99.9	100	99.0	99.8	99.9
no. of data/restraints/params	20266/27/1408	17415/7/1224	20035/556/1373	21855/22/1406	23568/9/1582
Goodness of fit on F^2	1.035	0.999	1.014	1.023	1.036
Final *R* indices ($I > 2\sigma(I)$)	$R_1 = 0.0297$, $wR_2 = 0.0694$	$R_1 = 0.0531$, $wR_2 = 0.0922$	$R_1 = 0.0365$, $wR_2 = 0.0793$	$R_1 = 0.0424$, $wR_2 = 0.1041$	$R_1 = 0.0346$, $wR_2 = 0.0648$
R indices (all data)	$R_1 = 0.0405$, $wR_2 = 0.0748$	$R_1 = 0.1229$, $wR_2 = 0.1154$	$R_1 = 0.0537$, $wR_2 = 0.0858$	$R_1 = 0.0598$, $wR_2 = 0.1141$	$R_1 = 0.0510$, $wR_2 = 0.0693$
Largest diff peak/hole ($e/Å^3$)	1.96/-1.80	1.07/-1.28	1.45/-0.92	2.10/-1.80	2.35/-1.87

Table S5. Selected bond lengths [Å] and angles [°] in structures of the complexes

Complex **1**	$Ir_1–C_1$	$Ir_1–C_{28}$	$Ir_1–N_1$	$Ir_1–N_3$	$Ir_1–O_4$	$Ir_1–O_3$	
	1.989(10)	2.020(10)	2.091(8)	2.056(8)	2.140(6)	2.181(6)	
	$C_1–Ir_1–C_{28}$	$N_1–Ir_1–C_{28}$	$C_1–Ir_1–N_3$	$C_1–Ir_1–O_3$	$C_{28}–Ir_1–O_4$	$N_1–Ir_1–O_3$	$N_3–Ir_1–O_4$
	95.0(4)	98.7(3)	95.3(4)	93.7(3)	85.5(3)	80.2(3)	80.9(3)
Complex **2**	$Ir_1–C_{28}$	$Ir_1–C_1$	$Ir_1–N_3$	$Ir_1–N_1$	$Ir_1–O_4$	$Ir_1–O_3$	
	1.979(11)	1.993(9)	2.072(7)	2.066(7)	2.155(6)	2.115(6)	
	$C_1–Ir_1–C_{28}$	$N_1–Ir_1–C_{28}$	$C_1–Ir_1–N_3$	$C_1–Ir_1–O_3$	$C_{28}–Ir_1–O_4$	$N_1–Ir_1–O_4$	$N_3–Ir_1–O_3$
	95.6(4)	79.5(3)	79.5(3)	86.2(3)	91.2(3)	81.8(3)	80.1(3)
Complex **3***	$Ir_1–C_1$	$Ir_1–C_{28}$	$Ir_1–N_1$	$Ir_1–N_3$	$Ir_1–O_4$	$Ir_1–O_3$	
	1.998(6)	1.989(6)	2.066(5)	2.063(5)	2.147(4)	2.152(4)	
	$C_1–Ir_1–C_{28}$	$N_1–Ir_1–C_{28}$	$C_1–Ir_1–N_3$	$C_1–Ir_1–O_3$	$C_{28}–Ir_1–O_4$	$N_1–Ir_1–O_3$	$N_3–Ir_1–O_4$
	96.9(2)	96.0(2)	97.5(2)	88.0(2)	90.2(2)	81.08(17)	80.69(19)
Complex **4**	$Ir_1–C_1$	$Ir_1–C_{28}$	$Ir_1–N_1$	$Ir_1–N_3$	$Ir_1–O_3$	$Ir_1–O_4$	
	1.993(3)	1.979(3)	2.053(3)	2.073(3)	2.173(2)	2.138(2)	
	$C_1–Ir_1–C_{28}$	$N_1–Ir_1–C_{28}$	$C_1–Ir_1–N_3$	$C_1–Ir_1–O_3$	$C_{28}–Ir_1–O_4$	$N_3–Ir_1–O_3$	$N_1–Ir_1–O_4$
	94.15(13)	80.06(12)	79.93(12)	95.14(11)	86.45(12)	80.10(10)	81.11(10)
Complex **5**	$Ir_1–C_1$	$Ir_1–C_{28}$	$Ir_1–N_1$	$Ir_1–N_3$	$Ir_1–O_4$	$Ir_1–O_3$	
	1.993(6)	1.988(6)	2.060(5)	2.068(5)	2.153(5)	2.161(4)	
	$C_1–Ir_1–C_{28}$	$N_1–Ir_1–C_{28}$	$C_1–Ir_1–N_3$	$C_1–Ir_1–O_3$	$C_{28}–Ir_1–O_4$	$N_1–Ir_1–O_3$	$N_3–Ir_1–O_4$
	98.0(2)	95.2(2)	99.2(2)	88.0(2)	88.5(2)	83.47(18)	80.2(2)

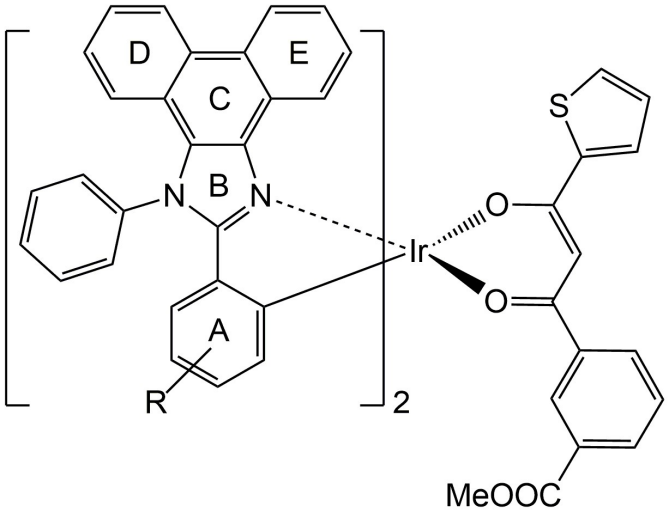

Figure S40. Labelling of planes in phenanthroimidazole ligands

Table S6. Angles between various planes in phenanthroimidazoles in structures of the complexes

Complex 1

Angle[°]	A	B	C	D	E
A		6.0(4)	9.5(4)	10.2(4)	13.5(4)
B	11.9(4)		5.0(4)	8.6(4)	8.9(4)
C	16.9(4)	5.1(4)		4.9(4)	4.0(4)
D	17.3(4)	7.5(4)	4.7(6)		6.2(4)
E	20.4(4)	8.8(4)	3.7(4)	5.1(4)	

Complex 2

Angle[°]	A	B	C	D	E
A		11.9(4)	15.2(4)	14.8(4)	17.5(4)
B	7.1(4)		3.8(3)	5.7(3)	6.2(4)
C	8.7(3)	3.5(3)		3.5(4)	2.4(4)
D	4.2(4)	3.4(4)	4.6(4)		3.9(3)
E	15.3(3)	10.8(3)	7.4(3)	11.5(3)	

Complex 3*

Angle[°]	A	B	C	D	E
A		7.5(3)	5.1(2)	3.2(3)	11.1(2)
B	12.9(3)		4.2(2)	7.8(3)	11.0(2)
C	18.5(2)	6.6(3)		7.2(2)	7.6(3)
D	18.2(2)	7.4(2)	2.1(3)		14.0(3)
E	22.1(2)	11.3(2)	5.0(3)	4.1(2)	

Complex 4

Angle[°]	A	B	C	D	E
A		11.1(3)	15.2(4)	12.8(4)	24.5(6)
B	12.2(3)		5.6(3)	9.6(4)	14.7(3)
C	12.1(4)	1.8(4)		7.6(4)	9.4(4)
D	11.7(4)	0.5(4)	1.5(4)		14.3(4)
E	12.6(4)	4.6(3)	2.8(5)	4.3(3)	

Complex 5

Angle[°]	A	B	C	D	E
A		2.8(4)	8.9(3)	11.1(4)	16.1(5)
B	16.8(3)		6.3(3)	10.0(4)	13.4(4)
C	20.9(4)	6.9(4)		7.2(4)	7.9(4)
D	18.0(4)	10.3(3)	6.4(4)		13.4(4)
E	29.2(4)	15.2(4)	8.7(4)	12.1(4)	

* in structure of complex **3** two independent molecules were observed, data is given for less disordered one

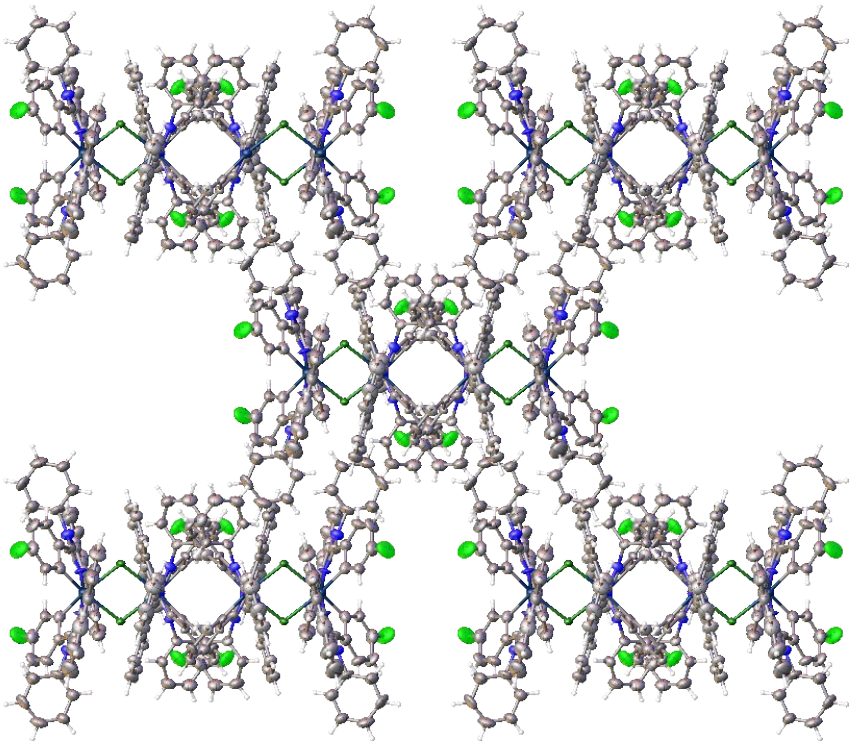

Figure S41. Fragment of the crystal packing of $[Ir(fphi)_2Cl]_2$ Image along 2 axis.

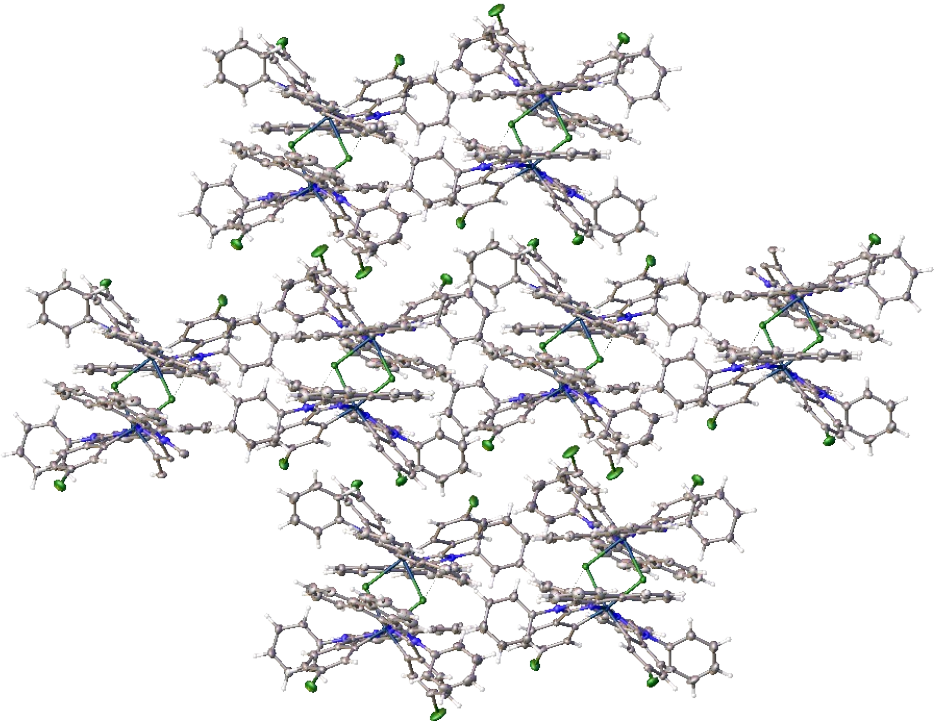

Figure S42. Fragment of the crystal packing of $[Ir(cphi)_2Cl]_2$ Image along 2 axis.

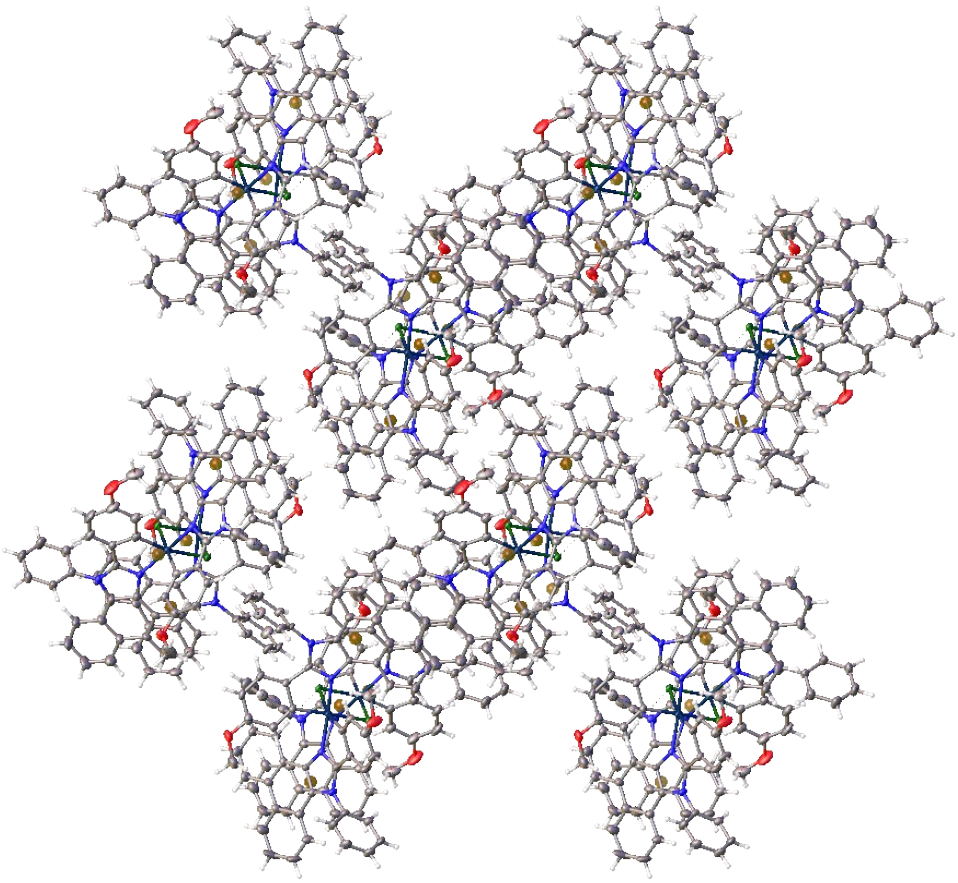

Figure S43. Fragment of the crystal packing of $[Ir(mphi)_2Cl]_2$

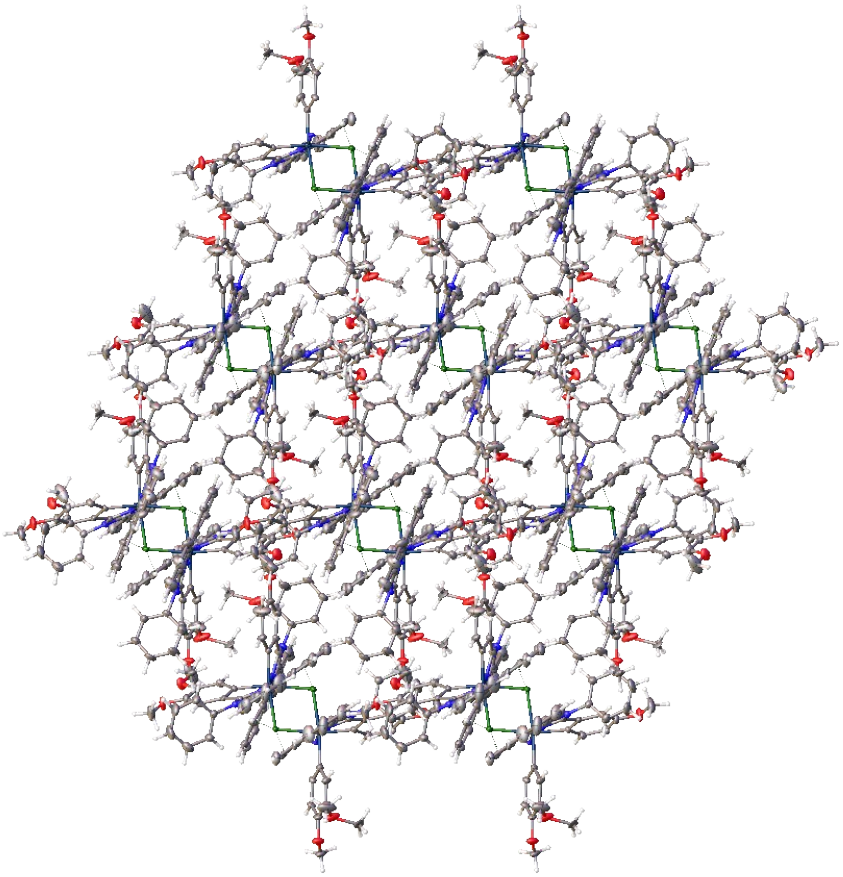

Figure S44. Fragment of the crystal packing of $[Ir(dmphi)_2Cl]_2$ Image along 2 axis.

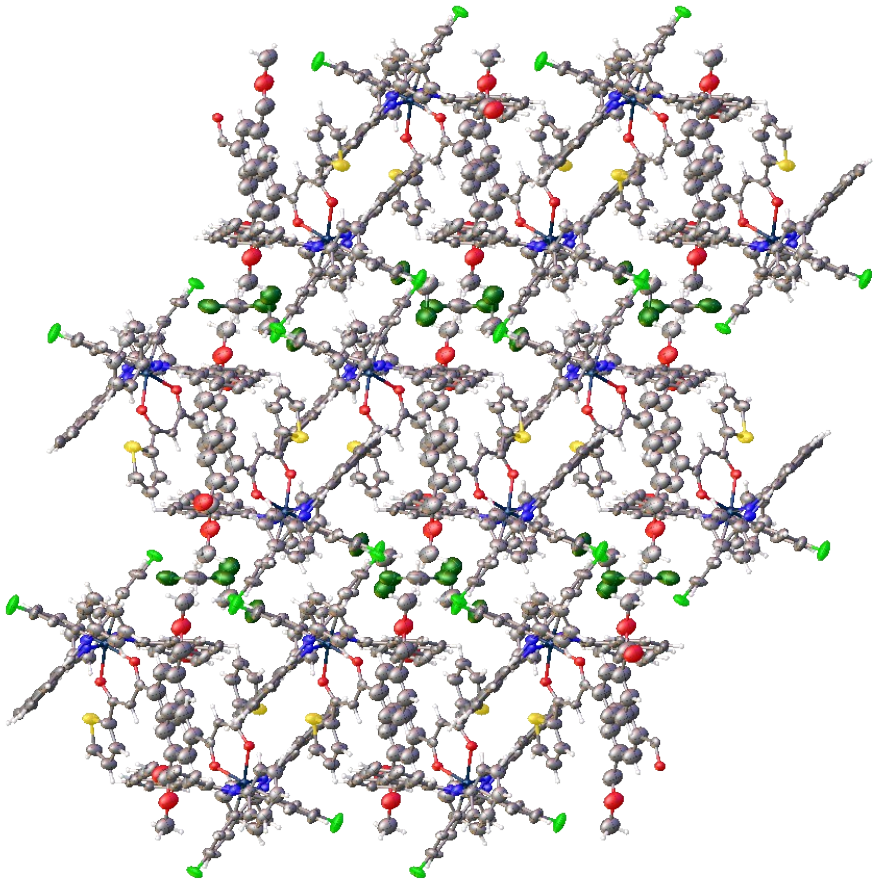

Figure S45. Fragment of the crystal packing of complex **1**. Image along 2 axis; minor components of disordered groups are not shown.

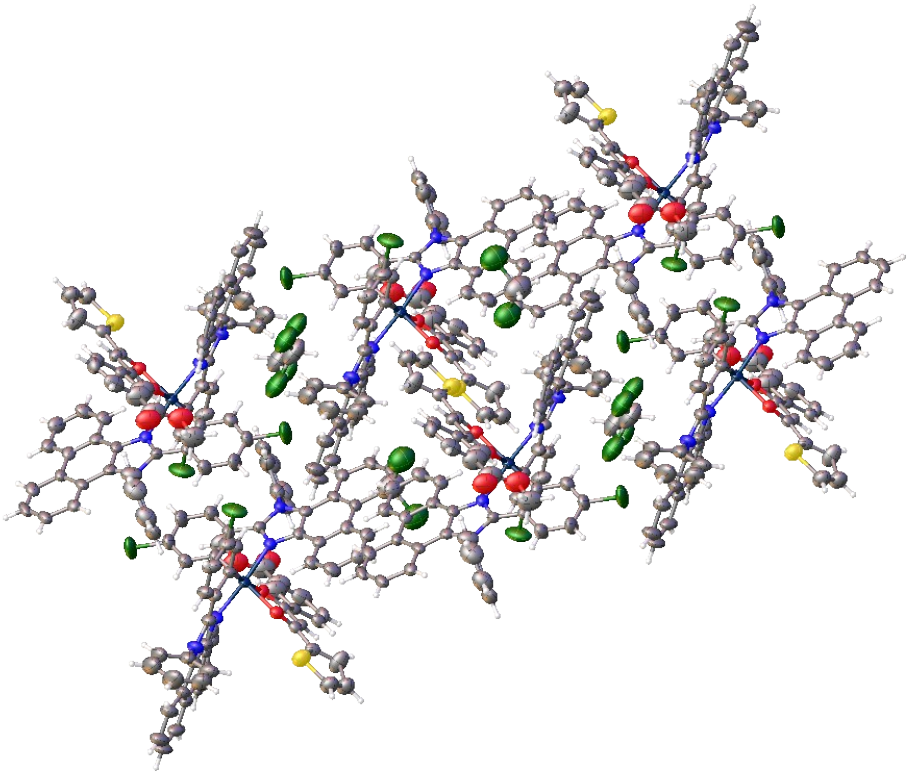

Figure S46. Fragment of the crystal packing of complex **2**. Minor components of disordered groups are not shown.

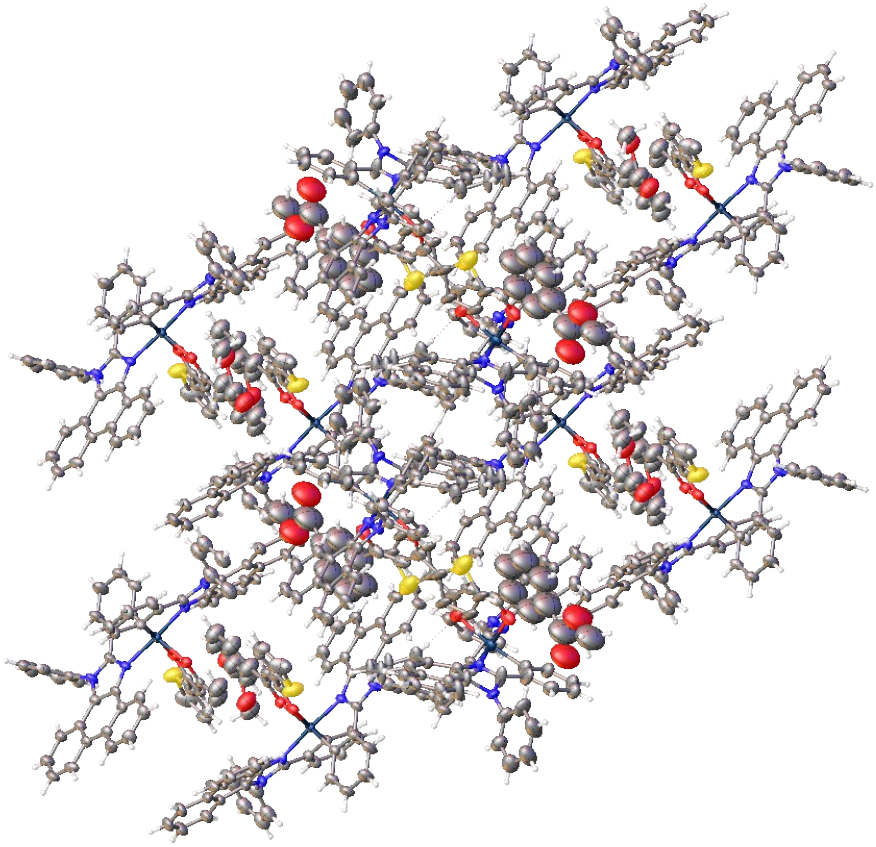

Figure S47. Fragment of the crystal packing of complex **3**. Minor components of disordered groups are not shown.

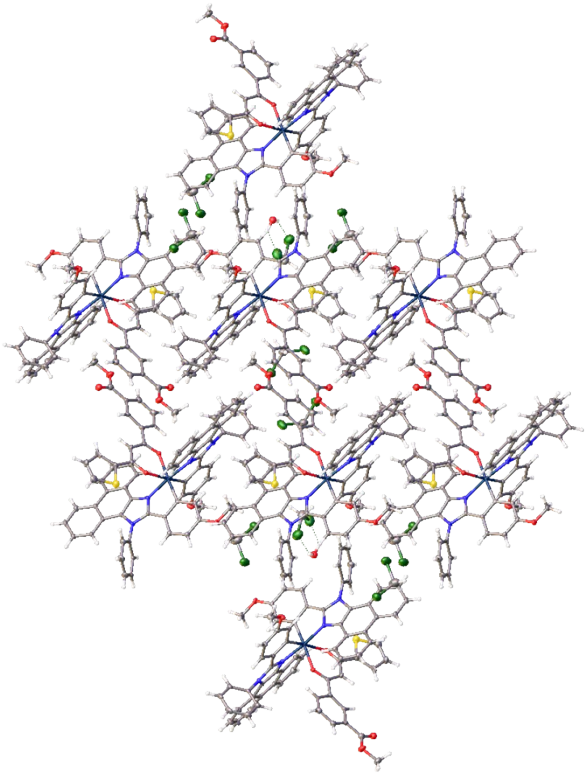

Figure S48. Fragment of the crystal packing of complex **4**.

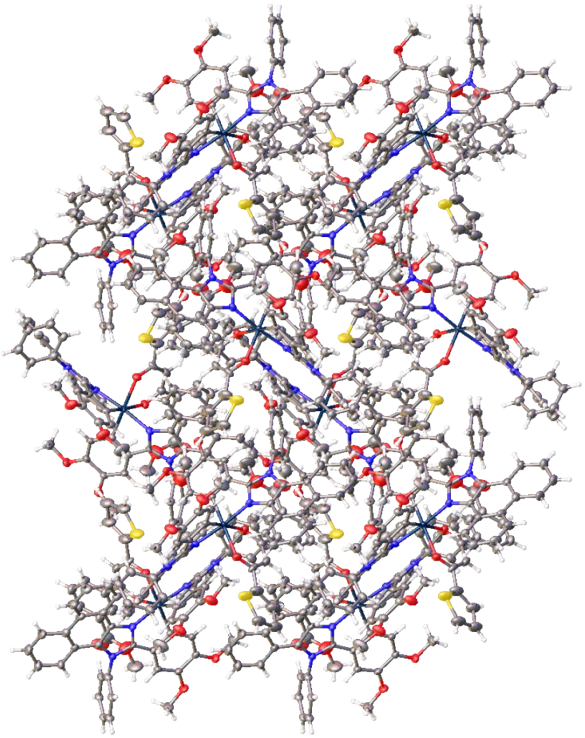

Figure S49. Fragment of the crystal packing of complex **5**. Image along 2_1 axis; minor components of disordered groups are not shown.

3. Redox and optical properties.

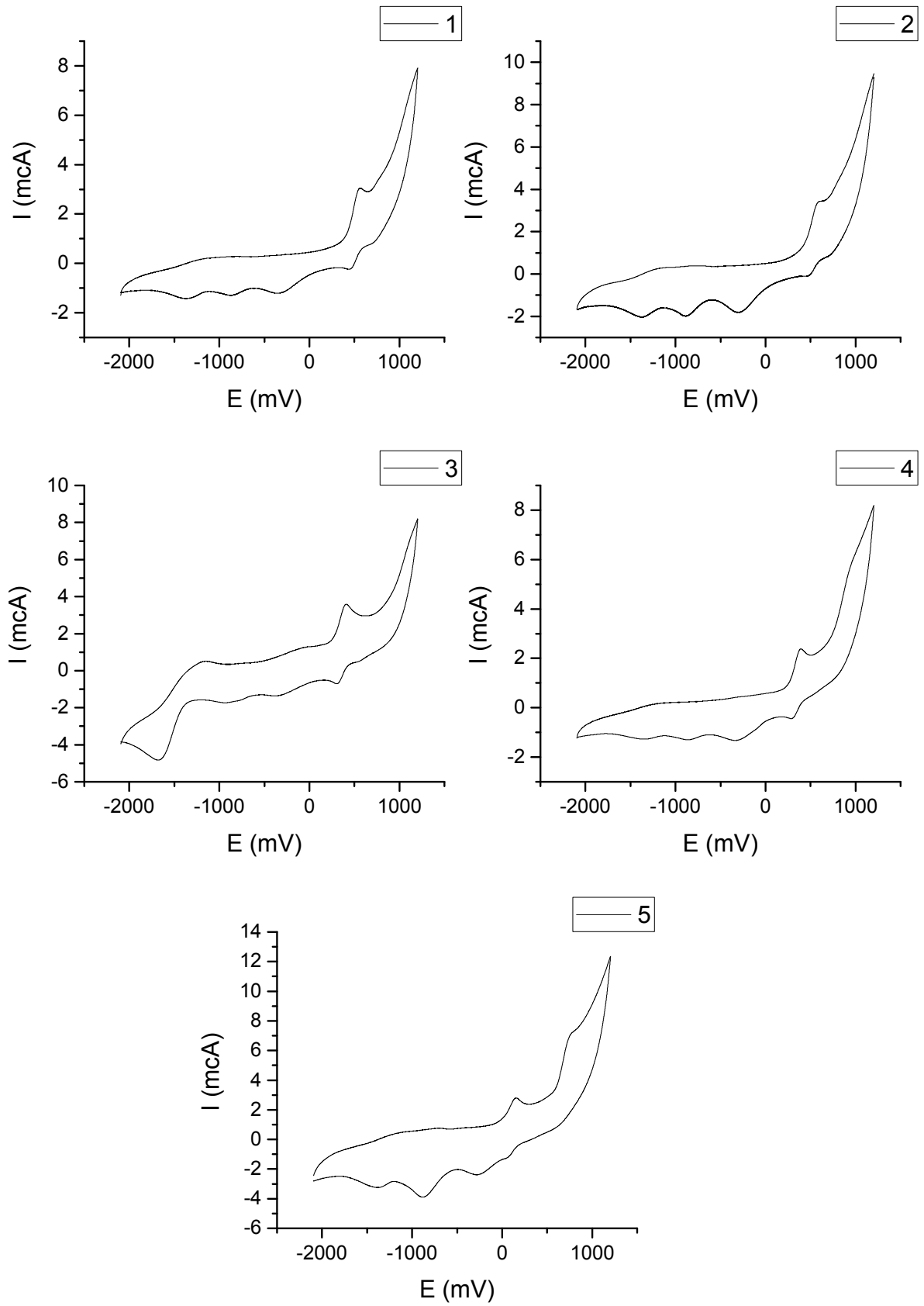

Figure S50. Cyclic voltammetry curves of complexes **1** – **5** measured versus ferrocene in Ar-saturated N,N-dimethylformamide (electrolyte – 0.1 M NBu_4PF_6) at a scan rate of 50 mV/s.

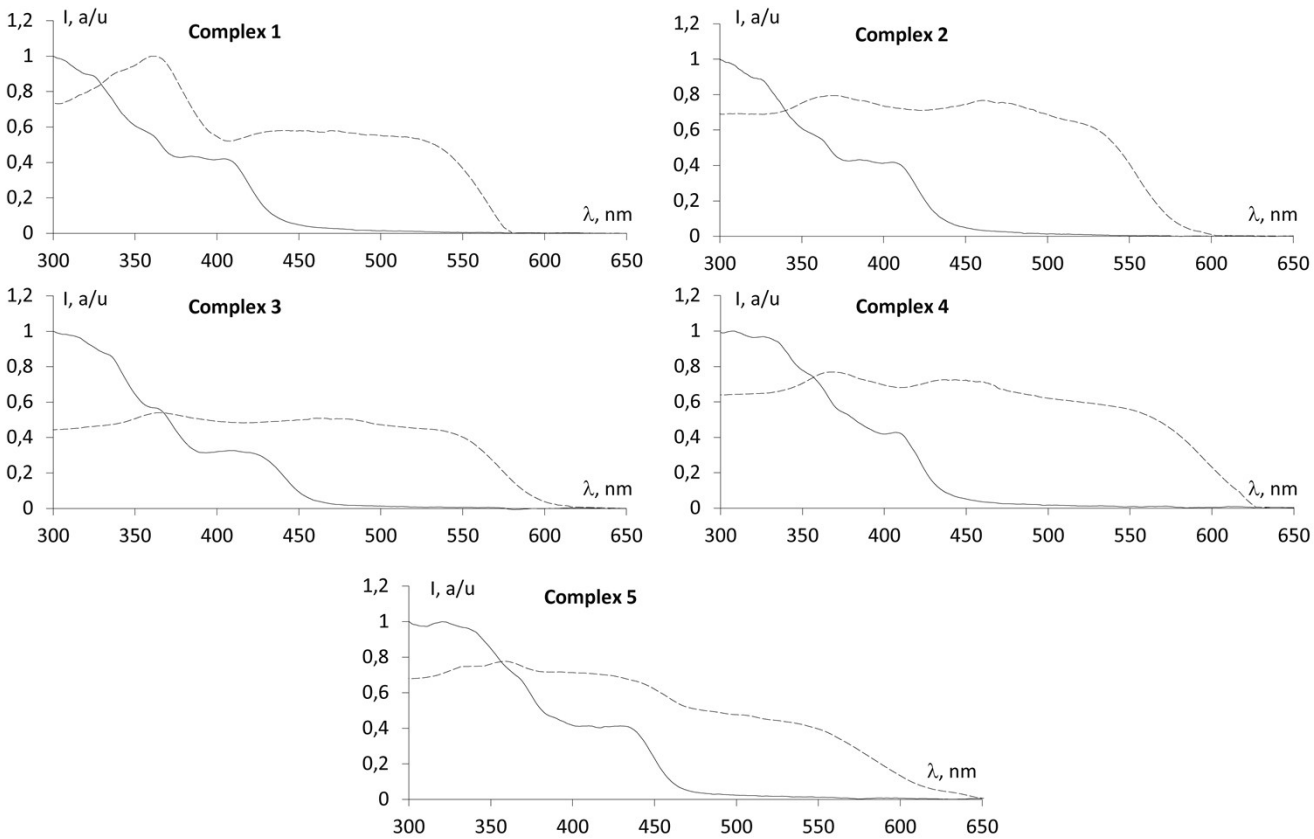

Figure S51. Excitation (---) and absorption (—) spectra of complexes **1** – **5** measured in CH_2Cl_2 at 25°C.

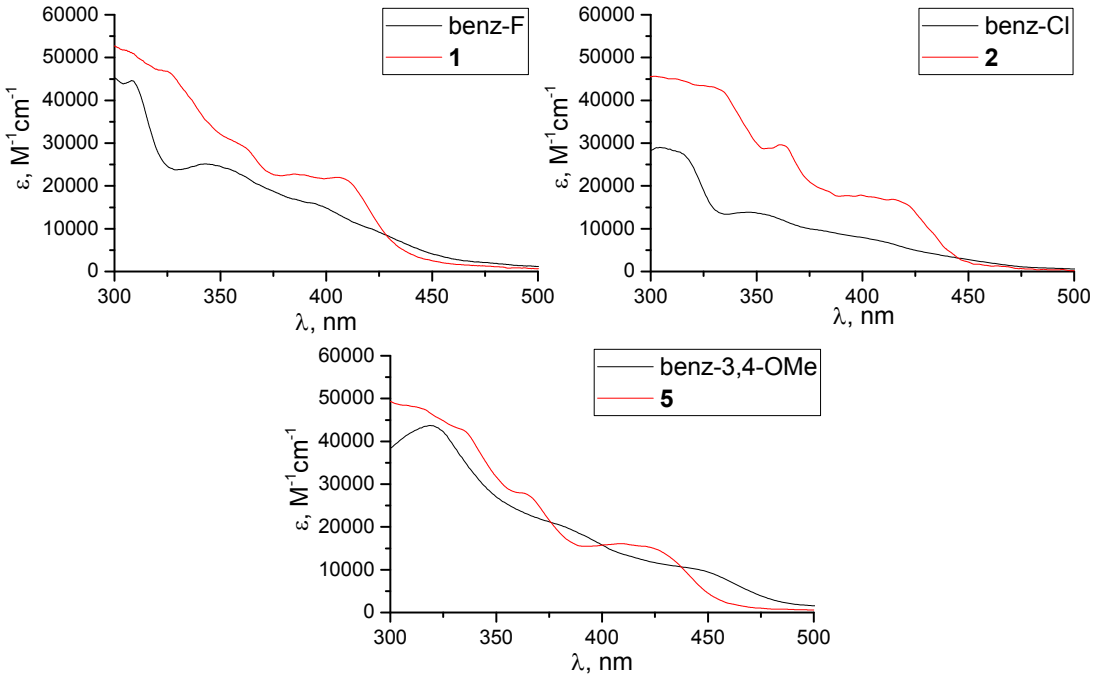

Figure S52. Comparison of absorption spectra of synthesized complexes (red) and benzimidazole-based complexes (black).

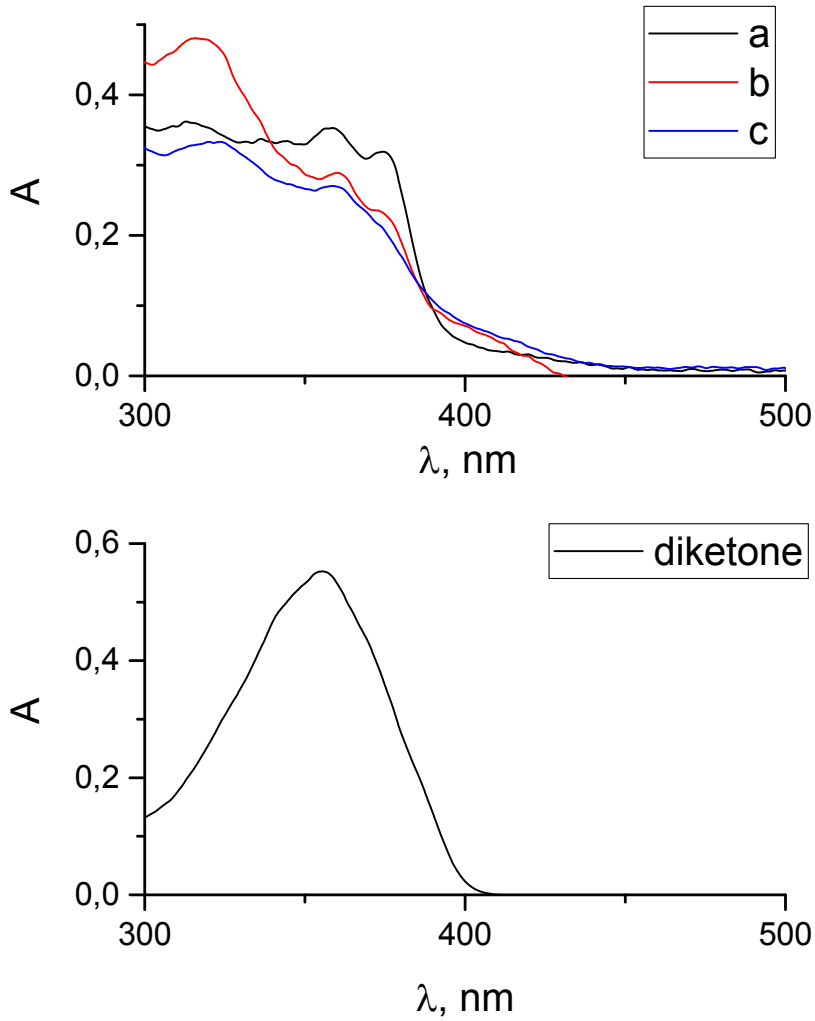

Figure S53. Comparison of absorption spectra of decomposition product of complex **3** in pure CH_2Cl_2 **(a)** with its chloride precursor **(b)** and decomposition product of complex **3** upon addition of CF_3SO_3H and NBu_4Cl **(c)** (upper) and absorption spectra of the β-diketone (lower).

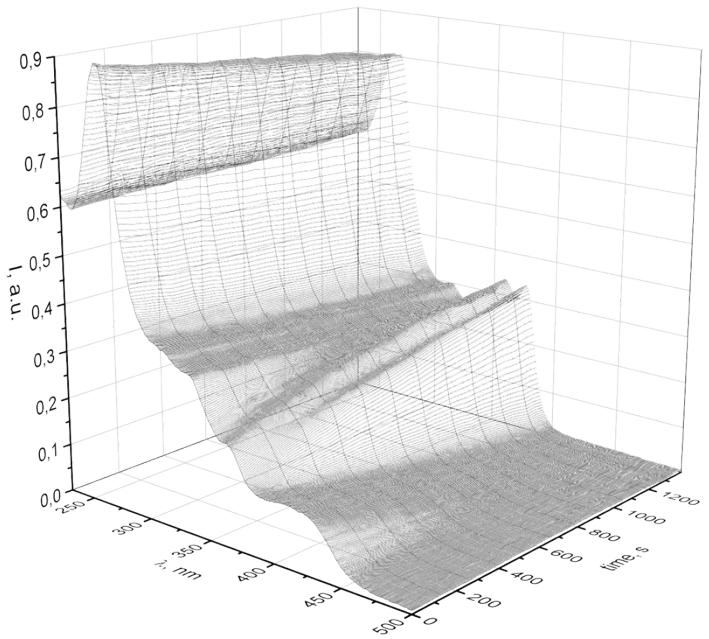

Figure S54. Changing of absorption spectra of complex **3** under continuous irradiation in time (measured in CH_2Cl_2 at 25°C).

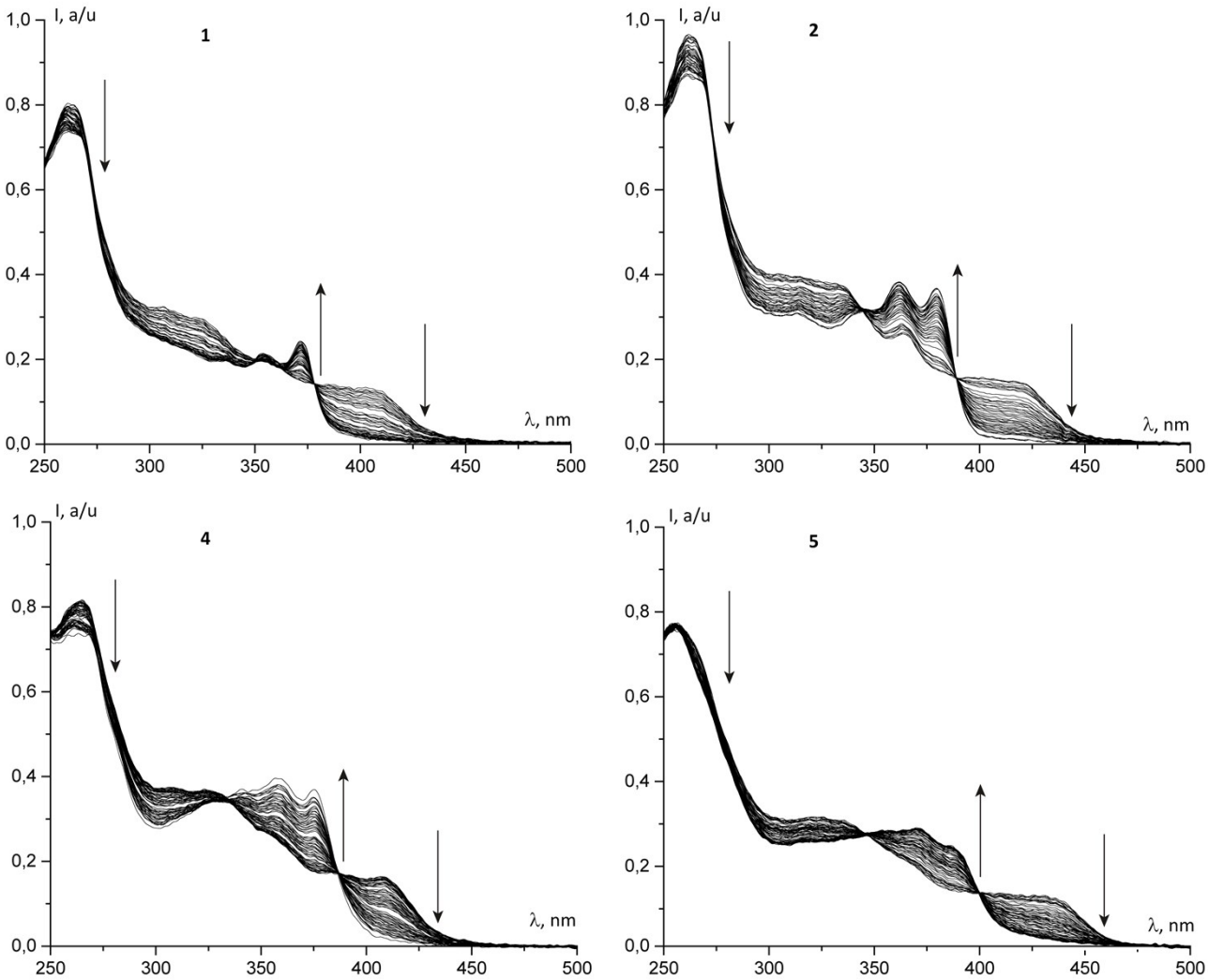

Figure S55. Changing of absorption spectra of complexes **1**, **2**, **4** and **5** under continuous irradiation (measured in CH_2Cl_2 at 25°C).

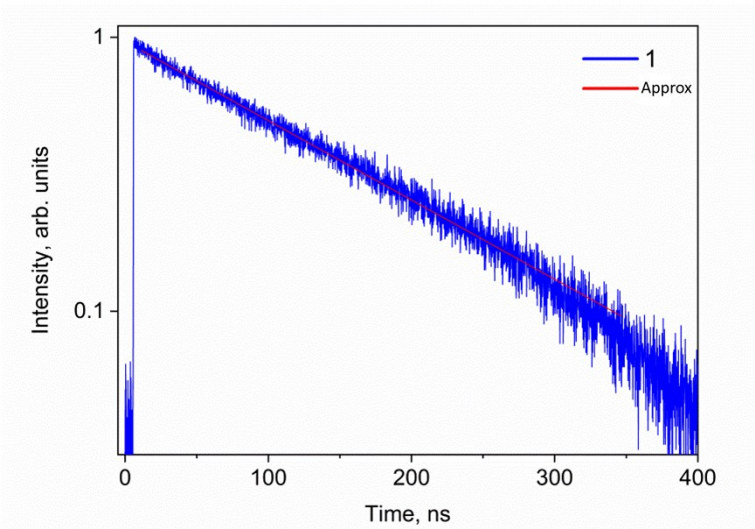

Figure S56. Photoluminescence decay curve of complex **1**with its approximation.

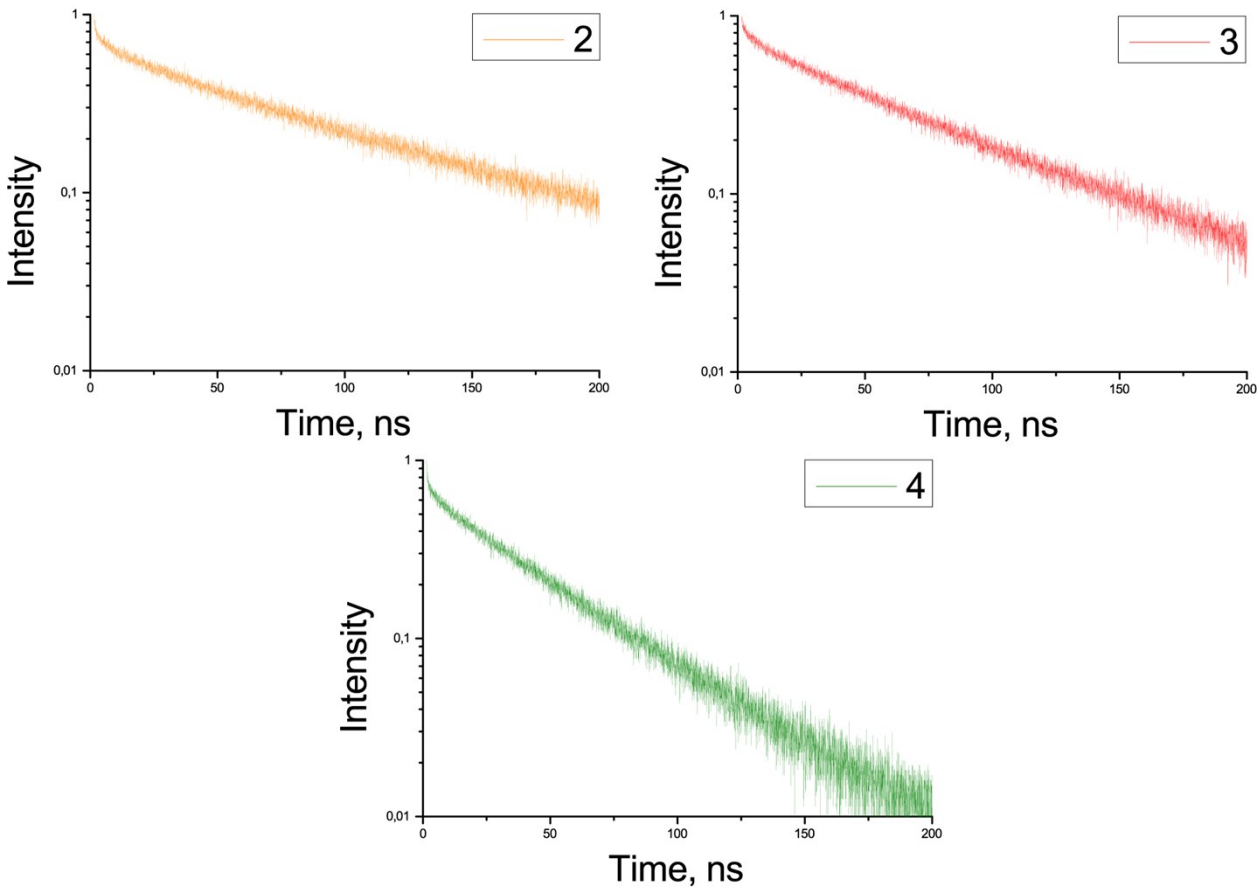

Figure S57. Photoluminescence decay curves of complexes **2** – **4**. (for complex **5** it was unable to record a decay curve due to weak luminescence)

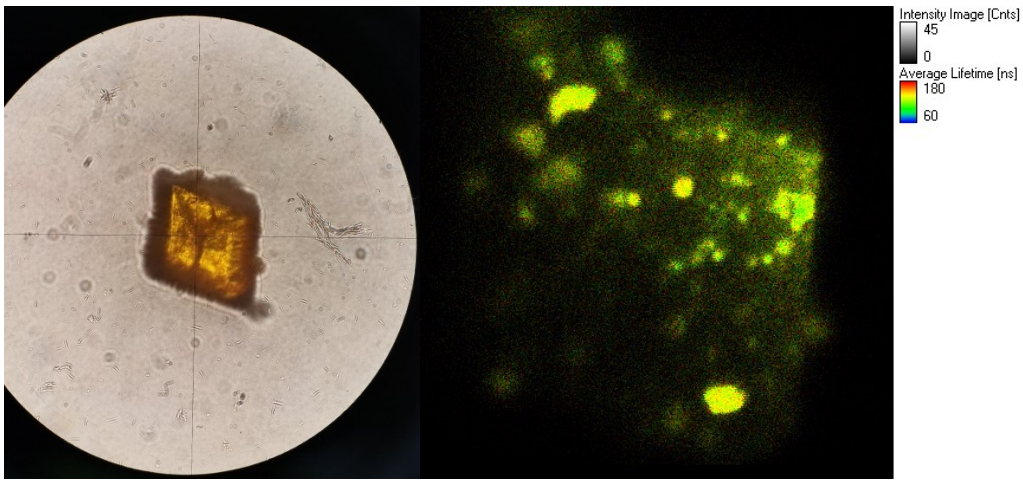

Figure S58. Mapping the surface of the selected crystallite (on the left) with spatial resolution by lifetime and luminescence intensity.

4. Calculation details.

Table S7. Composition (%) of frontier molecular orbitals for **1** – **5**.

complex		**1**	**2**	**3**	**4**	**5**
HOMO	Ir	43	43	48	38	38
	C^N	53	52	47	58	58
	O^O	4	5	5	4	4
	energy, eV	-4.97	-5.00	-4.79	-4.71	-4.55
LUMO	Ir	5	5	5	5	5
	C^N	11	11	11	11	11
	O^O	84	84	84	84	84
	energy, eV	-1.92	-1.94	-1.82	-1.79	-1.79

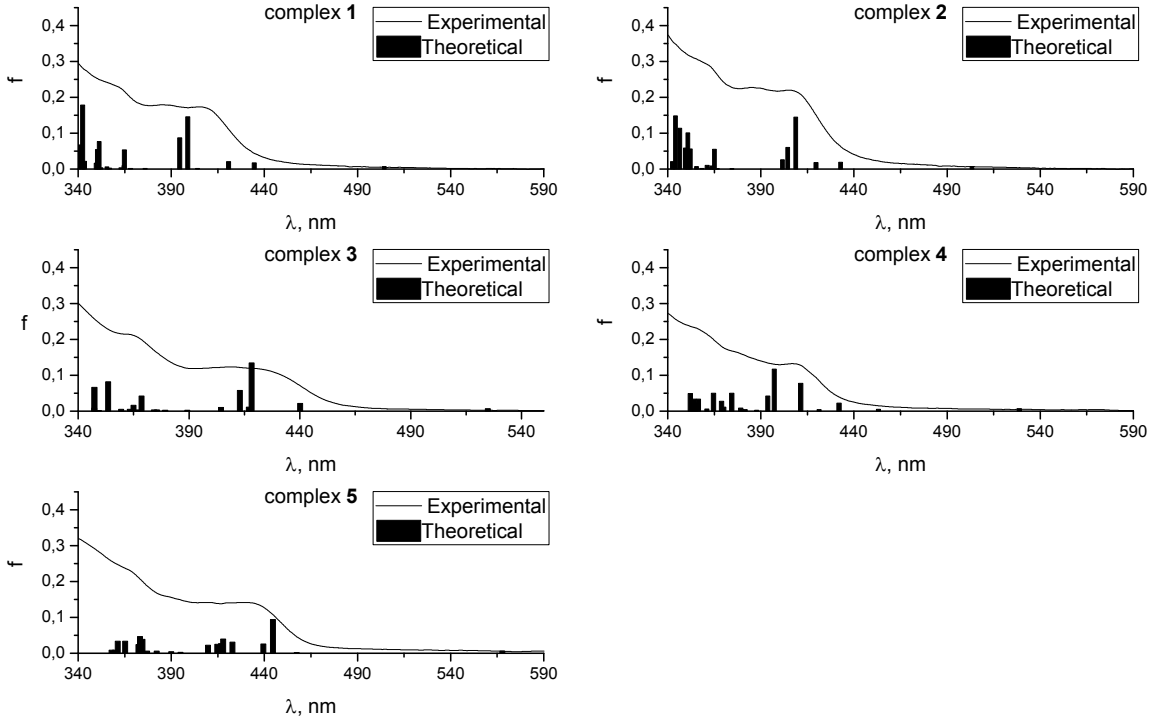

Figure S59. TDDFT electronic spectra of complexes **1**– **5**.

Table S8. Selected bond lengths in optimized structures of **1** – **5** at the ground and triplet excited states.

	1	**2**	**3**	**4**	**5**
Ir – C1 (S_0 / T_1)	1.9959 / 2.0103	1.9974 / 2.0110	1.9977 / 2.0125	1.9981 / 2.0132	1.9984 / 2.0094
Ir – C2 (S_0 / T_1)	1.9929 / 2.0038	1.9942 / 2.0050	1.9944 / 2.0057	1.9947/ 2.0068	1.9952 / 2.0027
Ir – N1 (S_0 / T_1)	2.0997/ 2.1005	2.0996 / 2.1002	2.0988 / 2.1014	2.0984 / 2.1001	2.0959 / 2.1015
Ir – N2 (S_0 / T_1)	2.0945 / 2.0944	2.0948 / 2.0945	2.0942 / 2.0942	2.0975 / 2.0965	2.1009 / 2.0978
Ir – O1 (S_0 / T_1)	2.1768 / 2.1287	2.1747 / 2.1282	2.1828 / 2.1247	2.1818 / 2.1248	2.1780 / 2.1187
Ir – O2 (S_0 / T_1)	2.1708 / 2.0897	2.1710 / 2.0892	2.1775 / 2.0791	2.1763 / 2.0821	2.1801 / 2.0748

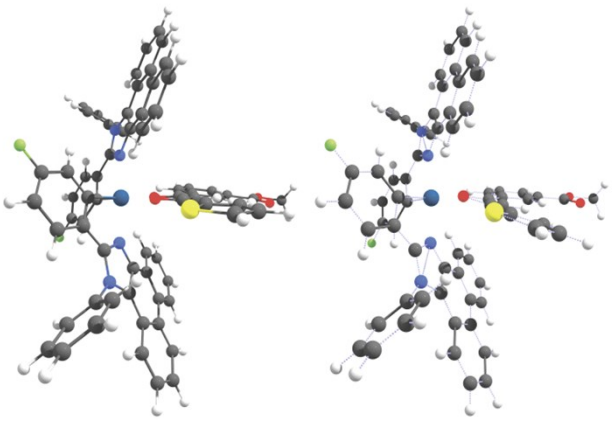

1

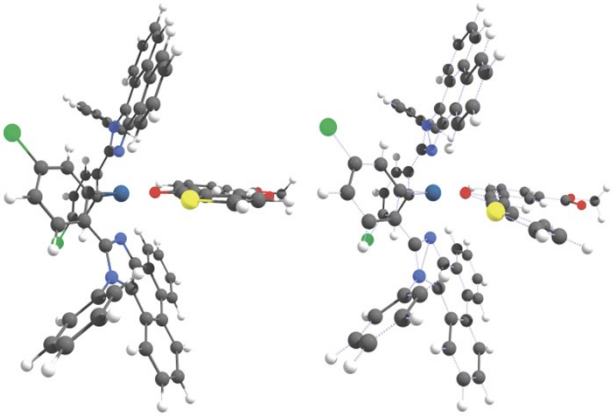

2

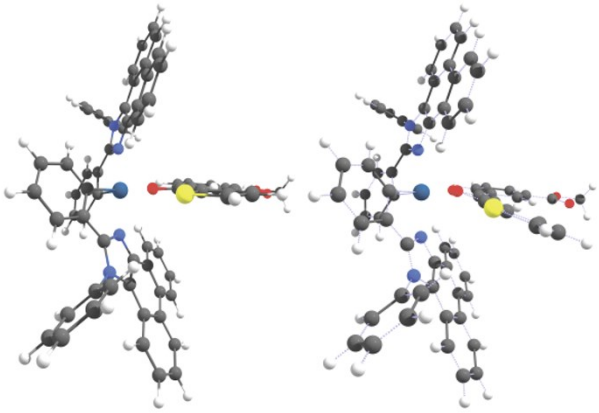

3

Figure S60a. Optimized geometries of S0(left) and T1(right) states of complexes **1** – **3**.

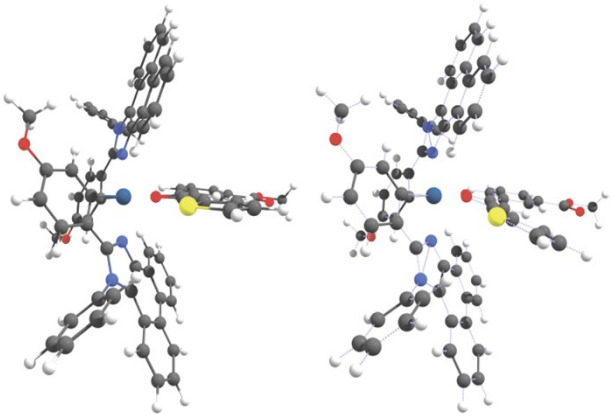

4

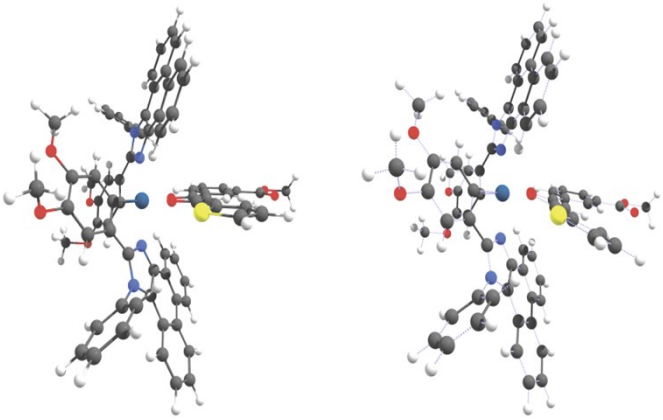

5

Figure S60b. Optimized geometries of S0(left) and T1(right) states of complexes **4** and **5**.

Table S9. TDDFT singlet excited states for **1** – **5**.

Compound	State	λ / nm (*f*)	Dominant monoexcitations
1	S_1	504 (0.007)	H → L (97%)
	S_2	435 (0.02)	H-2 → L (56%), H-1 → L (40%)
	S_3	421 (0.02)	H-1 → L (59%), H-2 → L (39%)
	S_5	399 (0.15)	H → L+1 (66%), H → L+2 (10%)
	S_6	395 (0.09)	H → L+3 (67%), H → L+1 (16%)
2	S_1	503 (0.007)	H → L (97%)
	S_2	432 (0.02)	H-2 → L (63%), H-1 → L (32%)
	S_3	420 (0.02)	H-1 → L (67%), H-2 → L (27%)
	S_4	409 (0.14)	H → L+1 (77%), H → L+2 (13%)
	S_5	404 (0.06)	H → L+2 (54%), H-3 → L (31%)
3	S_1	524 (0.007)	H → L (97%)
	S_2	440 (0.02)	H-1 → L (95%)
	S_3	418 (0.13)	H → L+1 (72%), H → L+2 (14%)
	S_4	416 (0.011)	H-2 → L (95%)
	S_5	412 (0.06)	H → L+3 (36%), H → L+2 (33%), H → L+1 (14%)
4	S_1	529 (0.006)	H → L (96%)
	S_3	432 (0.02)	H-2 → L (77%), H-1 → L (13%)
	S_5	411 (0.08)	H → L+1 (55%), H → L+2 (29%)
	S_6	397 (0.12)	H → L+4 (61%), H → L+2 (17%), H → L+1 (14%)
	S_7	394 (0.04)	H → L+2 (47%), H → L+4 (27%), H → L+1 (21%)
5	S_1	568 (0.006)	H → L (98%)
	S_3	444 (0.09)	H → L+1 (87%)
	S_4	439 (0.03)	H-2 → L (84%), H-1 → L (11%),
	S_5	423 (0.03)	H → L+3 (45%), H → L+4 (39%)
	S_6	418 (0.04)	H → L+2 (66%), H → L+5 (23%)

Only the singlet states in the visible spectral range are included. H = HOMO, L = LUMO.
All excitations are of combined MLCT / LLCT character. MLCT – metal-to-ligand charge transfer, LLCT – ligand-to-ligand charge transfer.

Table S10. Spin density distribution (%) for complexes **1** – **5** at their T_1 states.

complex		**1**	**2**	**3**	**4**	**5**
moiety	Ir	14	14	18	17	20
	O^O	83	82	76	78	70
	C^N	3	4	6	5	10

Table S11. Calculated emission wavelength for complexes 1 – 5 from the triplet excited state (calculated as $\lambda = hc/\Delta E$, where ΔE is $E(T_1)-E(S_0$ in T_1 geometry)

complex	**1**	**2**	**3**	**4**	**5**
λ, nm	658	657	697	687	727